Horizon 2020
European Union funding
for Research & Innovation

REDUCTION OF RADIOLOGICAL ACCIDENT CONSEQUENCES

Action	Research and Innovation Action NFRP-2018-1
Grant Agreement #	847656
Project name	**R**eduction of **R**adiological **C**onsequences of design basis and design extension **A**ccidents
Project Acronym	R2CA
Project start date	01.09.2019
Deliverable #	D4.4
Title	Final report on rod cladding failure during SGTR
Author(s)	G. Zullo, D. Pizzocri, L. Luzzi (POLIMI), F. Kremer (IRSN), N. Arnold, N. Muellner, R. Zimmerl (BOKU), J. Klouzal (UJV), D. Gumenyuk (SSTC), L.E. Herranz, R. Iglesias (CIEMAT), M. Cherubini, L. Giaccardi (NINE), A. Schubert, P. Van Uffelen (JRC), B. Bürger, Z, Hózer (EK)
Version	01
Related WP	WP4 SGTR
Related Task	T4.2. Fission product release from defective fuel rod during SGTR transient (POLIMI)
Lead organization	IRSN
Submission date	28.02.2023
Dissemination level	PU

This project has received funding from the Euratom research and training programme 2014-2018 under the grant agreement n° 847656

History

Date	Submitted by	Reviewed by	Version (Notes)
28.02.2023	L. Luzzi (POLIMI)	Z. Hózer (EK) N. Girault (IRSN)	01

Contents

List of figures and tables

Abbreviations

ANS	American Nuclear Society
BME NTI	Institute of Nuclear Techniques of the Budapest University of Technology and Economics
BWR	Boiling Water Reactor
DBA	Design Basis Accident
DEC	Design Extension Condition
EK	Energiatudományi Kutatóközpont / Centre for Energy Research
FG	Fission Gas
FGR	Fission Gas Release
FP	Fission Product
IFPE	International Fuel Performance Experiments
LOCA	Loss Of Coolant Accident
LWR	Light Water Reactor
MFPR-F	Module for Fission Product Release – France
NPP	Nuclear Power Plant
ODE	Ordinary Differential Equation
PWR	Pressurized Water Reactor
RELAP	Reactor Excursion and Leak Analysis Program
RING	Release of iodine and Noble Gas
SDA	Spectral Diffusion Algorithm
SGTR	Steam Generator Tube Rupture
VVER	Water Cooled Water Moderated Power Reactor

1. Introduction

The main objectives of Task 4.2 are to improve predictions of the complex fuel pellet behaviour of defective rods during a steam generator tube rupture (SGTR) transient and iodine accumulation phenomenon. This includes:

- Release of gaseous and volatile fission products (FPs), particularly iodine, from defective fuel rods during an SGTR transient.
- Complex fuel behaviour in defective fuel rods (especially oxidation, secondary hydriding).

This report summarizes the main achievements obtained in this task.

At UJV, TRANSURANUS code calculations were used to refine the conservative assumptions regarding the number of the failed rod in the core at the initiation of the SGTR. The gap inventory of ^{135}Xe, ^{133}Xe, ^{131}I and ^{137}Cs were assessed by TRANSURANUS model for both an intact fuel rod and a fuel rod with an assumed prior cladding breach. The calculated gap inventories were compared to the coolant activities measured in a VVER-1000 plant. Several cycles with varying number of leaking fuel rods were analyzed. No clear conclusion could be made for the release rates during the normal operation, including small activity spikes following power changes. On the other hand, the shutdown spike activity of ^{137}Cs always corresponds well to the gap inventory of the leaking rods assuming no enhanced diffusion from the fuel because of cladding failure. This conclusion helps to justify the application of the TRANSURANUS code for the gap inventory analysis.

At POLIMI, the coupling of TRANSURANUS [1] with SCIANTIX [2] has been upgraded to include the restart capability, allowing more precise simulations of validation cases (e.g., CONTACT1 experiment [3], [4]) of interest for the prediction of the gap activity from pressurized water reactor (PWR) fuel rods. The ANS 5.4-2010 methodology [5] has been implemented in TRANSURANUS (JRC) and SCIANTIX (POLIMI). POLIMI developed a methodology to bound the numerical error on the prediction of the release of radioactive volatile FPs [6]. This methodology has been applied in the newly developed physics-based model for the radioactive fission gas (FG) behaviour in the fuel. The model has been implemented in SCIANTIX and tested in both the stand-alone SCIANTIX version [7] and the version of TRANSURANUS coupled with SCIANTIX [8], thanks to the collaboration between JRC and POLIMI, against the CONTACT1 [3], [4] and the HATAC C2 [9] experiments. Results have been published in three journal papers [6]–[8].

IRSN proposed a new methodology for evaluating the release of radioactive isotopes from the fuel, by treating separately the release problem of (stable) elements, and the decay/release problem of radioactive isotopes. This allows to perform accurate assessment of the element release, and then to reuse this assessment for the calculation of radioactive isotope release. This methodology, called *decoupling approach*, uses two separate tools: the coupling of TRANSURANUS and MFPR-F codes, developed in collaboration with JRC, and a simple calculation tool for the formation, decay and transmutation of radioactive isotopes. This approach is applied as an illustration to an irradiation case taken from the Halden database (IFA-650.10).

BOKU has initiated a PhD position focused on modelling iodine spiking. A review of current literature was conducted. The simulations are done with RELAP5-3D. For WP2 transient calculations, the FP transport model of RELAP5-3D has already been implemented. A preliminary evaluation revealed that the FP behaviour model incorporated in RELAP5-3D is not including any physical retention effect on iodine (e.g., pool scrubbing) and is not suitable for simulating the iodine spike phenomenon without any post-processing. Therefore, an external function was introduced to improve the FP behaviour (see D4.1.1). Modelling of the radial redistribution of hydrogen in the zircaloy cladding (related to Task 4.3) was performed by the JRC (stand-alone model), harmonizing the transport models in cylindrical coordinates available in TRANSURANUS.

CIEMAT checked the applicability of fission product release models currently existing in MELCOR 2.2 (CORSOR and CORSOR-Booth models). The bases of the models were reviewed in the section 3.3 from the perspective of the iodine spike release in SGTR sequences. Despite the potential of these models to be used, the conditions underlying their bases are notably out the range of those concerning iodine spiking during SGTR DBA and DEC-A sequences. Therefore, an external MELCOR function has been built to model iodine spiking in SGTR DBA and DEC-A sequences.

NINE introduced in TRANSURANUS the modelling of FP release from defective fuel rods. The model considers two successive steps: (1) FP release from the fuel to the fuel-cladding gap, followed by (2) FP release from the fuel-cladding gap to the coolant. Furthermore, the model includes an upgraded section for the production of the

fission product isotopes. Such production considers a bigger number of isotopes with respect to the actual status of the code (iodine and other unstable gas has been included) and simulate them through an implicit scheme discretization of the Bateman's equations, i.e., considering decay and capture events as well as cumulative fission yields, the latter being verified through a comparison with the Serpent code. Regarding the diffusion of the isotopes in the fuel matrix, a new model option has been implemented considering a correction factor related to the fuel hyper-stoichiometry. Then, validation activity has been carried out for the fission gas release (FGR) from the fuel to the fuel-cladding gap against experimental data of CONTACT1 from IFPE database. Afterwards, the TRANSURANUS version extended by NINE has been extended to model the gap-to-coolant release from defective fuel rods. Then, it has been used to simulate the CRUSIFON1bis defective fuel rod experiment (IFPE database), and to calculate the phenomenological escape rates for short-lived FPs under equilibrium conditions.
The Centre for Energy Research (EK) further developed the Release of iodine and Noble Gases (RING) code against 18 new measured datasets obtained during power transients, reactor shutdown and start-up nuclear power plants. The targeted developments have been oriented to overcome the underestimation of the effect of the power change in the previous version of the code, and the introduction of new caesium spiking models (^{134}Cs and ^{137}Cs). The upgraded RING code has been applied to the simulation of iodine and caesium spiking effect in both SGTR, and collector cover opening conditions. In addition, it allowed to precise the activity release according to the specific power and pressure histories of the two events. In the updated transient model of the RING code, the release accelerates as a function of the variation in core power, primary pressure, and boric acid concentration. The original datasets used for the simulation of steady state and transient conditions with the RING code derived from the coolant analysis of the VVER Paks NPP performed before 2002. The improved acceleration factor for the release has been tailored and tested against recently collected new data from the Paks NPP, resulting in more reliable predictive capabilities of the code itself.
SSTC NRS reviewed the open literature about the investigation of fission product release from fuel rods under primary to secondary leaks. Main attention was paid on investigation approaches for iodine spike-effect modelling. With this respect SSTC NRS analysed the following sources:

- Kurchatov Institute document *Calculations of the fission products inventory under the cladding of hermetic and unhermetic fuel elements of VVER-1000 fuel assemblies (TVSA, TVS-2) with deep fuel burnup (60 MW * day / kg uranium for the fuel element) and the activity of the primary coolant. Report of the RRC KI, M: - 2004.*
- *Issue 197 "Iodine spiking phenomena" of document "NUREG-0933. Resolution of Generic Safety Issues (Formerly entitled "A Prioritization of Generic Safety Issues"), Main Report with Supplements 1–34, 2011.*
- *Regulatory Guide 1.183 "Alternative radiological source terms for evaluating design basis accidents at nuclear power reactors".*

As an option, SSTC NRS is considering collecting data for iodine spike-effect issues for Ukrainian NPPs.

2. Modelling the release of radioactive gas from fuel to gap

In the following, developments concerning the modelling of radioactive gaseous and volatile FPs from the fuel to the fuel-cladding gap are described.

To begin with, JRC has reprogrammed in modern Fortran the implementation of the semi-empirical model ANS 5.4-2010 [5] by V. Peri [10] in the TRANSURANUS code to predict the release-to-birth-ratio of some short-lived gaseous and volatile FPs. This model is limited to stationary conditions and relies on an empirical approach for the grain boundary behaviour of the FPs. In order to overcome this limitation, as a first step, POLIMI developed a methodology to bound a priori the numerical error on the prediction of both stable and radioactive FG/FP release [6]. The methodology is tailored to state-of-the-art spectral diffusion algorithms (SDAs) and is adopted in SCIANTIX [2] to guarantee an optimal discretisation of the intra-granular diffusion/diffusion-decay problem. In a second step, as an alternative to the state-of-the-art semi-empirical methodology ANS 5.4-2010 [5] to predict the release-to-birth-ratio of short-lived gaseous and volatile FPs, POLIMI developed a physics-based model to describe intra- and inter-granular behaviour of short-lived gaseous and volatile FPs in the fuel [7]. The model has been implemented in SCIANTIX [2] and tested (as a standalone code) against the CONTACT1 irradiation experiment [3], [4], from the IFPE database. Results include the comparison of the release-to-birth ratio of several short-lived isotopes of xenon and krypton against experimental measurements and ANS 5.4-2010 predictions [7].
To assess the aforementioned model from an integral point of view, the coupling interface between the integral fuel performance code TRANSURANUS and SCIANTIX has been upgraded, to account for the TRANSURANUS restart option. Then, the coupled code TRANSURANUS//SCIANTIX has been used to reproduce the CONTACT1 [3], [4] and the HATAC C2 irradiation experiment [9]. Results are collected in journal papers [6], [7], [11].

The TRANSURANUS version extended by NINE includes the intra-granular model for FP behaviour. This model considers the formation of radioactive FPs (unstable isotopes) and FGs (stable isotopes) within the fuel grains and their diffusion towards the grain boundaries. The intra-granular diffusion is modelled with the extension of the mechanistic model by Speight that considers the Brownian motion of bubbles, and the deriving intra-granular diffusivity can consider two contributions: a first term accounting for the fraction of in-solution FP atoms, available for single atom diffusion, and a second term accounting for the mobility of intra-granular bubbles. In addition, the intra-granular diffusivity is corrected with a factor that considers the increased FP diffusivity in hyper-stoichiometric fuel. The factor is applied to the intrinsic high-temperature component of the single atom diffusion coefficient given by Turnbull [12]. The TRANSURANUS version extended by NINE is currently being merged with other developments in TRANSURANUS.

A methodology for evaluating the inventory of radioactive isotopes released to the gap is proposed by IRSN. The underlying idea is that such evaluation must take into account two different aspects. Firstly, the release of fission products from fuel encompasses several complex phenomena, namely diffusion in UO2 grain, formation of precipitates (bubbles for noble gas, solid precipitates for chemically active FP), formation of volatile species at grain boundary and their release to open porosities. Secondly, determining the isotope vector associated to each fission product element requires to consider the transmutation and decay at each stage of the release, i.e., to solve the so-called Bateman equations extended with transfer rates associated with the mechanisms described above. Due to the difficulty to cover these two aspects in a single calculation tool, the proposed methodology consists of decoupling them, by using successively two different tools developed at IRSN. The first one is the MFPR-F code coupled with TRANSURANUS, evaluating the different steps of release mentioned above. The second tool, developed in the framework of WP5-Task2, calculates the formation and transmutation of radioactive isotopes (Bateman equations) as well as their transfer from the fuel to the gap based on simplified models for FP release. In the current approach, the parameters of these simplified models are to be determined from the results given by the TRANSURANUS//MFPR-F coupling.

2.1. Bounding of numerical error

Improving the current fuel performance codes used to reproduce the release of radioactive FGs from the fuel rod in transient conditions requires to develop suitable physically grounded description for the targeted FGs at the fuel grain scale. The meso-scale code SCIANTIX [2] has been upgraded to include the intra- and inter-granular behaviour of radioactive volatile FPs and radioactive FG (isotopes of xenon, krypton, iodine, tellurium, and caesium) with mechanistic models developed at the scale of the fuel grain.

From the intra-granular point of view, the following equation is used to model the production, diffusion, and decay of radioactive FPs:

$$\frac{\partial C(r,t)}{\partial t} = D(F,T)\nabla^2 C(r,t) - \lambda C(r,t) + S(F), \qquad r \in [0,a), t > 0 \tag{1}$$

Eq. 1 represents the FP diffusion in a spherical homogenous fuel grain of radius a (m) at uniform temperature T (K) and fission rate density F (fiss m^{-3} s^{-1}). The variables depend on the time t (s) and radial position r (m). C (at m^{-3}) is the intra-granular FP concentration, D (m^2 s^{-1}) is the diffusivity, λ (s^{-1}) is the decay rate, $S = yF$ (at m^{-3}s^{-1}) is the production rate of the FP and y (at fiss^{-1}) the fission yield. Besides, Eq. 1 takes advantage of the weak variation of the diffusivity D on the radial position r in the fuel grain, assuming that $-\nabla \cdot (-D(F,T)\,\nabla C(r,t)) = D(F,T)\nabla^2 C(r,t)$.

From Eq. 1, the spatial-averaged FP concentration is computed by using SDAs, powerful spectrum-temporal discretising techniques already explored to solve the stable FG diffusion [2], [13]. In addition, their extension to the radioactive case is straightforward.

When fast transient conditions and/or short-lived FPs are targeted, the discretising parameters (number of time-steps and of modes) must be consequently modified to ensure a high numerical accuracy. For this reason, an error analysis of the SDA employed to discretise Eq. 4 has been performed. The error analysis starts from the formulation of the non-dimensional version of Eq. 4, obtained by posing $\rho = r/a$, $\tau = tD/a^2$, $\phi = CD/a^2S$ and $\mu = \lambda a^2/D$:

$$\frac{\partial \phi(\rho,\tau)}{\partial \tau} = \widetilde{\nabla}^2 \phi(\rho,\tau) - \mu(\tau)\phi(\rho,\tau) + 1, \qquad \rho \in [0,1), \tau > 0 \tag{2}$$

The initial condition for Eq. 2 translates into $\phi_0 = C_0 D/a^2 S$ and the non-dimensional radial spherical Laplacian is noted as $\widetilde{\nabla}^2$. By applying the following modal expansion:

$$\phi(\rho,\tau) = \sum_{n=1}^{N_M} x_n(\tau)\,\psi_n(\rho) \tag{3}$$

with $\psi_n(\rho) = \frac{1}{\sqrt{2\pi}}\frac{\sin(\theta_n \rho)}{\rho}$ and $\theta_n = n\pi$ the eigenvalues, the unknown of the problem becomes the set of time coefficients $\{x_n(t)\}$. The latter are the solution of the problem:

$$\sum_{n=1}^{N_M} \frac{\mathrm{d}x_n(\tau)}{\mathrm{d}\tau}\delta_{nj} = -\sum_{n=1}^{N_M} x_n(\tau)\left(\theta_n^2 + \mu(\tau)\right)\delta_{nj} + \langle \psi_j | 1 \rangle \tag{4}$$

where $\langle \psi_n | \psi_j \rangle = \int_\Omega \psi_n \psi_j \,\mathrm{d}\Omega = \delta_{nj}$ is the Kronecker delta and $\langle \psi_j | 1 \rangle = \frac{(-1)^{j+1}}{j}\sqrt{\frac{8}{\pi}}$. For every time coefficient the following ordinary differential equation is hence to be solved:

$$\frac{\mathrm{d}x_j(\tau)}{\mathrm{d}\tau} = -\Lambda_j(\tau)x_j(\tau) + \langle \psi_j | 1 \rangle \tag{5}$$

where the mode eigenvalue is $\Lambda_j(\tau) = \theta_j^2 + \mu(\tau)$ and the initial condition comes from the projection $x_j(0) = < \psi_j | \phi_0 >$. Concerning the temporal discretisation, by exploiting the backward Euler scheme, for each time-step the numerical solution of Eq. 5 is:

$$x_{j,N}^{k+1} = \frac{x_{j,N}^k + \langle \psi_j | 1 \rangle \Delta\tau}{1 + \Lambda_j^{k+1}\Delta\tau} \tag{6}$$

where the superscript k indicates the discrete time $\tau^k = k\Delta\tau$. The numerical (N) spatial average of the concentration ($\bar{\phi} = \frac{3}{4\pi}\sum_{j=1}^{N} x_j \langle \psi_j | 1 \rangle$) is eventually reconstructed:

$$\bar{\phi}_N^{k+1} := \frac{3}{4\pi} \sum_{j=1}^{N_M} \frac{x_{j,N}^k + \langle \psi_j | 1 \rangle \Delta\tau}{1 + \Lambda_j^{k+1} \Delta\tau} \langle \psi_j | 1 \rangle \tag{7}$$

The refence formulation for the spatial average of the concentration $\bar{\phi}$, labelled with the subscript *A*, is given by the quasi-exact ANS 5.4 standard [14]

$$\bar{\phi}_A^{k+1} := \frac{3}{4\pi} \sum_{j=1}^{CN_M} \left(\frac{\langle \psi_j | 1 \rangle}{\Lambda_j^{k+1}} \left(1 - \exp\left(-\Lambda_j^{k+1} \frac{\Delta\tau}{M} \right) \right) + x_{j,A}^k \exp\left(-\Lambda_j^{k+1} \frac{\Delta\tau}{M} \right) \right) \langle \psi_j | 1 \rangle \tag{8}$$

Constant conditions are assumed within each time-step. The main difference with the latter formulation lies in the temporal coefficient $x_{j,A}^{k+1}$, evaluated at each time step from Eq. 5 with an incremental approach. Besides, Eq. 8 is obtained by using a higher number of time-steps $N_{\Delta\tau}$ (by a factor of $M \gg 1$) and a higher number of modes N_M (by a factor of $C \gg 1$) with respect to Eq. 7, to increase its accuracy.

To develop the error analysis, the following definition for the error between the numerical solution and the quasi-analytic solution is considered:

$$\mathrm{err}(N_{\Delta\tau}, N_M; \mu) := \max\left(\left| \frac{\bar{\phi}_A(\tau) - \bar{\phi}_N(\tau)}{\bar{\phi}_A(\tau)} \right| \right) \tag{9}$$

where $N_{\Delta\tau}$ and N_M are the number of time-steps and the number of modes used in the computation of the numerical solution. The diffusion-decay equation is numerically solved up to the equilibrium time. The error defined in Eq. 9 is then divided in two contributions: a temporal and a modal contribution ($\mathrm{err}(N_{\Delta\tau}, N_M; \mu) = \epsilon_{\Delta\tau}(N_{\Delta\tau}, N_M; \mu) + \epsilon_M(N_{\Delta\tau}, N_M; \mu)$). Exploiting the triangular inequality, the following upper bound is defined to proceed with the error analysis: $\epsilon(N_{\Delta\tau}, N_M; \mu) := |\epsilon_{\Delta\tau}(N_{\Delta\tau}, N_M; \mu)| + |\epsilon_M(N_{\Delta\tau}, N_M; \mu)|$.

The error analysis and the study of $\epsilon(N_{\Delta\tau}, N_M; \mu)$ results in two reference tables, complementary to the SDA, to select the spectrum-temporal discretization parameters ($N_{\Delta\tau}, N_M$) and provide a suitable *a priori* upper bound to the numerical error.
A fit of the upper bound $\epsilon(N_{\Delta\tau}, N_M; \mu)$ is considered. The fit depends on five parameters, (*A, B, C, D, E*) and its accuracy is ensured from $R^2 \geq 99.1\%$. Then, the fit function is:

$$\hat{\epsilon}(N_{\Delta\tau}, N_M) = 10^{A \log_{10} N_{\Delta\tau} + B} + 10^{C(\log_{10} N_M)^2 + D \log_{10} N_M + E} \tag{10}$$

From the performed error analysis, several values of μ are investigated and Table 1 and Table 2 are constructed, concerning the diffusion-decay problem in constant and transient conditions respectively.
The operative procedure to bound the error in constant conditions is given here below:

1. Fix the demanded upper bound (e.g., $U_B = 5\%$).
2. Estimate the constant value of $\mu = \frac{\lambda a^2}{D}$.
3. Determine the row, in Table 1, which best approximate the value previously estimated.
4. Choose ($N_{\Delta\tau}, N_M$) for which the fit function $\hat{\epsilon} \leq U_B$ (if the ratio between the simulated time interval and the equilibrium time is $t_s/t_e > 1$ then select $\frac{N_{\Delta\tau} t_s}{t_e}$ as time-step number) and use it in the implementation of the SDA.

Similarly, in transient conditions the operative procedure is structured as follows:

1. Fix the demanded upper bound (e.g., $U_B = 5\%$).
2. Compute the time-varying $\mu = \frac{\lambda a^2}{D}$ and its average value $\langle\mu\rangle$ over the time interval.
3. Determine the row, in Table 2, for which $\langle\mu\rangle \in [0, \mu_{max}]$
4. Choose $(N_{\Delta\tau}, N_M)$ for which the fit function $\hat{\epsilon} \leq U_B$ and use it in the implementation of the SDA.

Table 1: Reference table for constant conditions.

μ	A	B	C	D	E
0	-0.5028	-0.2662	-0.0397	-2.8320	1.4450
10	-0.5643	-0.1951	-0.7793	-0.2846	-0.4304
10^2	-0.6998	-0.0498	-0.5863	-0.2571	-0.4280
10^3	-0.8979	0.2502	-0.2448	-0.5961	-0.4140
10^4	-0.9764	0.3470	-0.1205	-0.7202	-0.4080
10^5	-0.9798	0.3367	-0.0841	-0.7575	-0.4062
10^6	-0.9797	0.3343	-0.0731	-0.7687	-0.4057
10^7	-0.9797	0.3340	-0.0702	-0.7716	-0.4056
10^8	-0.9797	0.3340	-0.0698	-0.7720	-0.4055
$>10^8$	-0.9797	0.3340	-0.0698	-0.7720	-0.4055

Table 2. Reference table for time-varying conditions.

$\langle\mu\rangle \in [0, \mu_{max}]$	A	B	C	D	E
[0;10]	-0.5633	-0.1979	-0.1460	-2.4400	1.3840
$[0;10^2]$	-0.4725	-0.1248	-1.1640	1.5660	-1.8260
$[0;10^3]$	-0.4705	-0.0781	-0.5503	0.3801	-1.1650
$[0;10^4]$	-0.4748	-0.0602	-0.1693	-0.5628	-0.5322
$[0;10^5]$	-0.4748	-0.0602	-0.1693	-0.5628	-0.5322
$[0;10^6]$	-0.4716	-0.0680	-0.0283	-0.9075	-0.3017
$[0;10^7]$	-0.4995	0.0052	-0.0218	-0.9272	-0.2885
$[0;10^8]$	-0.4760	-0.0540	-0.0192	-0.9300	-0.2867
$[0;10^9]$	-0.4964	-0.0015	-0.0130	-0.9450	-0.3219
$[0;10^{10}]$	-0.4912	-0.0143	-0.0130	-0.9450	-0.3219
$[0;10^{20}]$	-0.4874	-0.0227	-0.0130	-0.9450	-0.3219
$[0;10^{30}]$	-0.4889	-0.0237	-0.0130	-0.9450	-0.3219
$[0;10^{40}]$	-0.4716	-0.0581	-0.0130	-0.9450	-0.3219

2.2. Radioactive fission gas behaviour with SCIANTIX

The phenomenon of FG release from the fuel to the rod free volume is currently modelled in SCIANTIX [7] with a two-step process [15]–[18]:

1. FG atoms are uniformly generated within the fuel grains due to fission events. The dominant gas transport mechanism from the fuel to the rod free volume, is the atomic diffusion [12], [17]–[21], in the first place from within the grains to the grain boundaries, where the gas accumulates in grain-boundary bubbles.
2. The inter-granular bubbles grow by absorption of both FG and vacancies and can coalesce together, resulting in larger and fewer bubbles [20], [22]. Coherently with the state-of-the-art modelling [17], [18], [20] we assume that this process continues until the grain boundaries are sufficiently populated with large bubbles, and a network of interconnected bubbles is formed. This network constitutes a pathway through which fission gas is vented out of the fuel pellet, as soon as the network gets in touch with an easy escape route, e.g., a fuel crack. We assume that this release happens instantly, i.e., the gas is brought from the grain boundaries to the fuel rod free volume, neglecting all the intermediate mechanisms occurring [23].

This behaviour is supported by experimental observations of fractured surfaces of UO_2 showing that the grain boundaries are populated by large, lenticular bubbles [20]. If the grain-boundary bubble density is N_{gb} (bub m^{-2}) and the bubble average (projected on the grain boundary) area is A_{gb} (m_2), the fraction of the grain boundary covered with grain-boundary bubbles is $N_{gb}A_{gb}$, defined as fractional coverage F_c (/). The critical, or saturation, value of F_c that determines the interconnection of the grain boundary bubbles is set to F_c = 0.5, in line with experimental observations [20], [22], [24].

The intra-granular behaviour of radioactive FG is modelled as follows. Considering a spherical fuel grain, the diffusion of radioactive FG towards the grain boundary described following Booth formulation [25], according to Eq. 1, repeated here below:

$$\frac{\partial C(r,t)}{\partial t} = D_{\text{eff}}(F,T)\nabla^2 C(r,t) - \lambda C(r,t) + S(F) \tag{11}$$

Where λ (s^{-1}) is the decay rate and S = yF (at $m^{-3}s^{-1}$) is the production rate of the gas, being y (at $fiss^{-1}$) its cumulative fission yield. The concentration C (at m^{-3}) represents the residual amount of intra-granular FG. The effective diffusivity (D_{eff}) takes into account the ANS 5.4-2010 correction due to the first precursor, through a factor α(/). Also, it includes the combined effect of trapping-in [26] and irradiation-induced re-solution [27] from intra-granular bubbles, according to the work of White and Tucker [17]. In the end, being the trapping rate and the re-solution rate g and b, respectively, the effective diffusivity is then given by:

$$D_{\text{eff}} = \alpha \frac{b}{b+g} D \tag{12}$$

Where the adopted expression for the single-atom diffusivity is:

$$D = 7.6 \times 10^{-10} e^{-35000/T} + 5.64 \times 10^{-25} \sqrt{F} e^{-13800/T} + 2 \times 10^{-40} F \tag{13}$$

in line with the SCIANTIX validation for the modelling of inert gas behaviour [2].

The inter-granular behaviour of short-lived fission gases is modelled with the same physics-based approach, already implemented in SCIANTIX for the stable FG behaviour [2], [18], [20]. It is assumed that the grain-boundary venting is mainly driven by stable FG and that short-lived FG, negligible in mass with respect to stable isotopes, are not relevant in determining grain-boundary venting. Inter-granular bubbles develop on the grain boundaries and continuously absorb FG from the grains. Bubbles grow and coalesce on the grain boundaries until their saturation takes place, leading to the formation of a pathway connected with the pellet surface. Then,

the gas percolates through the interconnected porosity and is released to the fuel rod free volume [17], [18], [20]. The grain-boundary saturation process represents an incubation time for the onset of the thermal release [28]. The delay is caused by the initially closed porosity of the fuel microstructure. In the case of short-lived radioactive FGs, this delay is significant. Hence, suitable modelling of this incubation period is required. From the modelling point of view, the grain-boundary bubble behaviour, based on the work of Pastore et al. [18], is exploited. With respect to the modelling of stable FG, the concentration of radioactive FG accumulated at the grain boundary C_b is given by:

$$\frac{dC_b}{dt} = -\left(\frac{3}{a} D_{\text{eff}} \frac{\partial C}{\partial r}\right)_{r=a} - \lambda C_b - R \tag{14}$$

The release rate R (at m^{-3} s^{-1}) accounts for the FG atoms accumulated on grain boundaries, that are released to the fuel rod free volume as soon as the grain-boundary venting occurs, computed according to [2], [7], [18].

2.2.1 Model testing as standalone version in SCIANTIX

The model outlined in Section Radioactive fission gas behaviour with SCIANTIX has been implemented into the current version of SCIANTIX [2] and tested as a standalone code to simulate the CONTACT1 experiment [3], [4]. The CONTACT1 test involved an in-pile study of short fuel rods composed of UO_2 pellets wrapped in a Zr-4 cladding. We focus on the CONTACT1 - FRAMATOME rodlet since this case is dominated by diffusional release, whereas the other experiments are performed at lower power and burn-up and thus dominated by athermal release, which is currently not considered in the SCIANTIX code.
In CONTACT1, the pellet stack was thermally isolated at both ends by alumina oxide pellets and an Inconel spring ensured its axial holding. The capsule was in a PWR loop, at 13 MPa (to best represent the effect of the cladding creep down) and the nucleate boiling regime provided an external cladding temperature of 330°C. The linear power, the fuel centreline temperature (FCLT), the cladding outer diameter at power, the release of stable inert fission gases and the release-to-birth ratios of some short-lived isotopes (between ^{133}Xe and ^{89}Kr) were measured.
The SCIANTIX simulation required as input quantities the fuel temperature, fission rate density and fuel hydrostatic stress. These quantities are obtained with the TRANSURANUS code [1] for which the CONTACT1 input file is available. In particular, the radial average of the fuel temperature and hydrostatic stress are used in the SCIANTIX code, providing an acceptable 0D representation of the irradiation experiment.
By using SCIANTIX, the release-to-birth ratios for the short-lived FG isotopes between ^{133}Xe and ^{88}Kr are calculated. In Figs. 1-6 the calculations are compared with both experimental measurements and ANS 5.4-2010 predictions.
The release kinetics predicted with the SCIANTIX code are in qualitative agreement with the experimental data[1]. Likely, the measured R/B values increase with fuel burnup due to the development of intergranular porosity with the irradiation. This behaviour is predicted by SCIANTIX calculations due to the physical description of grain-boundary bubble development [2], [18]. Instead, ANS 5.4-2010 reproduces this mechanism through a modified empirical Vitanza threshold [28], implemented in the methodology.
The fact that measured R/B values reach an approximately constant value after 10 MWd/kgU is due to the achievement of radioactive equilibrium between the phenomena of production, diffusion, and decay. SCIANTIX accounts for this behaviour by solving Eq. 11 with a dedicated spectral approach (outlined in Section 2.1) while ANS 5.4-2010 only considers the equilibrium solution of Eq. 11 [5]. This is the reason why the ANS 5.4-2010 is

[1] As stated in the IFPE documentation of the CONTACT programme [3], [4] and in [5], [7] measured values for ^{133}Xe at 10 MWd/kgU (Fig. 4) shows a significant increase. The CONTACT documentation exhibits a lack of information about the experimental uncertainty of the measurements. Nevertheless, the ^{133}Xe is known to be subjected to larger uncertainty in comparison with that on other isotopes [5]. It is reasonable to ascribe the ^{133}Xe release-to-birth ratio increase to instrumentation errors because it is not reflected in the other release curves. Furthermore, the linear connection between the points measured at successive time points should not be confused with real release evolution points.

not applicable in transient scenarios (e.g., accidental scenarios), as opposed to the model described in Section Radioactive fission gas behaviour with SCIANTIX.
From the ANS 5.4-2010 report [5] it is possible to extract an uncertainty band, of a factor of 5 wide, on the measured R/Bs, which encloses both the ANS 5.4-2010 predictions and the SCIANTIX calculations.
The root mean square error on the predicted R/Bs with respect to the experimental data, for the model implemented in SCIANTIX [29] and the semi-empirical ANS 5.4-2010 methodology [5] is shown in Table 3. The SCIANTIX predictions results in satisfactory agreement with the experimental data and in most cases at least as good as the ANS 5.4-2010 predictions. This is a non-trivial result, given that the model described in Section 2.2 is based on physical parameters [2], [7], while the ANS 5.4-2010 methodology [5] adopts parameters calibrated on its validation database (e.g., grain radius and single-atom diffusivity).

Table 3: Root mean square error (RMSE) of release-to-birth ratios with respect to the experimental data, for the model implemented in SCIANTIX [29] and the semi-empirical ANS 5.4-2010 methodology [5].

Isotope	RMSE – ANS 5.4-2010	RMSE – SCIANTIX
^{133}Xe	4.57 x 10^{-3}	5.28 x 10^{-3}
^{135m}Xe	2.10 x 10^{-5}	1.60 x 10^{-4}
^{135}Xe	5.37 x 10^{-5}	3.55 x 10^{-4}
^{85m}Kr	1.27 x 10^{-4}	1.50 x 10^{-4}
^{87}Kr	3.86 x 10^{-6}	1.15 x 10^{-4}
^{88}Kr	4.57 x 10^{-3}	5.28 x 10^{-3}

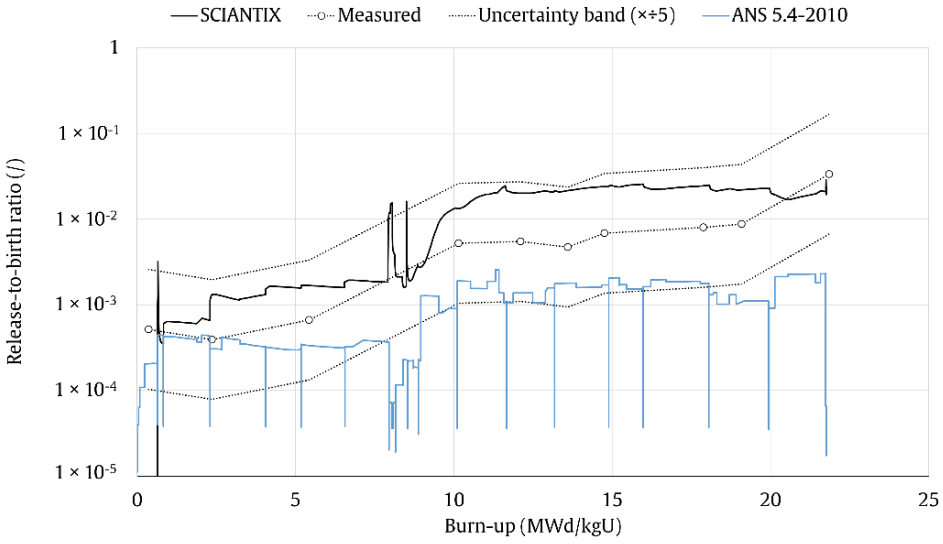

Fig. 1: Comparison of the release-to-birth ratio measured during the CONTACT 1 experiment (white dots) against the SCIANTIX prediction (black solid line) and the ANS 5.4-2010 prediction (blue line), for the short-lived ^{85m}Kr.

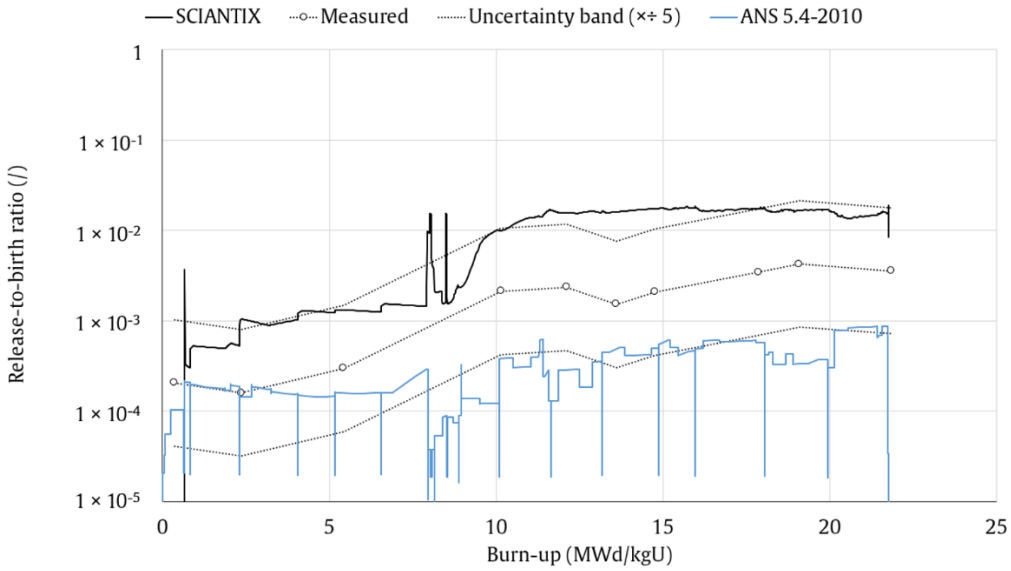

Fig. 2: Comparison of the release-to-birth ratio measured during the CONTACT 1 experiment (white dots) against the SCIANTIX prediction (black solid line) and the ANS 5.4-2010 prediction (blue line), for the short-lived ^{87}Kr.

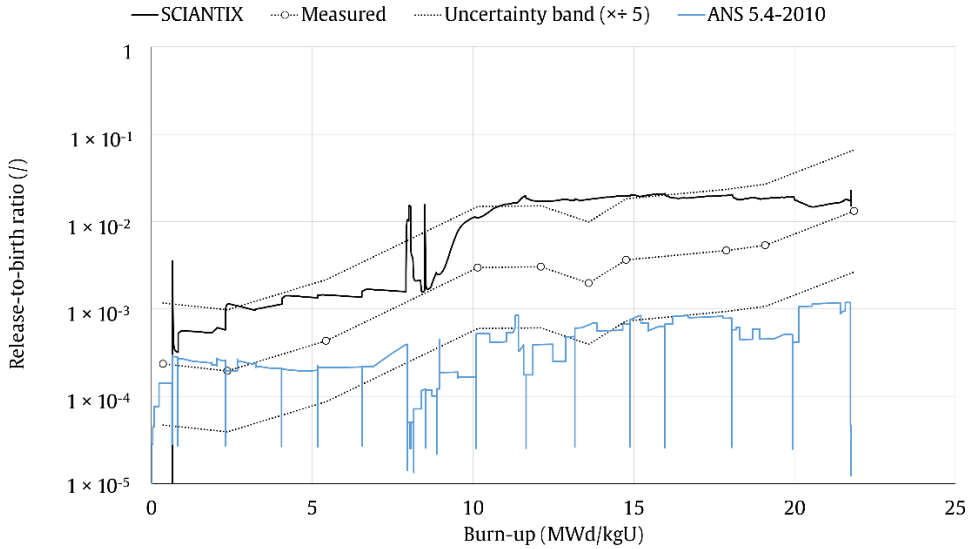

Fig. 3: Comparison of the release-to-birth ratio measured during the CONTACT 1 experiment (white dots) against the SCIANTIX prediction (black solid line) and the ANS 5.4-2010 prediction (blue line), for the short-lived ^{88}Kr.

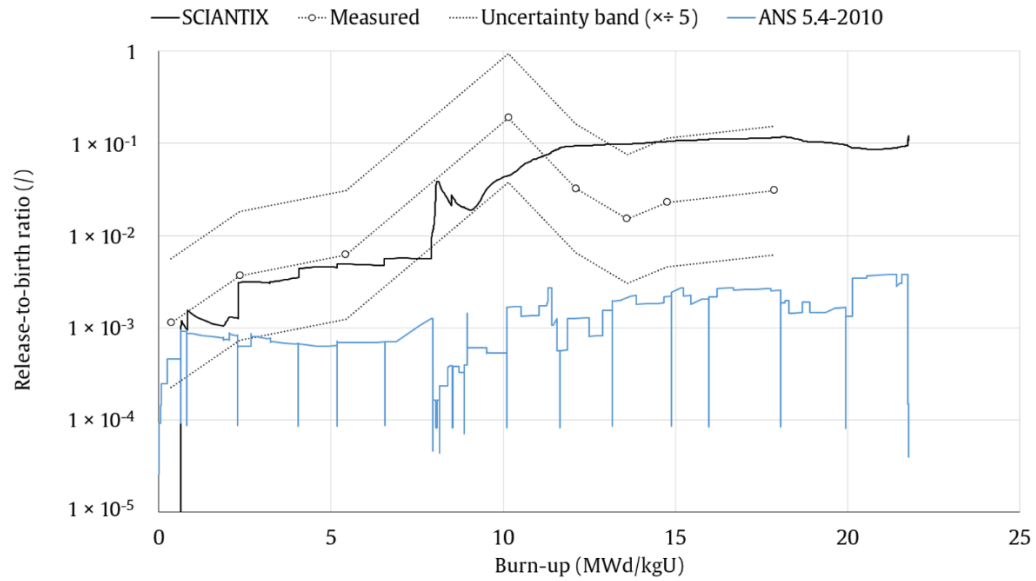

Fig. 4: Comparison of the release-to-birth ratio measured during the CONTACT 1 experiment (white dots) against the SCIANTIX prediction (black solid line) and the ANS 5.4-2010 prediction (blue line), for the short-lived ^{133}Xe.

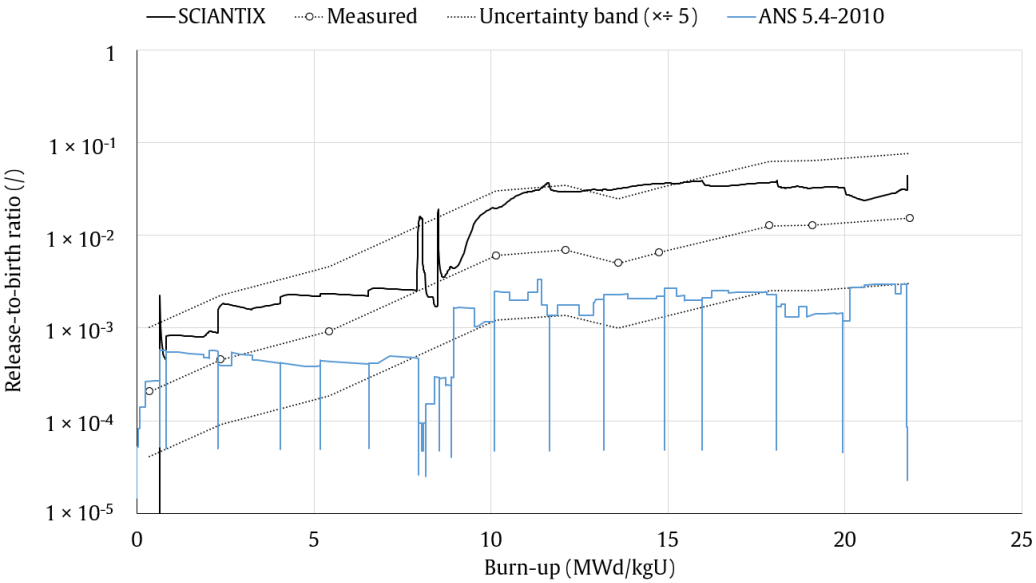

Fig. 5: Comparison of the release-to-birth ratio measured during the CONTACT 1 experiment (white dots) against the SCIANTIX prediction (black solid line) and the ANS 5.4-2010 prediction (blue line), for the short-lived ^{135}Xe.

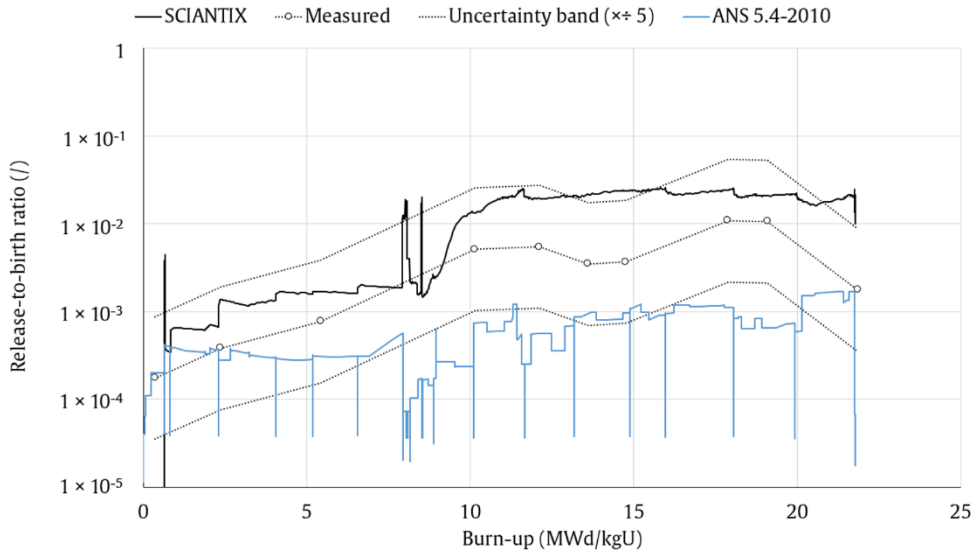

Fig. 6: Comparison of the release-to-birth ratio measured during the CONTACT 1 experiment (white dots) against the SCIANTIX prediction (black solid line) and the ANS 5.4-2010 prediction (blue line), for the short-lived ^{135m}Xe.

2.2.2 Model testing with TRANSURANUS coupled with SCIANTIX

The TRANSURANUS fuel performance code [1], coupled with SCIANTIX [2] (here identified as TRANSURANUS//SCIANTIX) is employed to test at the rod scale the physics-based model that describe the radioactive gas behaviour in the UO_2 fuel.

Two irradiation experiments from the IFPE database, CONTACT 1 [3], [4] and HATAC C2 [9] are considered. As mentioned in the previous section, CONTACT 1 focuses on the fuel rod behaviour irradiated in stationary conditions. HATAC C2 investigates the fuel behaviour during a sequence of power transients.

The comparative analysis on the CONTACT 1 case is again supported by applying the ANS 5.4-2010 semi-empirical methodology [5] to evaluate the release-to-birth ratio of short-lived fission gases.

The assessment against the HATAC C2 experiment is performed by comparing the release rate of the short-lived ^{133}Xe.

From Fig. 7 and Fig. 8, the behaviour of the release-to-birth ratio of the short-lived isotopes ^{133}Xe and ^{85m}Kr is analysed. The R/B dynamics predicted by TRANSURANUS//SCIANTIX show an increase with burnup. This is a consequence of the model implemented in SCIANTIX (Section 2.2) describing the fundamental phenomena of production, (intra-granular) diffusion and decay as inter-related and mutually interactive [7]. The predicted R/Bs approach to their asymptotic values (this is more evident after 12 MWd/kgU) from the competition among production, diffusion, and radioactive decay (as expressed by Eq. 11). This prediction differs from the one given by the semi-empirical ANS 5.4-2010 methodology, based on the asymptotic solution of the diffusion-decay equation [5].

In particular, the ANS 5.4-2010 methodology is not designed to describe the time evolution of radioactive fission gas due to the physical phenomena of intra-granular diffusion, grain-boundary accumulation and release due to bubble interconnection. Rather, it aims to produce a conservative estimation of R/B as a function of local values of fuel temperature and linear heat rate [5]. As previously concluded, the application of SCIANTIX to the description of radioactive gas behaviour leads to predictions that include crucial physical aspects (production, diffusion, decay, interaction with intra- and inter-granular bubbles) that in the end impact the radioactive release. Conventional fuel performance codes (e.g., TRANSURANUS) may benefit from this aspect because of the possibility to apply the code in both stationary and transient conditions, without calibration processes.

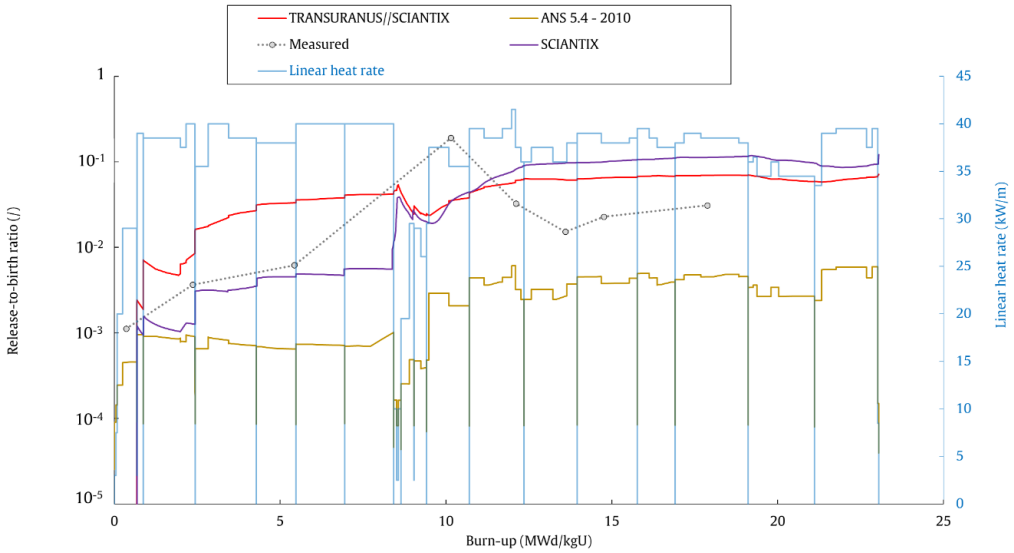

Fig. 7: Comparison of the ^{133}Xe measured release-to-birth ratio (grey dots) with the release-to-birth ratio predicted by the ANS 5.4-2010 methodology [5] (gold solid line), the stand-alone version of the SCIANTIX code [2], [7] (purple solid line) and TRANSURANUS//SCIANTIX (red solid line), as a function of the fuel rod burn-up, during the CONTACT 1 experiment [3], [4]. Also, the input linear heat rate is included on the secondary axis (blue line).

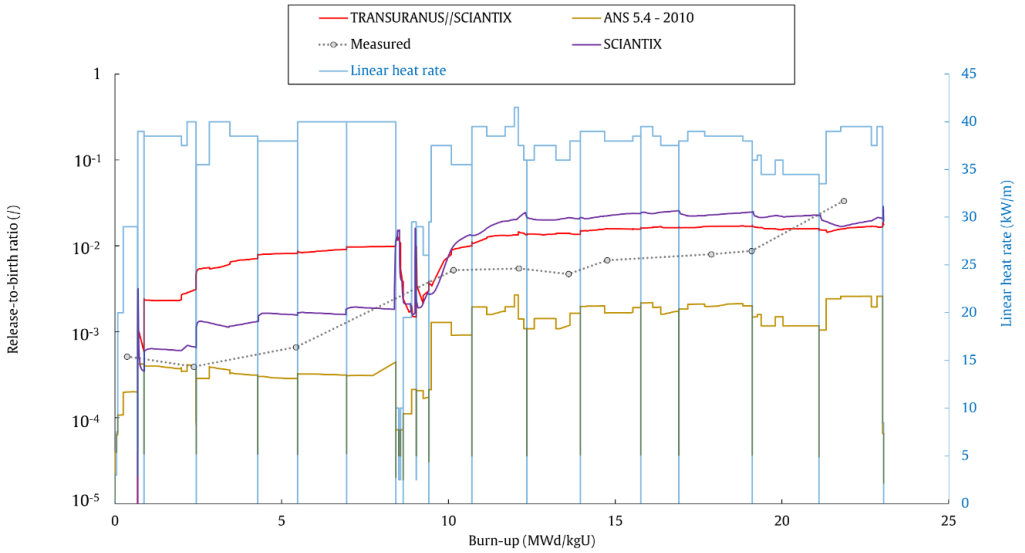

Fig. 8: Comparison of the ^{85m}Kr measured release-to-birth ratio (grey dots) with the release-to-birth ratio predicted by the ANS 5.4-2010 methodology [5] (gold solid line), the stand-alone version of the SCIANTIX code [2], [7] (purple solid line) and TRANSURANUS//SCIANTIX (red solid line), as a function of the fuel rod burn-up, during the CONTACT 1 experiment [3], [4]. Also, the input linear heat rate is included on the secondary axis (blue line).

The use of the SCIANTIX module within TRANSURANUS allows the calculation of the time-dependent release of short-lived fission gases, because of the model described in Section 2.2.
Fig. 9-Fig**. 16** show the predictions of the ^{133}Xe release rates measured during the last seven power transients. The comparative analysis reveals a good qualitative behaviour of the calculations.

A general summary of the release rate pattern observed in the analysed transients can be proposed as follows:

- During power increases, the ^{133}Xe accumulated at the grain-boundary is vented out from the fuel. This corresponds to the first increase in the release rate.
- During intermediate phases at constant power, the ^{133}Xe diffusion-decay process tends towards the equilibrium and the release rate approach a constant value.
- During power decreases, the associated stress variations lead to the gas venting from the fuel and a concomitant spike in the release rate.

Among the various sources of uncertainty, for example due to experimental accuracy needed to detect the short-lived ^{133}Xe [5], or due to our simplified grain-boundary modelling, the model for burst gas release due to micro-cracking is discussed. In fact, having a semi-empirical nature, its applicability to this specific power cycling experiment may alter the release rate kinetics. In Fig. 9Fig. **16**, the experimental data[2] are compared against the calculated release rates, with and without the effect of the burst release due to micro-cracking.

It is noted that the behaviour of the computed release rates is generally closer to the behaviour measured during the power increase and the successive constant power holding, rather than during the power decrease. Because the release rate evolution is qualitatively unaffected by the inclusion of the burst release due to micro-cracking (during the power increases and constant power holding), it is reasonable to assume that the release dynamics is controlled by the diffusional release model. On the contrary, during the power decrease, it is evident that the burst release due to micro-cracking produces an overestimation of the release rate (i.e., of one order of magnitude on the value of the release rate). Although in this case the diffusional contribution alone produces an overestimation of the data, it appears that forthcoming developments of the micro-cracking effects are possible and should consider the asymmetric representation of the release during power increases and decreases.

Another source of model-related uncertainty, which may impact the calculations, concerns the description of grain-face, grain-edge, and grain-corner porosity in SCIANTIX. As a qualitative assessment, it is possible that the high release rate measured during the first power increase may lead to a sudden emptying of the grain edge porosity, resulting in depressurization and collapse mechanism of the interconnected porosity. This mechanism would in turn cause a lower experimental release rate measured at the depressurization stage [17], [30]–[32]. Nevertheless, a complete description of the grain-boundary porosity is a complex task that calls for the use of empirical parameters and assumptions affected by uncertainty and a follow-up in this direction would require more supporting experimental data to rely on.

The presented results show that SCIANTIX, either used standalone or coupled with TRANSURANUS, reproduce the dynamics of the radioactive release, increasing during irradiation. This aspect constitutes a milestone in the modelling of radioactive gas without calibration of specific parameters, as in the ANS 5.4-2010 methodology [5], under both constant and transient conditions. In addition, ANS 5.4-2010 predictions are solely by the imposed linear heat rate. Nevertheless, the calculated release rates of the short-lived ^{133}Xe isotope require further attention, also considering the large uncertainties pertaining to ^{133}Xe measurements. They reveal only a partial agreement with the measurements, the error reaching even an error of an order of magnitude. From a preliminary analysis of the model for burst release due to grain-boundary micro-cracking, the need to revise this model emerges, especially during power reductions. However, a more detailed and more elaborate analysis is necessary to draw definite conclusions. Lastly, from the analysis of the results of the two complementary cases analysed (CONTACT 1 and HATAC C2), the potential of the coupled version of TRANSURANUS with SCIANTIX could be highlighted.

[2]In the IFPE documentation [9], it is indicated that the released fission gas was collected from the helium stream, dispatched to an analysis laboratory, and measured with a Ge-Li detector. The data sets for fission gas release fraction and release rates were then derived from a computer program. Therefore, the reported experimental measurements were not instantaneous but processed *a posteriori*, and thus may suffer from an additional contribution of uncertainty, which however was not quantified.

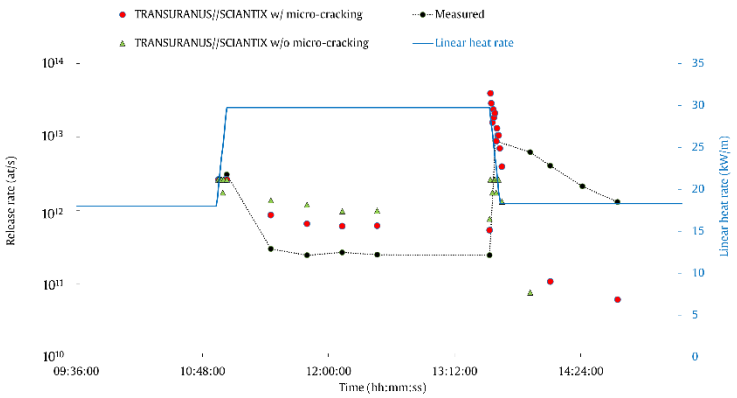

Fig. 9: ^{133}Xe release rate measured during the third power transient. The measurements (black dots) are compared against the TRANSURANUS//SCIANTIX calculation considering the burst release contribution from the micro-cracking (red dots) and neglecting it (green triangles).

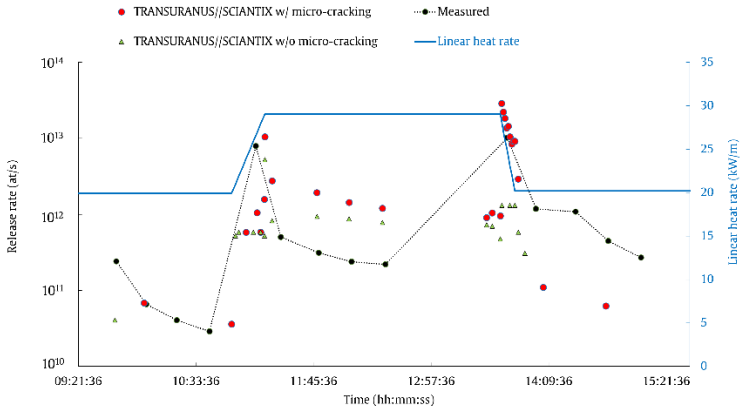

Fig. 10: ^{133}Xe release rate measured during the fourth power transient. The measurements (black dots) are compared against the TRANSURANUS//SCIANTIX calculation considering the burst release contribution from the micro-cracking (red dots) and neglecting it (green triangles).

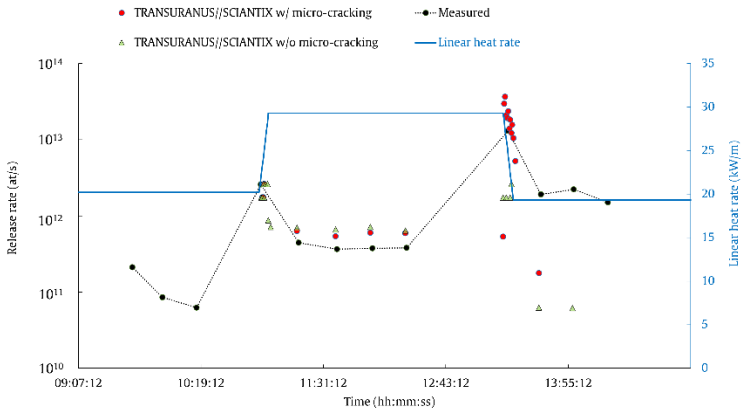

Fig. 11: ^{133}Xe release rate measured during the fifth power transient. The measurements (black dots) are compared against the TRANSURANUS//SCIANTIX calculation considering the burst release contribution from the micro-cracking (red dots) and neglecting it (green triangles).

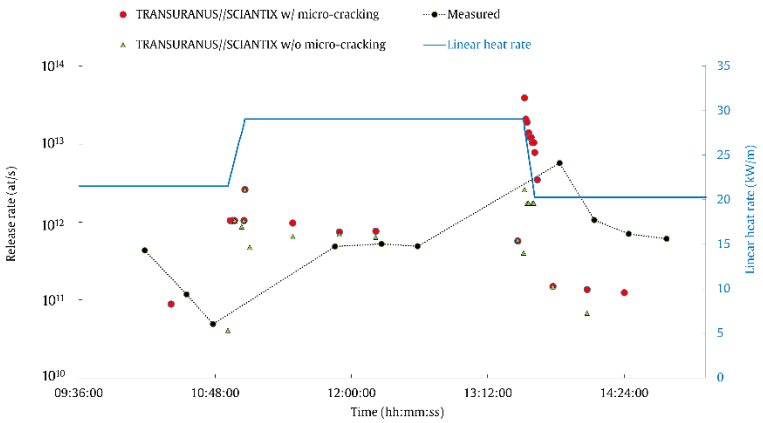

Fig. 12: ^{133}Xe release rate measured during the sixth power transient. The measurements (black dots) are compared against the TRANSURANUS//SCIANTIX calculation considering the burst release contribution from the micro-cracking (red dots) and neglecting it (green triangles).

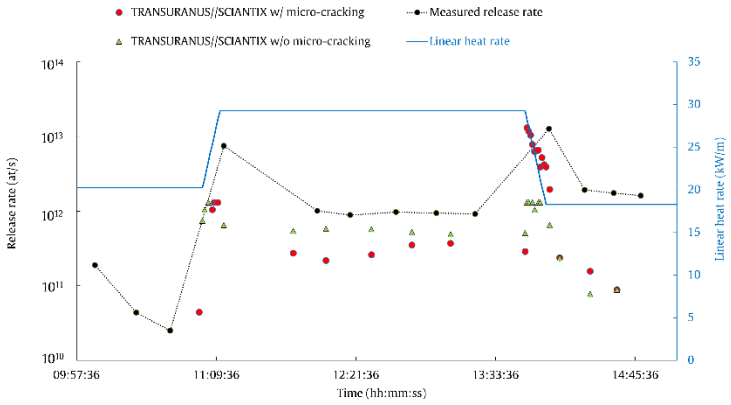

Fig. 13: ^{133}Xe release rate measured during the seventh power transient. The measurements (black dots) are compared against the TRANSURANUS//SCIANTIX calculation considering the burst release contribution from the micro-cracking (red dots) and neglecting it (green triangles).

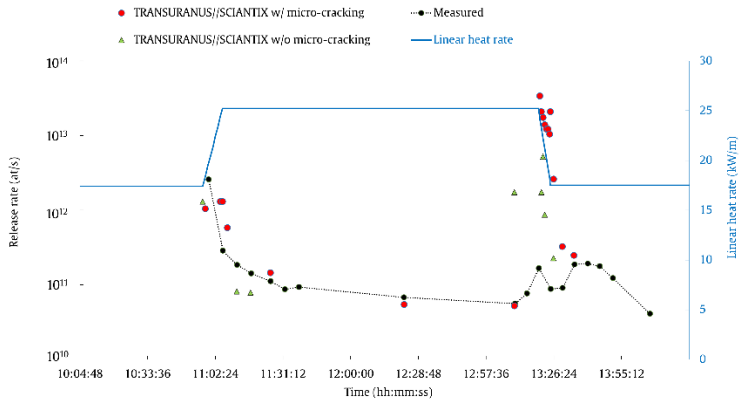

Fig. 14: ^{133}Xe release rate measured during the eighth power transient. The measurements (black dots) are compared against the TRANSURANUS//SCIANTIX calculation considering the burst release contribution from the micro-cracking (red dots) and neglecting it (green triangles).

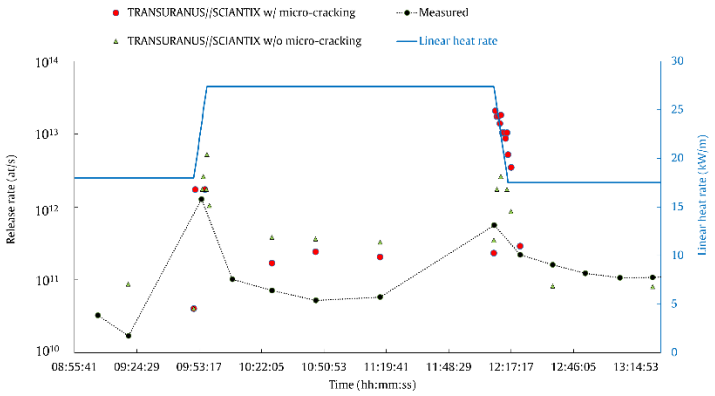

Fig. 15: ^{133}Xe release rate measured during the ninth power transient. The measurements (black dots) are compared against the TRANSURANUS//SCIANTIX calculation considering the burst release contribution from the micro-cracking (red dots) and neglecting it (green triangles).

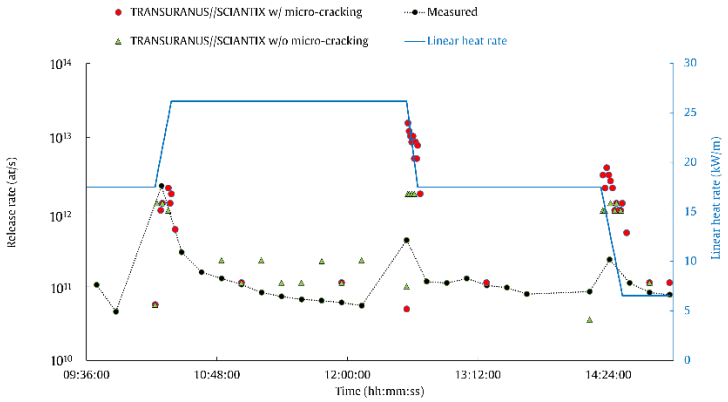

Fig. 16: ^{133}Xe release rate measured during the tenth power transient. The measurements (black dots) are compared against the TRANSURANUS//SCIANTIX calculation considering the burst release contribution from the micro-cracking (red dots) and neglecting it (green triangles).

2.3. Development of the TRANSURANUS code

Fission product transport mechanisms inside and outside the fuel differ according to species (e.g., due to different chemical affinity), and among isotopes of the same species (e.g., due to radioactive decay). When the release outside the cladding is considered in defective fuel rods, the decay rate of different isotopes plays a relevant role in evaluating the coolant activity [17], [18], [20]. For these reasons, thoroughly studying transport and concentration of different fission products in nuclear systems requires to evaluate each isotope separately.

At the current state of development, the TRANSURANUS code[3] considers many stable isotopes of Xe, Kr, Cs and Nd, and the following unstable isotopes: ^{133}Xe, ^{135}Xe, and ^{85}Kr. The code simulates the production of these isotopes through fission events, and by correcting the fission yields of the unstable isotopes with multiplication factors to account for the equilibrium concentrations. Then, the production of each species is calculated as the sum of the production of all the isotopes of such species, e.g., the sum of ^{133}Xe, ^{135}Xe and the stable isotopes of xenon give the final production of xenon. Doing this, the information referred to single isotopes is lost.

Besides, in TRANSURANUS, the release of gaseous and volatile radioactive (in particular, short-lived) fission products can be calculated by using the ANS 5.4-2010 methodology [5]. This semi-empirical approach yields the release-to-birth ratio of some isotopes of xenon, krypton, and iodine, and when coupled with corresponding fission gives the gap activity.
To endow TRANSURANUS with a more robust option to assess the production and release of gaseous and volatile radioactive FPs, NINE considered an alternative option, separating the contribution of each isotope of interest and extending the mechanistic modelling of stable fission gases to radioactive isotopes[4].

The list of isotopes considered is the following:

- ^{128}Xe, ^{129}Xe, ^{130}Xe, ^{131}Xe, ^{132}Xe, ^{133}Xe, ^{134}Xe, ^{135}Xe, ^{136}Xe, ^{137}Xe, ^{138}Xe
- ^{80}Kr, ^{82}Kr, ^{83}Kr, ^{84}Kr, ^{85}Xe, ^{86}Xe, ^{87}Xe, ^{88}Xe, ^{89}Xe
- ^{133}Cs, ^{135}Cs, ^{137}Cs, ^{138}Cs
- ^{131}I, ^{132}I, ^{133}I, ^{134}I, ^{135}I, ^{136}I, ^{137}I, ^{138}I

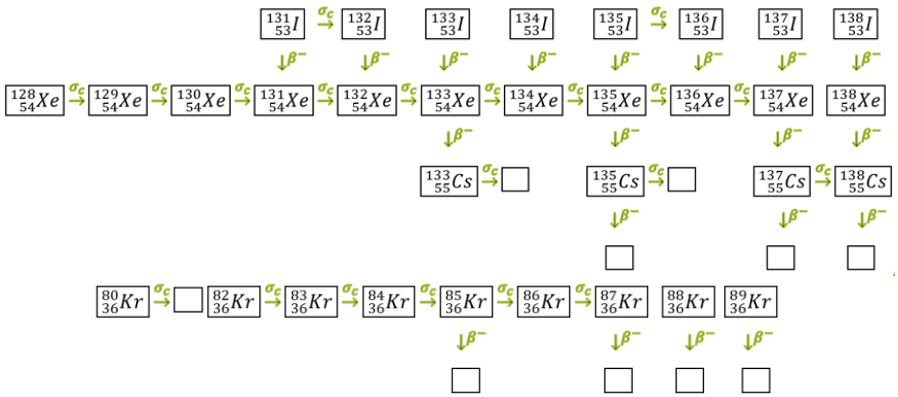

Fig. 17: Relationship among radioactive decay and capture events for the list of isotopes considered in the developments of the TRANSURANUS code.

[3] The reference TRANSURANUS version is the v1m6j21.
[4] In the current work, chemical interactions between non-inert FPs are neglected, and will be object of further developments involving thermo-chemical libraries.

To compute the FP inventory in the fuel the following equation has been considered for each isotope:

$$\frac{d\,{}^{A}_{Z}N(t)}{dt} = y_f \cdot q - \lambda_{{}^{A}_{Z}N} \cdot {}^{A}_{Z}N(t) - \sigma_{c\,{}^{A}_{Z}N} \cdot \Phi \cdot {}^{A}_{Z}N(t) \tag{15}$$

In Eq. (15), ${}^{A}_{Z}N$ is the concentration of the considered isotope, $\sigma_{c\,{}^{A}_{Z}N}$ is the neutron capture cross section evaluated at thermal energy, and Φ is the thermal neutron flux. Cumulative fission yields, decay constants and neutron capture cross sections are evaluated from the JEFF-3.3 library [17], [18], [20]. Numerically, Eq. (15) is discretized by applying backward Euler method.

The outlined approach has been implemented in TRANSURANUS and assessed through a comparison with the Serpent code [33]. The calculation of the release of radioactive isotopes is based on the mechanistic TRANSURANUS option to describe the stable (xenon and krypton) fission gas behaviour [17], [18], [20]. Namely, stable FGs are produced inside the UO_2 grains, they migrate towards the grain boundaries predominantly via thermal or irradiation-induced diffusion and accumulate in grain-boundaries bubbles. The intra-granular diffusion of stable fission gas in TRANSURANUS is governed by:

$$\frac{\partial C(r,t)}{\partial t} = D_{\text{eff}}(F,T)\nabla^2 C(r,t) + S(F) \tag{16}$$

The intra-granular effective diffusivity can be chosen among different options. Notwithstanding, none of them considers the possibility to diffuse in a hyper-stoichiometric fuel matrix, that may occur in presence of a cladding defect. Indeed, if the coolant enters the fuel-cladding gap, oxidation of both fuel and cladding occurs. It is known that in oxidizing conditions the release of the fission products increases due to changes in the intra-granular diffusivity [34]–[40], hence it is of interest to account for this process. In the work carried out by Killeen and Turnbull [40], there are reported a series of experiments in which the release of ^{85}Kr from hyper-stoichiometric uranium dioxide was measured under annealing conditions, in CO/CO_2 atmospheres [17], [18], [20] and an expression for the intra-granular diffusivity is given. Nevertheless, the equation is somewhat inconvenient for a fuel rod modelling code due to its complexity and the presence of many empirical constants and parameters, which may vary depending on the isotope and atmosphere considered. For this reason, Kim [39] provided a simplified practical expression for the intra-granular diffusivity of fission gas in UO_{2+x}. In Kim's formulation the intrinsic thermal contribution D_1 is corrected with a factor that accounts for the observed enhanced diffusivity under hyper-stoichiometric conditions, resulting in:

$$D_1 = 7.6 \cdot 10^{-10} e^{-\frac{35000}{T}} f(x) \tag{17}$$

$$f(x) = 1 + 493x + 32182x^2 \tag{18}$$

The variable x (/) indicates the deviation from stoichiometry. Eqs. (17) and (18) are considered valid in the hyper-stoichiometry range $0.005 \leq x \leq 0.12$ and in the temperature range $1000\ \text{K} \leq T \leq 1600\ \text{K}$. Afterwards the modification of the single-atom intra-granular diffusivity D_s, the effective diffusivity, according to [41], is:

$$D_{\text{eff}} = \frac{b}{b+g} D_s + \frac{g}{b+g} D_b \tag{19}$$

The effective diffusion coefficient D_{eff} is decomposed in two components: the first one considering only the fraction of FPs not trapped in intra-granular bubbles and the second one referring to the population of FPs trapped into bubbles and available to diffuse only through bubble mobility[5] D_b.
As previously stated, in this work the mechanistic description of stable fission gas diffusion, available in TRANSURANUS, has been extended to gaseous and volatile radioactive fission products. Eq. (16) can be solved by both URGAS and FORMAS algorithms [42]–[44] that are tailored for the diffusion equation without the decay loss, providing an approximation to the description of the diffusion of short-lived fission products.
In the current implementation, the stoichiometry deviation x equals the radially averaged oxygen-to-metal ratio in each section (or slice) of the discretized fuel rod. Further developments of this description will consider the development of a dedicated solver for Eq. (11) in TRANSURANUS as well, and the formulation of an oxygen redistribution model inside the fuel matrix (including local stoichiometry variations) and the analysis of the thermal effect on the hyper-stoichiometry conditions.

The TRANSURANUS version extended by NINE has been used to reproduce the CONTACT 1 irradiation experiment, from the IFPE open database [3], [4]. In Fig. 18 we show the calculated ^{133}Xe R/B. To detail a better comparative analysis, we include the calculations of TRANSURANUS using the ANS 5.4-2010 methodology, and TRANSURANUS//SCIANTIX, shown before in Fig. 7. When TRANSURANUS adopts the semi-empirical ANS 5.4-2010 methodology [5] to predict ^{133}Xe R/B (green line in Fig. 18), the calculation underestimates the data (black dots in Fig. 18), hence the gap activity as well. This underprediction has revealed to be systematic in the simulation of this case (see Section 2.2) [7], [11], and it can be attributed to the calibration behind the semi-empirical nature of the ANS 5.4-2010 methodology, that is trained on a different experimental database [5], [45]. In addition, the release dynamic is not well represented since the methodology essentially follows the input linear heat rate (Fig. 7). This constitutes a crucial limitation when considering fast transient scenarios and their dynamics (such as in the case of a fuel failure event) potentially resulting in the unreliability of the ANS 5.4-2010 methodology, that can be overcome with the help of TRANSURANUS//SCIANTIX (Fig. 7 and Fig. 8) or TRANSURANUS-NINE (Fig. 18).
Detailing the performance of the TRANSURANUS code extended by NINE, Eq. (16) is solved with the URGAS algorithm [46] (including Eq. (17) with $\mathrm{x} = 0$ in absence of cladding defect and oxidating environment). The resulting flux of atoms from the intra-granular region is then combined with the TRANSURANUS mechanistic inter-granular gas modelling [18], [41] and the inventory calculation (Eq. (15)) to estimate the release-to-birth ratio of short-lived FG isotopes. The predicted R/B curve in Fig. 18 (blue line) follows a behaviour qualitatively similar to the one detailed for the previous simulation case (Fig. 7, TRANSURANUS//SCIANTIX), namely increasing with the burnup, with differences due to the inherent FG/FP modelling (e.g., Eq. (11) and Eq. (16)).

[5] The intra-granular bubble mobility, appearing in the fission gas diffusion equation through the term D_b, has been investigated in several works [41], [67]–[71]. Its use was exploited to investigate the large fission gas release at high temperatures (above 1600°C) in annealing conditions and during transients, while it provides a negligible contribution to the fission gas release in normal PWR conditions [41].

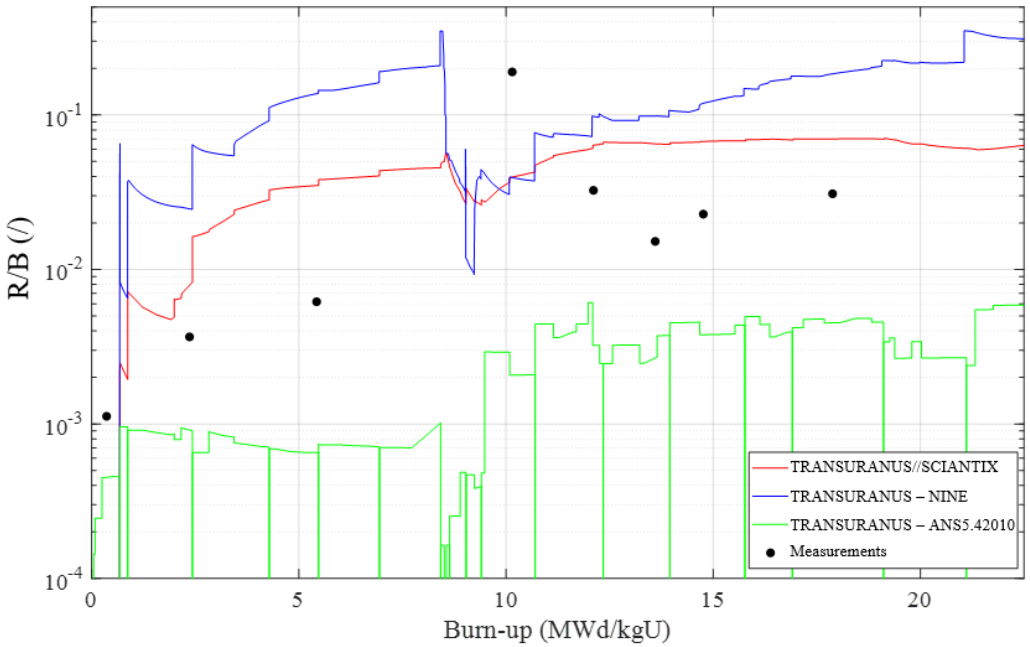

Fig. 18: Release-to-birth ratio of ^{133}Xe isotope, measured during the CONTACT 1 experiment (data reported as black dots) along with code calculation results. The green line represents the prediction from ANS 5.4-2010 methodology, the semi-empirical algorithm recently implemented in TRANSURANUS [5], [11]. The red line represents the calculation from the TRANSURANUS//SCIANTIX version [7], [11]. The blue line represents the calculation from the mechanistic TRANSURANUS fission gas behaviour model, extended to the radioactive isotopes, performed in this work.

2.4. Evaluating isotope inventory released to the gap

The decoupling approach implies to calculate the release of FP from fuel under specific conditions with a mechanistic tool, in that case the TRANSURANUS//MFPR-F code, and then, from the obtained release rates, to estimate parameters of the simplified isotope release modelling used in the decay-transmutation-transfer calculation tool. The MFPR-F modelling includes the chemical interactions of FP (other than noble gas) between them and with the UO_2 crystal, as well as fuel oxidation by the gap atmosphere. These two features are important in the context of a defective fuel rod, because they strongly affect the release of FP, such as Iodine and Caesium, and thus the amount of radioactive isotopes released to the gap.

Here, details about the calculation tools relevant for the decoupling approach will be presented, then preliminary results obtained on a demonstration case are presented. This case corresponds to a cladding failure occurring at the beginning of the 2nd irradiation cycle of a fuel rod, the subsequent release of radioactive isotopes being estimated using the decoupling approach.

2.4.1 Modelling of chemically active FP and of oxygen redistribution in MFPR-F

The modelling of chemically active FPs is illustrated on **Fig. 19**. Fission products created by fissions are incorporated into the fuel matrix under atomic or oxide form and diffuse toward grain boundaries treated as a segregation zone. The grain boundary is then considered as a multiphase system consisting of multicomponent phases:

- The **solid solution** of FP elements and oxygen in UO2 matrix
- The **metal phase**, modeling the white inclusions, are composed of Mo and Ru
- The **phase of complex ternary compounds**, modeling the grey phase precipitates in the fuel, includes molybdate, uranate and zirconate of Ba, Sr and Cs
- The separate **solid phase of CsI**

- The **gas phase** including noble gas and all gaseous compounds of FP elements

The role of the gas phase, which interacts with the solid solution and solid precipitates, is played by the grain face bubbles. A thermochemical equilibrium gives the speciation of FP which can be in solid solution, trapped in separate phases or under gaseous form. The FP fraction in solid solution obtained from this equilibrium determines the boundary condition for the grain diffusion mentioned above.

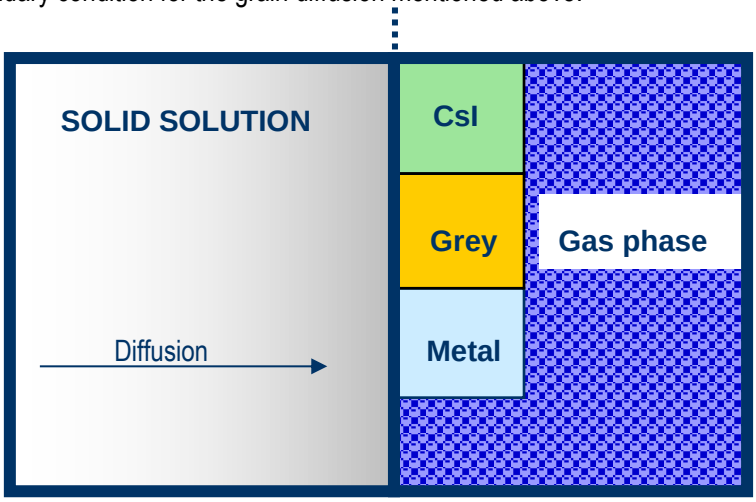

Fig. 19: Schematic FP behaviour in MFPR-F.

The oxygen liberated by uranium fission is considered, unlike FP, as homogeneous in the grain (diffusion is instantaneous), and also participates to the thermochemical equilibrium. The O content is thus between a "bonded" part (that is the part associated to U or to FP as simple oxides or trapped into separate phases) and a "free" part, see Fig 21. The O "free" fraction defines the fuel deviation stoichiometry x in UO_{2+x} and the fuel oxygen potential μ_{Ox} via the Lindemer-Besmann correlation [47].

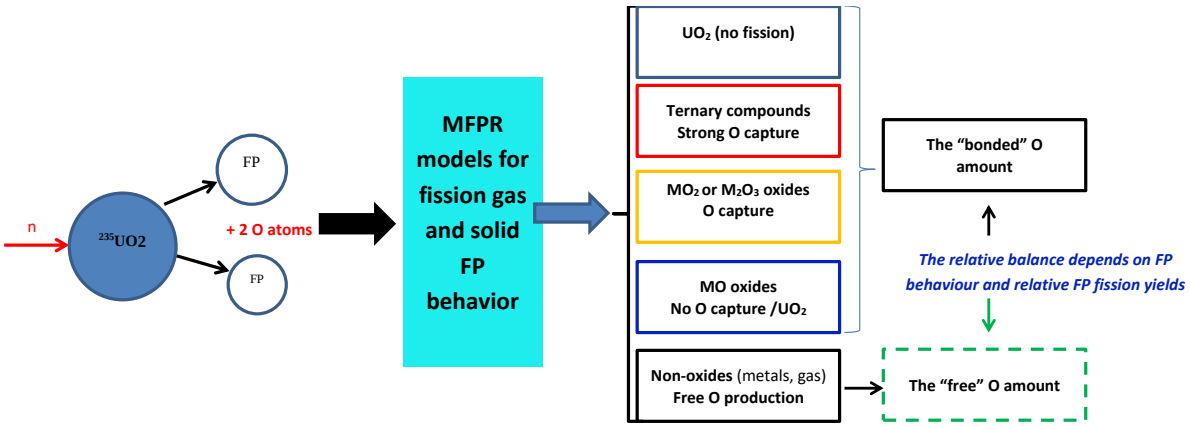

Fig. 20: Schematic oxygen production and partition resulting from fission process in MFPR-F.

On the global (pellet) scale where spatial variation of temperature is significant, the oxygen potential should be considered as a function of coordinate r and, according to the non-equilibrium thermodynamics [47], gradients of $\mu_{Ox}(x(r),T)$ and $T(r)$ are the driving force of the oxygen diffusion. The evolution of the oxygen concentration profile is described by the diffusion equation:

$$\frac{\partial}{\partial t}C_{Ox}^{(tot)} = \frac{1}{r}\frac{\partial}{\partial r}rD\left[\frac{\partial C_{Ox}^{(free)}}{\partial r} + C_{UO_2}\chi\frac{\partial T}{\partial r}\right] + V_{gr}^{-1}S_{Ox}(r,t) + V_{gr}^{-1}R_{Ox}(r,t) \qquad (20)$$

where $C_{Ox}^{(tot)}$ is the concentration of total (bonded+free) oxygen, $C_{Ox}^{(free)} = C_{UO_2}x$, C_{UO_2} is the Urania volume concentration, S_{Ox} is the source of oxygen liberated by uranium fissions, R_{Ox} is the oxygen release (through the release of FPs as oxides) and V_{gr} is the grain volume. D is the oxygen diffusion coefficient, assumed independent from the oxygen concentration, and χ is the so-called Soret coefficient, controlling the thermodiffusion. The boundary conditions for the above equation are defined as:

$$\frac{\partial}{\partial r} C_{Ox}^{(free)}(r,t)\Big|_{r=0} = 0, \tag{21}$$

$$\left[D\frac{\partial}{\partial r} C_{Ox}^{(free)}(r,t) + DC_{UO_2}\chi\frac{\partial T}{\partial r}\right]_{r=R_{pellet}} = J_{Ox}(x_s) \tag{22}$$

where R_{pellet} is the pellet radius, $J_{Ox}(x_s)$ is the external oxygen flux through the pellet surface, which is given as a function of the surface stoichiometric deviation x_s. This flux is determined by the partial pressures of oxygen, steam, and hydrogen at the vicinity of the pellet surface [35]. Note that it is equal to 0 in case of inert atmosphere around the fuel.

2.4.2 Modelling of release of radioactive isotopes

A tool calculating the decay, transmutation and transfer of radioactive isotopes between the fuel, gap and coolant regions has been developed in the framework of WP5 and it is used in the current approach to estimate the activity in the gap. This tool includes a simple modelling for release of isotopes from the fuel, briefly described here. Considering a decay chain of radioactive isotopes, the Bateman equations extended with release terms provide a balance equation for the number N_i of each isotope in the fuel:

$$\frac{dN_i}{dt} = B_i - \lambda_i N_i - R_i \tag{23}$$

where B_i, λ_i and R_i are the birth, decay and release rates, respectively. Effects of transmutation can be included in the birth and decay rates by considering cumulative coefficients. The R_i term encompasses two distinct release contributions, namely from fuel surface and fuel volume. The former is due to the recoil mechanism expressed as a release-to-birth ratio:

$$\left(\frac{R}{B}\right)_{rec} = \frac{d_{gap}}{R_{pellet}}\frac{\mu_f}{\mu_g} \tag{24}$$

where d_{gap} is the gap width, and μ_f and μ_g are ranges of fission fragment in the fuel and gap, respectively. The contribution from fuel volume is express as a diffusive process, following the Booth expression [25]:

$$\left(\frac{R}{B}\right)_{diff}^{i} = 3\sqrt{\frac{D_i}{\lambda_i R_{gr}^2}}\left(coth\sqrt{\frac{\lambda_i R_{gr}^2}{D_i}} - \sqrt{\frac{D_i}{\lambda_i R_{gr}^2}}\right) \tag{25}$$

where R_{gr} is the grain radius and D_i the diffusion coefficient of the considered isotope. Finally, by multiplying the R/B expressions by the birth rate, the release term is obtained:

$$R_i = B_i\left[\left(\frac{R}{B}\right)_{rec} + \left(\frac{R}{B}\right)_{diff}^{i}\right] \tag{26}$$

This modeling assumes that release from fuel volume is controlled by diffusion only, which is a strong simplification with respect to the complex mechanisms considered in MFPR-F. In the present context of decoupling approach, where the parameters of the isotope release model are fitted on results given by MFPR-F

calculations, some adaptations must be made for cases where the release is not controlled by diffusion. In such cases, a first-order kinetic model is used, as it will be illustrated in the following paragraph.

2.4.3 Demonstration of decoupling approach

To illustrate the decoupling approach on a concrete case, the irradiation history of the fuel rod used in the Halden IFA 650.10 case, represented on **Fig. 21**, is considered with a hypothetical event: a defect appearing in the cladding at beginning of the 2nd irradiation cycle (t = 6500h). The aim of the approach is to estimate, after the defect opening, the inventory of some isotopes of interest, namely of xenon and iodine.

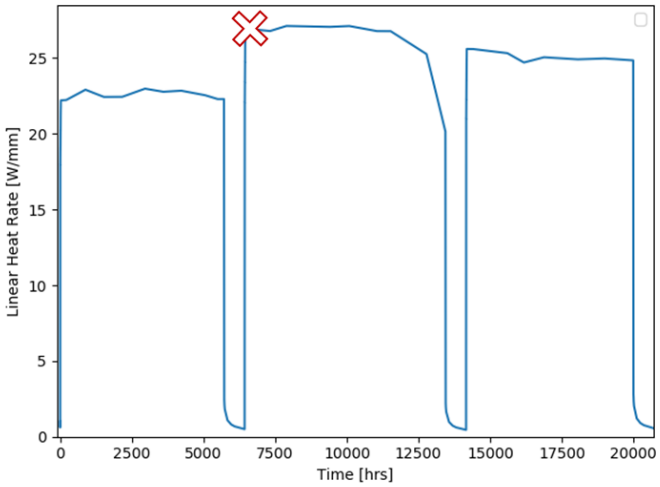

Fig. 21: Halden Ifa 650.10 case: irradiation of the fuel rod. The red cross represents the instant of cladding failure at t = 6500h.

The first step of the decoupling approach is to predict and analyse the release of xenon (referred to as fission gas (FG) in what follows) and iodine elements from the fuel using the coupled TRANSURANUS//MFPR-F code. To apply the oxidation model of MFPR-F, a composition of the gap atmosphere must be provided, which is not possible in the current state of TRANSURANUS. For the sake of simplifying the current study, the hypothesis is made that the atmosphere is composed of pure steam, which is not the case due to several phenomena, namely the transient stage after failure, when the coolant enters the gap, and the steam progressively replaces the filling gas, the subsequent cladding interior oxidation, and the radiolysis of steam. These two last phenomena induce the constant production of hydrogen in the gap.

The steam atmosphere in contact with the pellet rim leads to an oxidation of the pellet, as illustrated on Fig. 22. The O/M ratio, initially equal to 2 and homogeneous over the pellet radius (t = 7000h), progressively increases up to an average of 2.1 (t = 11000h) and exhibit important radial variations across the pellet radius. A peak is indeed observed at the pellet rim, followed (moving toward the pellet center) by a depression, and finally by a gentle increase up to the pellet centre. The external peak is due to the inflow of oxygen at the pellet rim, whereas the increase toward pellet centre can be attributed to the thermodiffusion: in case of hyperstoechiometric fuel, oxygen is indeed known to migrate toward hotter regions [48].

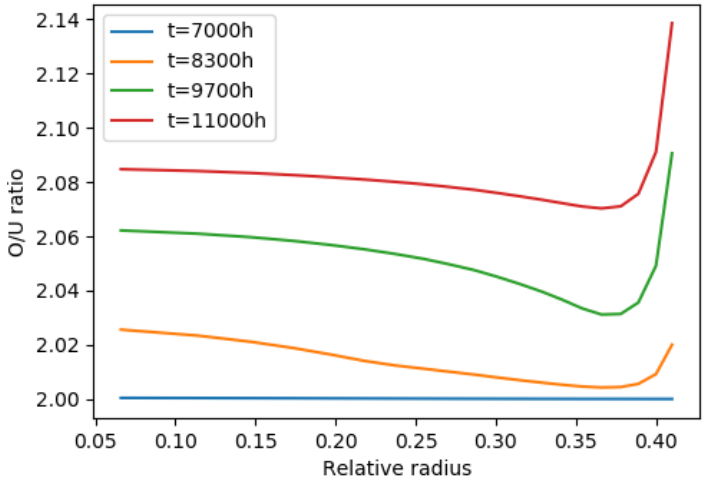

Fig. 22: Radial distribution of O/U ratio calculated by MPFR-F at several instants in the second irradiation cycle.

The fuel oxidation enhances FG diffusivity by a factor of about 500 (for O/U = 2.08) at the pellet centre. The effect of this higher diffusivity can be seen on Fig. 23. Initially, about half of FG is dissolved in the UO_2 bulk, the other half being in the intragranular bubbles. After t = 7500h, i.e., when the O/M ratio starts to increase, most of the dissolved gas gets trapped in the intragranular bubbles, whereas a small fraction gradually diffuses out of the grain. After a period corresponding to sufficient FG accumulation in grain boundary bubbles for them to interconnect, the flow of FG going out of the grain is directly released to open porosities. The released fraction reaches 8% at t = 12000h.

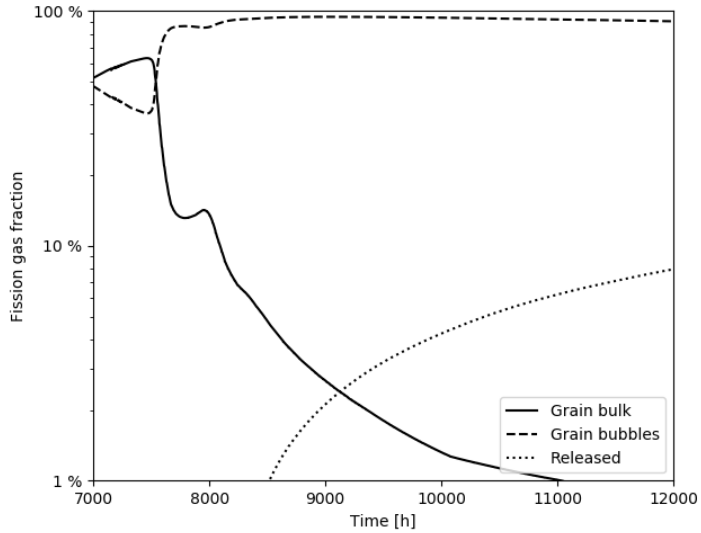

Fig. 23: Evolution of the fractions of FG inventories (in logarithmic scale) inside the grain as atom (plain), in intragranular bubbles (dash), and released (dot), at the pellet center, during the 2nd cycle of irradiation, at the pellet centre. Fraction of FG inventory located in intergranular bubbles remains under 1%, hence it is not represented on the figure.

The behaviour of iodine, represented on **Fig. 24**, appears to be very different from that of FG. At t = 7000h, more than 98% of iodine has already migrated outside the grain and formed CsI precipitates. Small amounts of iodine gaseous species (I and CsI) then appear in the intergranular bubbles, and begin to be released at t = 8500h, that is when the accumulation of gaseous species (mostly FG) led to interconnexion of intergranular bubbles. The role of fuel oxidation on the release of iodine is not straightforward, although a simulation of the same case, but without oxidation (not shown here), led to lower levels of released iodine. A direct effect of fuel oxidation could be the formation of ternary oxides (Cs_2MoO_4, Cs_2UO_4) consuming caesium atoms from the CsI phase and freeing

iodine atoms subsequently transferred to the gas phase. An indirect effect would be that the enhancement of FGR led to a stronger venting of the intergranular bubbles, thus allowing more evaporation from the CsI precipitates.

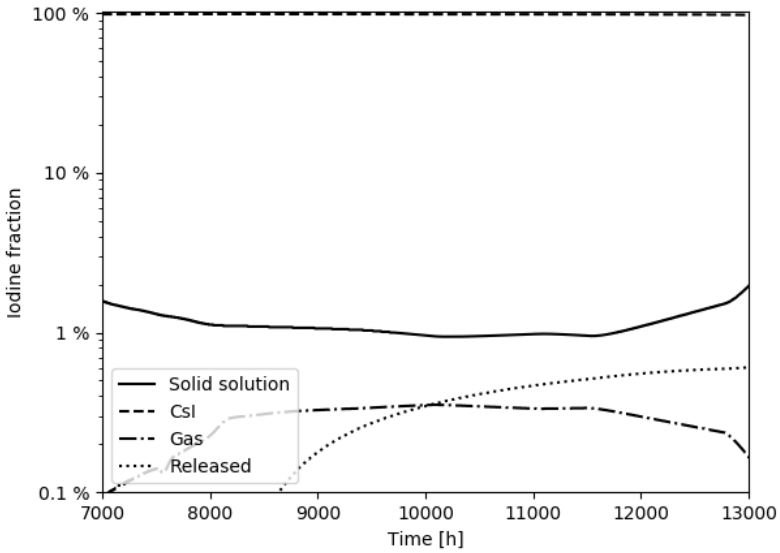

Fig. 24: Evolution of the fractions of iodine inventories (in logarithmic scale) dissolved in grain (plain), at grain boundary in CsI precipitates (dash) or gaseous phase (dash-dot), and released (dot), at the pellet center, during the 2nd cycle of irradiation.

The above analysis highlighted the essential difference of the release mechanisms between xenon and iodine, that is xenon release is controlled by diffusion inside the grain, whereas iodine release is controlled by both the thermochemical equilibrium between solid and gaseous phases and the venting of the gas phase (itself dependant on FG release) at grain boundary. This difference must be considered for evaluating the release of isotopes, as presented below.

The second step of the approach is to estimate the release of radioactive isotopes from the fuel, using the calculation tool described in Paragraph 2.4.2. Before that, fitting of parameters – and potentially adaptations – of the release formula (25) must be made, based on the results obtained with TRANSURANUS//MFPR-F. Note that this fitting concerns the release from fuel volume only, because the release from surface by recoil mechanism (24) is independent from the isotope. Regarding xenon, the above analysis showed that the Booth model can be applied. The formula (25) is plotted on **Fig. 25** (left) with parameters $R_{gr} = 4 \times 10^5 m$ and $D_i = 1.5 \times 10^{-20} m^2 s^{-1}$, which provide a good agreement with the TRANSURANUS//MFPR-F results. Unlike for xenon, the Booth model is unsuitable for the release process of iodine. A first-order kinetic model, in which release rate is proportional to the amount of the considered isotope ($R_i = \nu_i N_i$), is rather used. A coefficient $\nu_i = 4.8 \times 10^{-11} s^{-1}$provides a good agreement, as shown on **Fig. 25** (right).

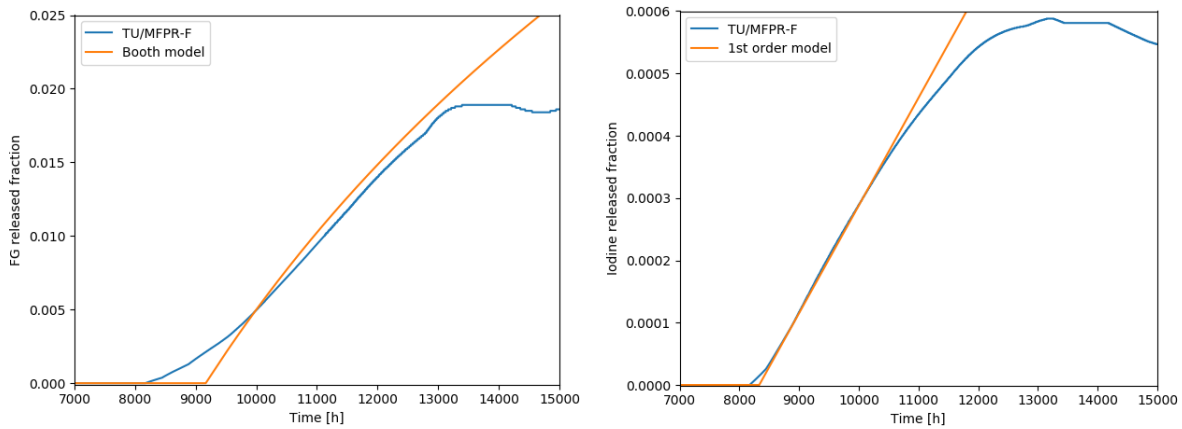

Fig. 25: Fraction of FG (left) and iodine (right) released as a function of time, as calculated by TRANSURANUS//MFPR-F (blue) and by a Booth or 1st order kinetic model (orange).

The calculation tool is then applied to a set of isotopes including iodine and fission gases (xenon and Krypton), for which the fitted release terms are applied. The release-to-birth ratios are represented for FG and iodine on Fig. 26, in logarithmic scale. The ratios calculated for FG follow a -1/2 slope, as expected for a Booth release model. By contrast, the iodine isotopes have a very low R/B ratio, which is consistent with the very low levels of iodine release calculated by TRANSUNANUS//MFPR-F. In such situation, the release from fuel surface by the recoil mechanism, which is at least of the order of $d_{gap}/R_{pellet} \sim 10^{-4}$ (for $d_{gap} = 1\mu m$), would be dominant for iodine isotopes.

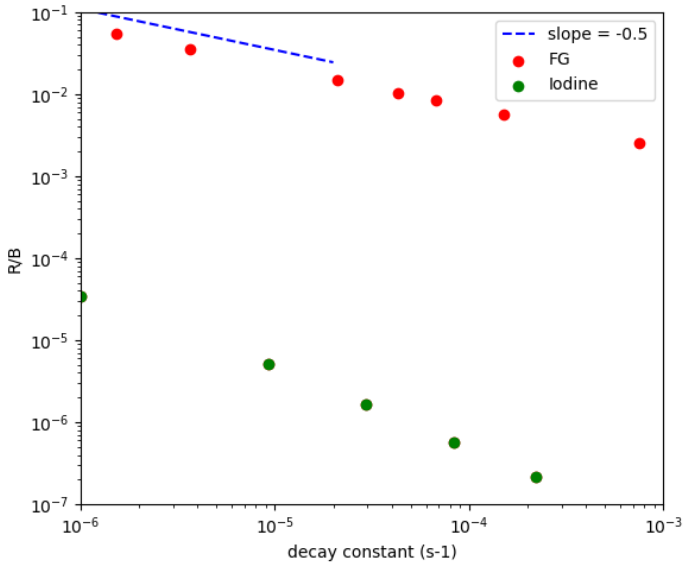

Fig. 26: Release-to-birth ratios of FG and iodine isotopes as a function of decay constant, as calculated for the fuel region by the calculation tool applied with fuel release terms fitted on TRANSURANUS//MFPR-F results.

To complete the present study, an evaluation of the gap inventory would have to be carried out with the calculation tool. Also, the study would have to be extended to other elements, such as caesium which is relevant for radiological consequences but also for its chemical interactions with iodine, or tellurium which is an important precursor of iodine. However, the aim of this study is for now to demonstrate the relevance of the decoupling approach for evaluating release of isotopes from fuel, and further estimate the activity in the gap of a defective fuel rod, which constitutes the reservoir of the rod source term in case of an SGTR transient.

The presented methodology combines mechanistic models for the release of elements, and a more empirical modelling for the decay/transfer of radioactive isotopes. The decoupling approach could nevertheless

accommodate more physical modelling for the second step. The next milestones for this approach to be fully effective are:

- developing a model for the composition of the gap atmosphere in a defective fuel rod,
- validate the predictions of the approach on experimental data.

Regarding the first point, a model is currently in preparation in the TRANSURANUS code. For the validation, data from the CRUSIFON experiment from the IFPE (International Fuel Performance Experiments) database is planned to be used.

3. Modelling release from gap to coolant

The progress in modelling the FP release from the fuel-cladding gap to the coolant are delineated in the next subsections.

The previous fuel-to-gap model developed by NINE is complemented with a gap-to-coolant model for the FP release. Indeed, the previous process of intra-granular diffusion and release from the fuel acts as a source for the concentration of FP/FG in the fuel-cladding gap, then the release from the defective fuel rods is modelled with a phenomenological first order kinetic model. The model is developed based on the open literature models for release from defective rods, and it has been implemented in the TRANSURANUS version extended by NINE.

EK upgraded the RING code against new 18 nuclear power plants data (during power transients, reactor shutdown and start-up). The developments aimed at overcoming the limitations of previous version of the code, and a new caesium spiking models (^{134}Cs and ^{137}Cs) has been introduced. The upgraded RING code has been applied to the simulation of iodine and caesium spiking effect in SGTR, and collector cover opening conditions. In addition, it allows better evaluating the activity release according to the specific power and pressure histories of the two events.

CIEMAT checked the applicability of fission product release models currently existing in MELCOR 2.2 (CORSOR and CORSOR-Booth models). The bases of the models were reviewed. Despite the potential of these models to be used, the conditions underlying their bases are notably out the range of those concerning iodine spiking during SGTR DBA and DEC-A sequences. Therefore, an external MELCOR function has been built to model iodine spiking in SGTR DBA and DEC-A sequences.

BOKU has initiated a PhD position focused on modelling iodine spiking. A review of current literature was conducted. The simulations are done with RELAP5-3D. A preliminary evaluation revealed that the FP behaviour model incorporated in RELAP5-3D is not including any physical retention effect on iodine (e.g., pool scrubbing) and is not suitable for simulating the iodine spike phenomenon without any post-processing. Therefore, an external function was introduced to improve the FP behaviour (see D4.1.1).

SSTC NRS reviewed the open literature about the investigation of fission product release from fuel rods under primary to secondary leaks. Main attention was paid on investigation approaches for iodine spike-effect modelling. As an option, SSTC NRS is considering collecting data for iodine spike-effect issues for Ukrainian NPPs.

3.1. Development of the TRANSURANUS code

Here it is described the development that has been included in the TRANSURANUS version extended by NINE, towards the prediction of radioactive release from defective fuel rods, and, ultimately, the estimation of the phenomenological escape rate coefficients. The selected gap-to-coolant model, when there are defective fuel rods and which was also suitable for straightforward implementation in TRANSURANUS, considers the generalized Lewis model [49], echoed in the recent work of Veshchunov [50]. The model follows a phenomenological first-order kinetic approach and the gap-to-coolant transport of gaseous and volatile FPs through the cladding defect is described with:

$$\frac{dn_i}{dt} = q_i - R_i - \lambda_i n_i \tag{27}$$

where the mean concentration of the i-th isotope in the fuel rod free volume (i.e., including the volumes of fuel-cladding gap and fuel rod plenum) is n_i $\left(\frac{at}{m^3}\right)$, the release rate of the i-th isotope from the fuel (per unit volume of the fuel rod free volume) is q_i $\left(\frac{at}{m^3 s}\right)$ and the release rate from the gap into the coolant is R_i $\left(\frac{at}{m^3 s}\right)$. R_i is assumed to be proportional to n_i through a phenomenological escape rate coefficient ε $\left(\frac{1}{s}\right)$:

$$R_i = \varepsilon n_i \tag{28}$$

If an equilibrium between the fuel-to-gap release and the gap-to-coolant release is reached, the following relation can be used to estimate the escape rate ε:

$$q_i = R_i = \varepsilon n_i \text{ with } \varepsilon = \frac{q_i}{n_i} \tag{29}$$

In the present discussion, axial transport phenomena are neglected, and the focus is on PWR conditions, for which a weak dependence of ε on the defect size can be assumed [50]. Evaluating phenomenological escape rate coefficients (defined in the first-order kinetic model for FG gap-to-coolant release by Eq. (28)) is crucial to estimate the primary coolant activity in the event of fuel failure [50]. Escape rate coefficients can be estimated using Eq. (29) and used to calculate the radioactive release from defective fuel rods.

There is a small number of experimental data available in open literature about the coolant activity due to radioactive gaseous and volatile FPs released from a defective fuel rod. The IFPE open database includes data from the CRUSIFON program [51], [52], that are irradiation experiments in which a cladding failure was mechanically imposed.

Fig. 27 shows the results of the application of the TRANSURANUS version extended by NINE to calculate the escape rate ε for ^{133}Xe with Eq. (29). Up to 4×10^5 s, calculated escape rates are distributed between values from about 10^{-6} to 10^{-4} s^{-1}. In this first half of the plot, the agreement with escape rates for noble gas evaluated in past works is considered as satisfactory, these being indeed distributed in the same interval [49], [50]. From 6×10^5 s on, calculated escape rates increase of about one order of magnitude. It must be noted that during each power ramp (decreasing and/or increasing), and also after these power ramps, the equilibrium assumption made to derive the escape rate with Eq. (29) may not hold, hence producing variations in the calculated escape rates.

Also, developments that have been implemented in the TRANSURANUS version extended by NINE, currently neglect axial transport phenomena and release mechanisms that involves the accurate prediction of local temperature and partial pressures of non-condensable gases. The gap pressure evolution in defective fuel rods is a complex phenomenon that requires an accurate description of the thermal-hydraulic dynamics coupled to the fuel performance analysis. This is an interesting area for future improvements of fast-running FPCs (as TRANSURANUS) when evaluating the radiological consequences of accidental scenarios, e.g., in fuel rod failure events.

In addition to moving towards a complete phenomenological first-order kinetic model, as in Refs. [49], [50], it would be also interesting to enrich the methodology described here by the coupling between TRANSURANUS, that can calculate the fission gas production and release from the fuel, the temperature distribution and the

oxidation in the fuel and cladding, with a thermal-hydraulic code as RELAP5-3D, able to properly simulate the water evaporation and steam condensation inside the gap, the partial pressures evolution and the non-condensable gas release from the gap into the coolant.

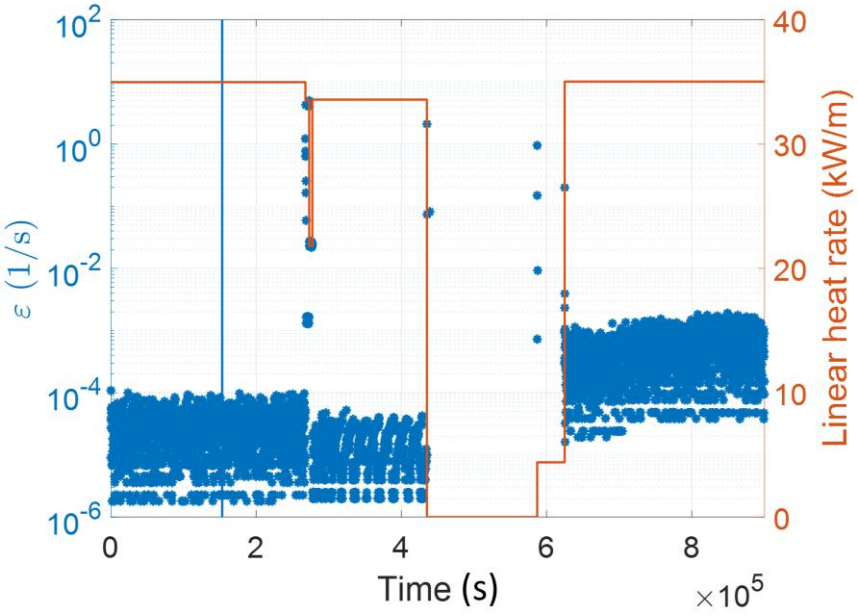

Fig. 27: The red line of the figure represents the input linear heat rate for the CRUSIFON1bis simulation in TRANSURANUS. The initial time coincides with the instant when the cladding defect has been forcibly opened, according to the IFPE documentation [51], [52]. The blue points represent the phenomenological escape rate, for the short-lived ^{133}Xe, calculated by TRANSURANUS extended by NINE according to Eq. (29).

3.2. Development of the RING code

The thermal hydraulic safety analyses of steam generator tube rupture (SGTR) accidents in NPPs indicated that fuel failure during the accident cannot be expected, since the fuel cladding temperatures in the reactor core will not reach high values. However, if defective fuel rods are in the core, the iodine spiking phenomenon would result in significant increase of coolant activity. The transient conditions could initiate some outflow from the defective fuel rod and some part of the activity stored in the free volume of the fuel rod could be released into the coolant. Among the potential consequences of SGTR accidents these effects must be taken into account.

EK developed the Release of iodine and Noble Gases (RING) code for the analyses of coolant activity concentrations in VVER-440 NPPs. The RING code is able to estimate the number of defective fuel rods and the amount of tramp uranium on the surface of the reactor core. The transient module of the code can predict the peak activity concentration during transients. This transient module includes a correlation which considers the changes in primary pressures, reactor power and boric acid concentration. The original version of the code was capable to predict only ^{131}I activity peaks, but as a result of recent development [53], two caesium isotopes (^{134}Cs and ^{137}Cs) are also calculated.

The RING code can also be used for the simulation of activity release during SGTR events. At the beginning of the calculations the steady state activity concentration of ^{131}I, ^{134}Cs and ^{137}Cs isotopes in the primary coolant must be given. As boundary conditions, the time dependent variation of primary pressure, core thermal power and coolant boric acid concentration must be given. These parameters can be taken from thermal hydraulic calculations.

Two critical scenarios were selected for the analyses of VVER-440 NPPs in the framework of R2CA project:

- Break of three steam generator tube and
- Opening of collector cover.

The results of these calculations are summarized in the present section.

The iodine spiking model of the RING code has been updated against new 18 NPP measured datasets (during power transients, reactor shutdown and start-up). In detail:

- The effect of the power change was underestimated by the previous version of the code, in predicting the coolant activity due to iodine spiking.
- New caesium spiking models (^{134}Cs and ^{137}Cs) have been introduced.

The upgraded RING code has been applied to the simulation of iodine and caesium spiking effect in SGTR, and collector cover opening conditions. In addition, it will allow to precise the activity release according to the specific power and pressure histories of the two events.

During a SGTR event the reactor parameters change and the associated release of activity through iodine spiking from defective fuel rods is expected. It is important to estimate the activity released from defective fuel rods and the computer codes applied should be validated against nuclear power plants (NPPs) measurement of released iodine during transient, from defective fuel rods.

The RING computer code [54], [55] has been developed for the simulation of leaking fuel rods under steady state and transient conditions for a VVER-440. This code proved to be capable to predict the number of leaking fuel rods and the amount of tramp uranium during single cycles and several years of operation, based on the measured primary coolant activity (due to iodine, xenon and krypton).

In the transient model of the RING code, the release accelerates as a function of the variation in core power (Q), primary pressure (P) and boric acid concentration (c_{bor}). The correction factor S describing the acceleration of activity release form the leaking fuel rod is approximated by the following equation:

$$S^n = 1 + a_1 \frac{\Delta \mathrm{Q}^{\mathrm{n}}_{\mathrm{core}}}{Q^{\mathrm{nom}}_{\mathrm{core}}} + a_2 \frac{\Delta P^{\mathrm{n}}}{P^{\mathrm{nom}}} + a_3 \frac{\Delta c^{\mathrm{n}}_{\mathrm{bor}}}{c^{\mathrm{nom}}_{\mathrm{bor}}} \quad (30)$$

The data for Q, P and c_{bor} in nominal (nom) reactor conditions are required as a function of time. The initial activity concentration is set from steady state data (i.e., nominal power assumed before transient).

The spiking model in first version of the RING code was fitted to reactor shutdown data. Seven sets of data were available that time. During the last decade several transients with iodine peaks were recorded and it allowed the improvement of the spiking model. Nowadays, twenty-four sets of data are available, eight of them are power change transients, twelve of them are shutdown transients and the other four are start-up transients.
The original RING code has been used to estimate the iodine activity released in the coolant. Afterwards, the correction factor S^n (Eq. 34) has been upgraded by introducing a new a_1, providing better estimates of the maximum ^{131}I activity concentration in several cases.

During the fitting of new coefficients for the iodine spiking model, the following feedback was received:

- Running calculations on the new data set with the old coefficients: the model gives a good estimation for the time and magnitude of ^{131}I activity peak by the shutdown transients but underestimates the magnitude of ^{131}I activity peak by the power change transients (Fig. 28).
- Increasing the coefficient of the power-term until the magnitude of the calculated activity peak close to the measured magnitude by the power change transients (Fig. 29). Running calculations on the shutdown transients with the new power-term coefficient: the model still gives good estimation for the magnitude of ^{131}I activity peak.

By comparing the measured ^{131}I, ^{134}Cs and ^{137}Cs activity concentrations it is visible that the concentration increase between the steady-state and the peak values are similar in the case of the caesium isotopes than in the case of iodine. For this reason, the introduced ^{134}Cs and ^{137}Cs spiking models were similar to ^{131}I model described by Eq. 34. The calculations are illustrated in Fig. 30.

Detailed description of RING spiking model development is available in the technical report:
Berta Bürger (EK), Zoltán Hózer (EK): Improvement of the iodine and caesium spiking models in the RING code, EK-2021-437-1-4-M0

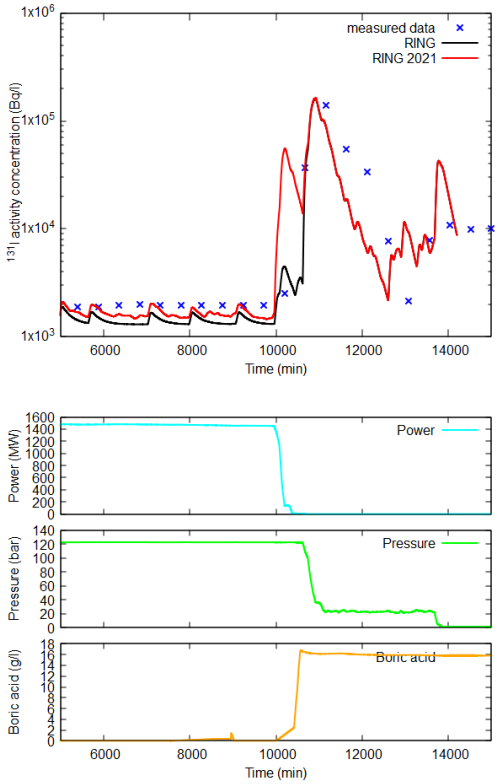

Fig. 28: Measured and calculated ^{131}I primary coolant activity concentrations (above), the technological parameters as a function of time (below) on reactor shut-down dataset

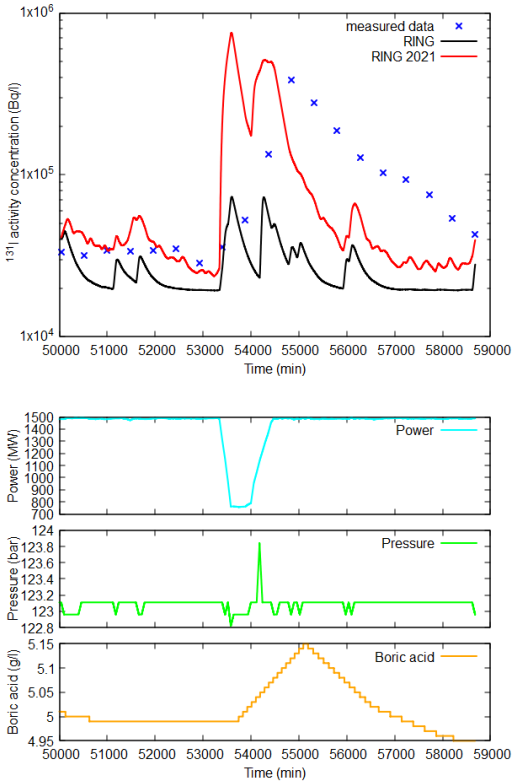

Fig. 29: Measured and calculated ^{131}I primary coolant activity concentrations (above), the technological parameters as a function of time (below) on power change dataset

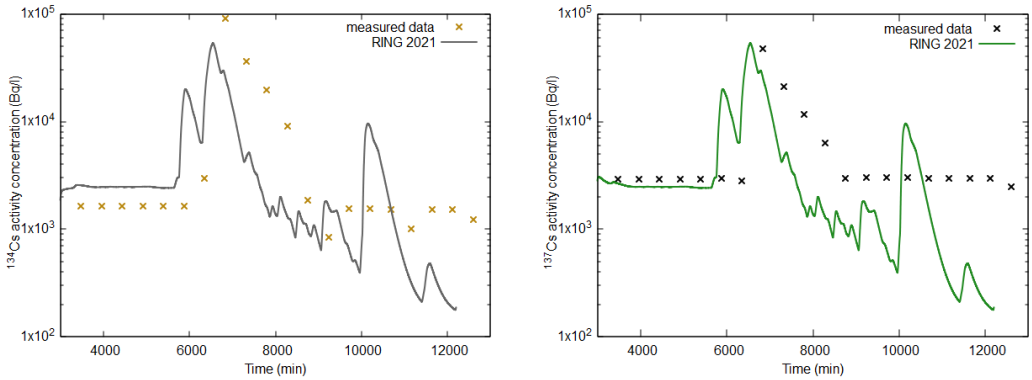

Fig. 30: Measured and calculated ^{134}Cs (left) and ^{137}Cs (right) primary coolant activity concentrations on power change dataset

3.2.1 Simulation of SGTR event with the break of 3 tubes

Initial and boundary conditions

The nuclear power plants have operational limits for some of radioactive isotopes in the coolant. In the Hungarian regulation there are limits for some activated corrosion products and five iodine isotopes.

The limit for ^{131}I is $4.6 \cdot 10^6$ Bq/dm^3. There is no direct limit for the caesium isotopes, however, those values could be calculated using models for defective fuel rods and considering sources from tramp uranium.

The activity concentration limits do not depend on primary coolant purification flow rates. For this reason, in the safety analyses both minimal and maximal purification flowrates are taken into account and two sets of data are evaluated. In case of high flowrate, the corresponding number of defective fuel rods is high, and the related data can be used to support activity release calculations. The calculated data for low flowrate case can be used for the evaluation of radiation (dosimetry) conditions in the vicinity of primary circuit. The initial values of activity concentrations for the RING calculations are listed in Table 4.

Table 4: Primary coolant activity concentrations in normal operation.

Isotope	Core inventory (Bq)	Activity concentrations in the primary coolant with minimal purification flowrate (Bq/dm^3)	Activity concentrations in the primary coolant with maximal purification flowrate (Bq/dm^3)
^{131}I	$1.85 \cdot 10^{18}$	$4.59 \cdot 10^6$	$4.58 \cdot 10^6$
^{134}Cs	$3.81 \cdot 10^{17}$	$9.35 \cdot 10^6$	$8.75 \cdot 10^6$
^{137}Cs	$2.47 \cdot 10^{17}$	$6.06 \cdot 10^6$	$5.67 \cdot 10^6$

In the present calculations both low and high flowrate cases were considered. As we will see, the maximum activity concentrations during SGTR accidents would correspond to the high flowrate case, when the number of leaking fuel rods was much higher.

The pressure history was determined by RELAP5 calculation. The reactor power history corresponds to the actuation of reactors scram. The boric acid concentration was calculated considering the emergency core coolant system (ECCS) flows and break flow. The reactor power drops quickly to decay heat value in the beginning of the scenario. The primary pressure decreases significantly after 30 s and stabilizes at around 30 bars. The boric acid concentration is monotonously increasing with the ECCS injection.

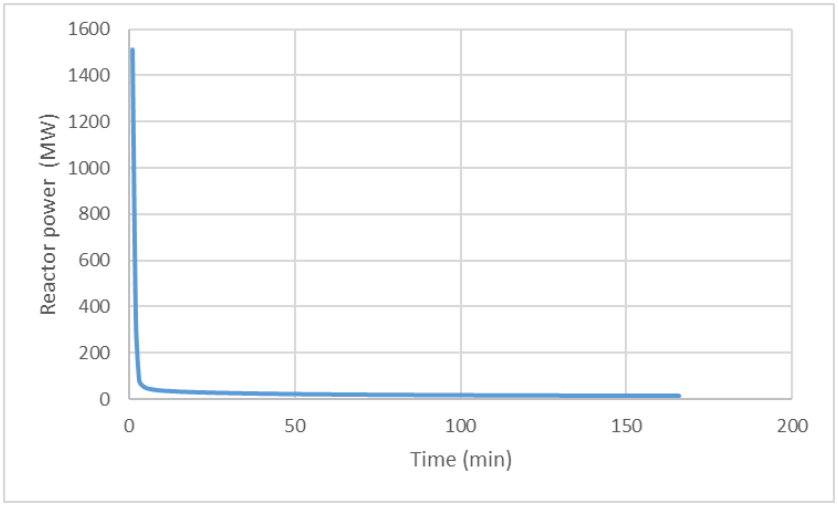

Fig. 31: Reactor power during the break of 3 steam generator tube event.

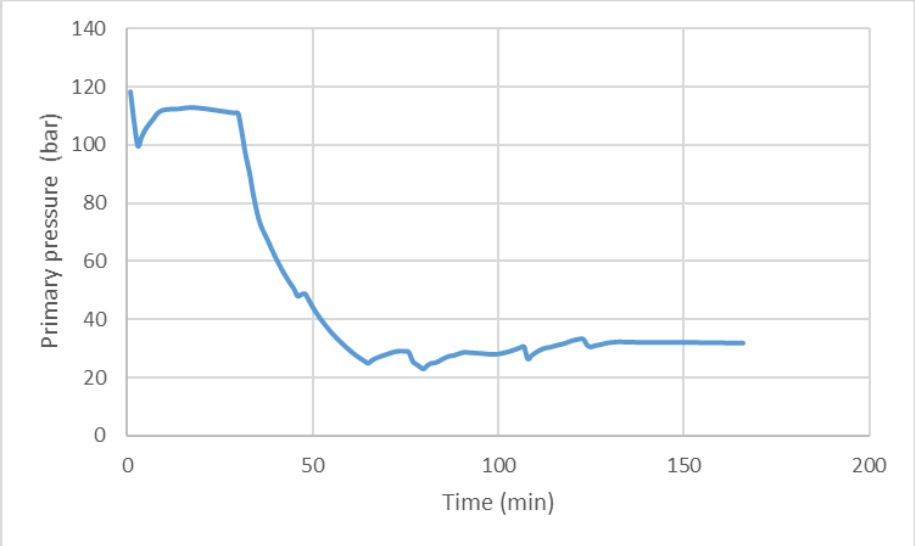

Fig. 32: Primary pressure during the break of 3 steam generator tube event.

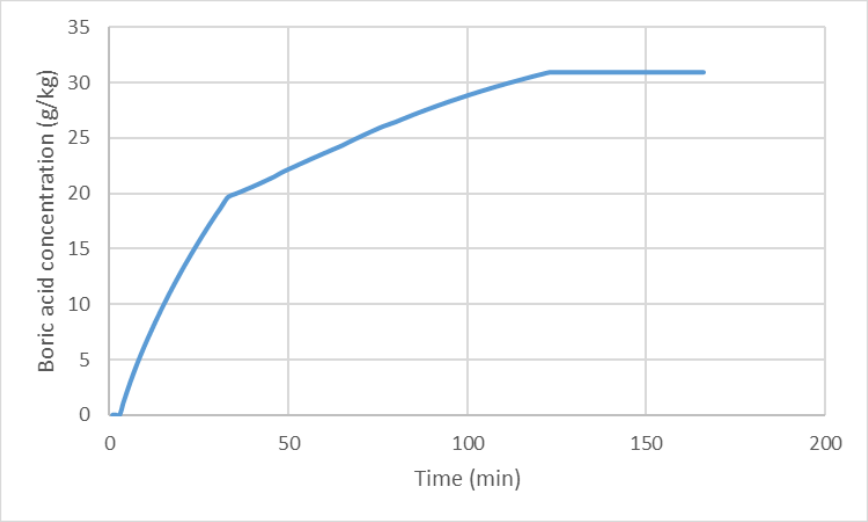

Fig. 33: Boric acid concentration of the primary coolant during the break of 3 steam generator tube event.

Coolant activity concentrations

The calculated activity concentration histories represent the conditions in an intact primary circuit, since the RING code cannot handle break and ECCS flows. The histories for ^{131}I, ^{134}Cs and ^{137}Cs calculated by the RING code are presented in Fig. 34 and Fig. 35. The strongest releases can be seen between 30-70 minutes, when the primary pressure drops from 115 bars to 31 bars.

The maximum activity concentrations were reached for the cases with high steady state purification rate and the corresponding values were $2 \cdot 10^9$ Bq/dm^3 (^{131}I), $4.1 \cdot 10^8$ Bq/dm^3 (^{134}Cs) and $4.1 \cdot 10^8$ Bq/dm^3 (^{137}Cs).

In order to determine the activity concentrations corresponding to the 3-tube break SGTR scenario, additional calculations were performed. Using the data from the RING calculations and taking into account the break and ECCS flows, the activity concentrations for the three isotopes were determined for each time step. The results are presented in Fig. 37. The following maximum activity concentrations were reached $1.36 \cdot 10^9$ Bq/dm^3 (^{131}I), $2.7 \cdot 10^8$ Bq/dm^3 (^{134}Cs) and $2.7 \cdot 10^8$ Bq/dm^3 (^{137}Cs).

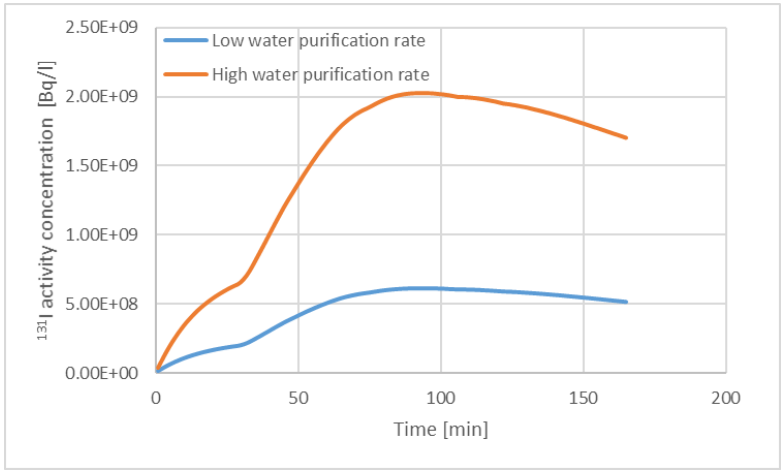

Fig. 34: Calculated ^{131}I activity concentration of the primary coolant during the break of 3 steam generator tube event.

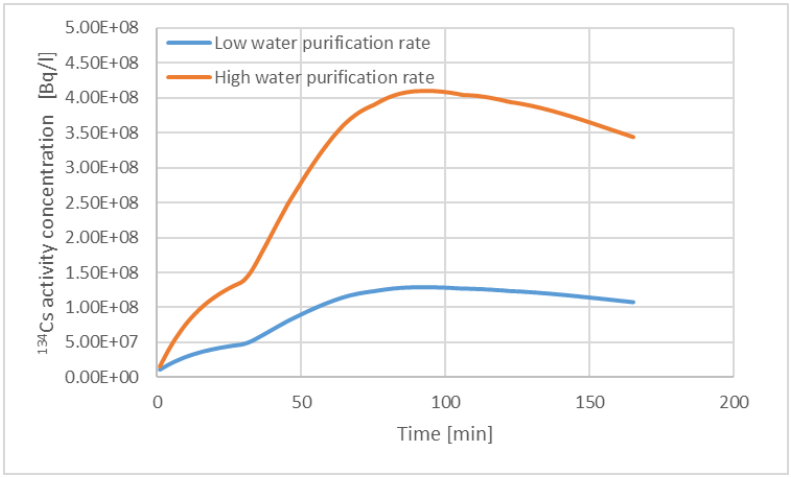

Fig. 35: Calculated ^{134}Cs activity concentration of the primary coolant during the break of 3 steam generator tube event.

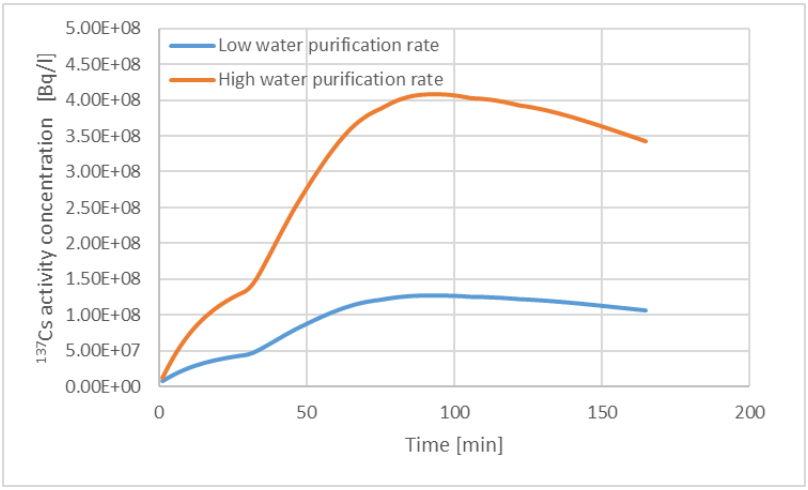

Fig. 36: Calculated ^{137}Cs activity concentration of the primary coolant during the break of 3 steam generator tube event.

The results clearly showed that the maximum concentrations corresponded to the high water purification rate cases for all three isotopes. For this reason, in the further analyses only the data from high water purification rate cases were evaluated.

The results of RING calculation showed the activity concentration history for a reactor system without break. In the RING model only intact primary circuit is handled, and the activity concentration decrease takes place mainly due to the operation of water purification system.

In order to estimate the activity concentration during SGTR event additional calculations were performed using the data from the RING iodine spiking simulation with the following steps.

- calculation of the primary coolant mass using break and ECCS flowrates,
- calculation of primary coolant activity concentrations starting from the RING data and adding the effect of break flow.

In these calculations the decay of radioactive isotopes was not taken into account, since the three selected isotopes have long half-life compared to the simulated time (3 hours). The maximum coolant activity concentrations were lower by about 30% in the broken circuit compared to the RING calculation. The stabilisation of the concentrations at 120 min time correspond to the isolation of the affected steam generator, when the break flow stopped.

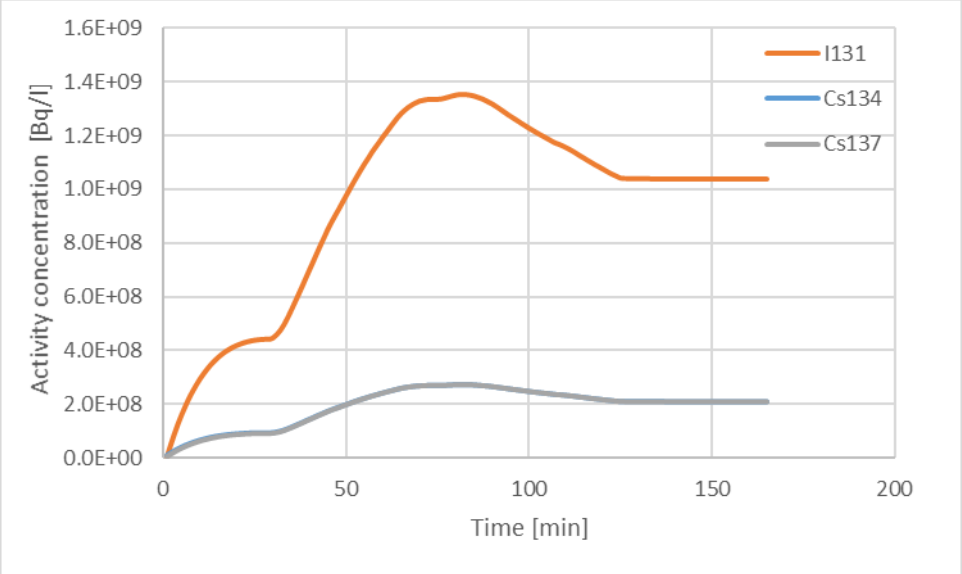

Fig. 37: ^{131}I, ^{134}Cs and ^{137}Cs corrected activity concentrations of the primary coolant during the break of 3 steam generator tube event (^{134}Cs and ^{137}Cs data are very close to each other and cannot be seen separately).

Integrated activity releases from the defective fuel rods

Parallel with the calculation of activity concentrations, the activity release from the leaking fuel rods are determined by the RING code. The calculated values for the three isotopes are summarized in Table 5.

Table 5: Integrated activity release from defective fuel rods during the break of 3 steam generator tubes.

Isotope	Integrated release (Bq)
^{131}I	$4.5 \cdot 10^{14}$
^{134}Cs	$8.95 \cdot 10^{13}$
^{137}Cs	$8.95 \cdot 10^{13}$

Released activity to the steam generator

Taking into account the primary coolant activity and break flowrate, the release to the steam generator was calculated for the three isotopes (Fig. 38). The activity release to the SG terminates when the breakflow stops.

The calculated results (Table 6) shows that roughly 40% of the activity released from the leaking fuel rods (Table 5) arrives to the secondary side of the steam generator.

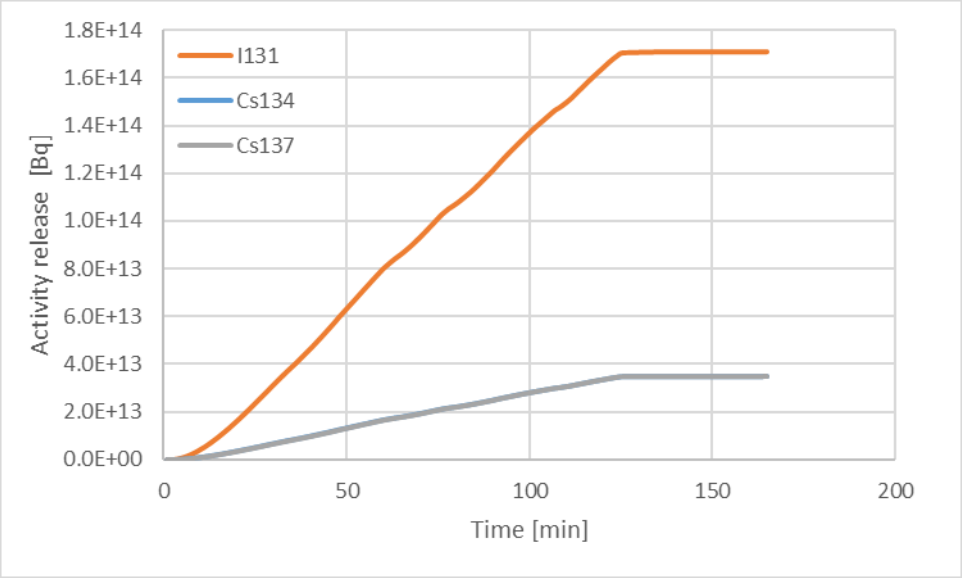

Fig. 38: ^{131}I, ^{134}Cs and ^{137}Cs activity release to the steam generator during the break of 3 steam generator tube event (^{134}Cs and ^{137}Cs data are very close to each other and cannot be seen separately).

Table 6: Integrated activity release to steam generators during the break of 3 steam generator tubes.

Isotope	Integrated release (Bq)
^{131}I	$1.71 \cdot 10^{14}$
^{134}Cs	$3.5 \cdot 10^{13}$
^{137}Cs	$3.47 \cdot 10^{13}$

This is the final result of the calculations. The activity release data to the steam generator can be used in further activity transport calculations to evaluate the doses in the rooms of nuclear power plant and to simulate activity release to the environment.

3.2.2 Simulation of SGTR event with the collector cover opening

Initial and boundary conditions

In the collector cover opening scenario the same initial conditions were used as in the case break of three SG tubes. The primary coolant activity concentration data used for VVER-440 nuclear power plants safety analyses were summarized in Table 4. Similarly, to the three tubes break, the collector cover opening scenario was calculated with both minimal and maximal purification flowrates.

The pressure history was determined by RELAP5 calculation [1]. The reactor power history corresponds to the actuation of reactors scram. The boric acid concentration was calculated considering the emergency core coolant system (ECCS) flows and break flow. The reactor power drops quickly to decay heat value in the beginning of the scenario. The primary pressure decreases significantly from the beginning of the transient and stabilizes around 50 bars after 110 minutes. The boric acid concentration is monotonously increasing with the ECCS injection. The power, pressure and boric acid concentration histories were selected from thermal hydraulic calculations.

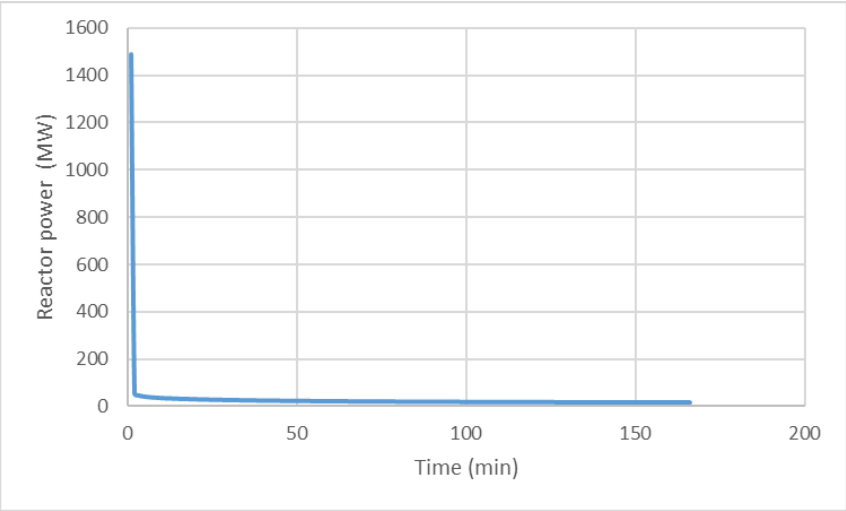

Fig. 39: Reactor power during the collector cover opening event.

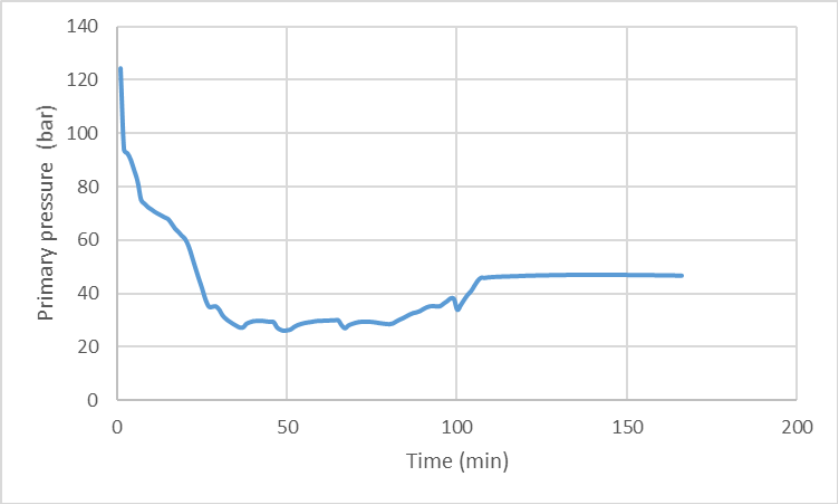

Fig. 40: Primary pressure during the collector cover opening event.

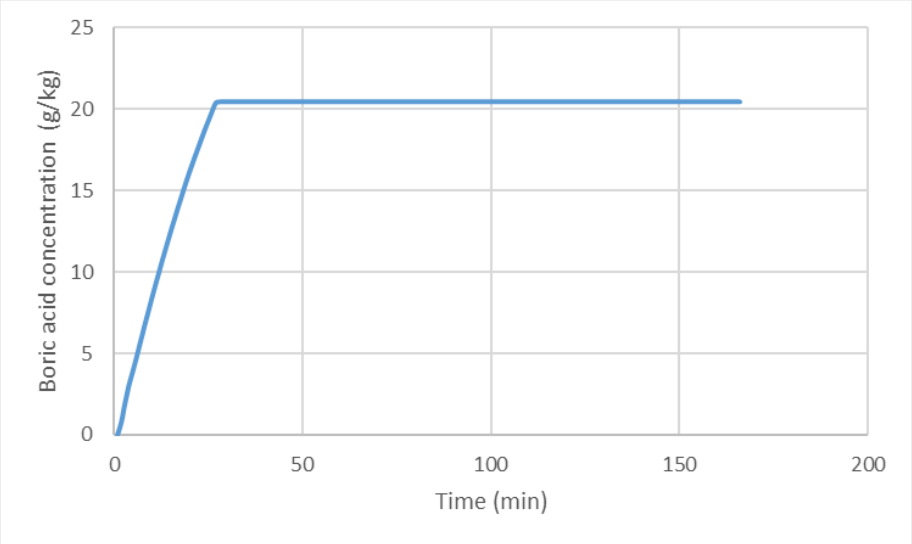

Fig. 41: Boric acid concentration of the primary coolant during the collector cover opening event.

Coolant activity concentrations

The calculated activity concentration histories represent the conditions in an intact primary circuit, since the RING code cannot handle break and ECCS flows. The histories for ^{131}I, ^{134}Cs and ^{137}Cs calculated by the RING code are presented in Fig. 43-Fig. **44**. The strongest releases can be seen in the first 80 minutes, when the primary pressure drops from 125 bars to 25 bars.

The maximum activity concentrations were reached for the cases with high steady state purification rate and the corresponding values were $1.25 \cdot 10^9$ Bq/dm^3 (^{131}I), $2.56 \cdot 10^8$ Bq/dm^3 (^{134}Cs) and $2.54 \cdot 10^8$ Bq/dm^3 (^{137}Cs).

In order to determine the activity concentrations corresponding to the collector cover opening scenario, additional calculations were performed. Using the data from the RING calculations and taking into account the break and ECCS flows, the activity concentrations for the three isotopes were determined for each time step. The results are presented in Fig. 45. The following maximum activity concentrations were reached: 10^9 Bq/dm^3 (^{131}I) $2 \cdot 10^8$ Bq/dm^3 (^{134}Cs) and $2 \cdot 10^8$ Bq/dm^3 (^{137}Cs).

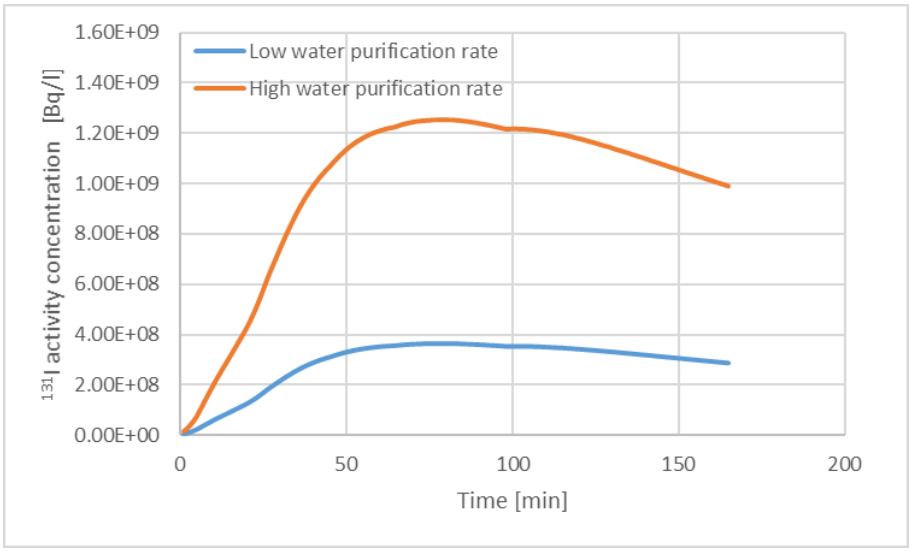

Fig. 42: Calculated ^{131}I activity concentration of the primary coolant during the collector cover opening event.

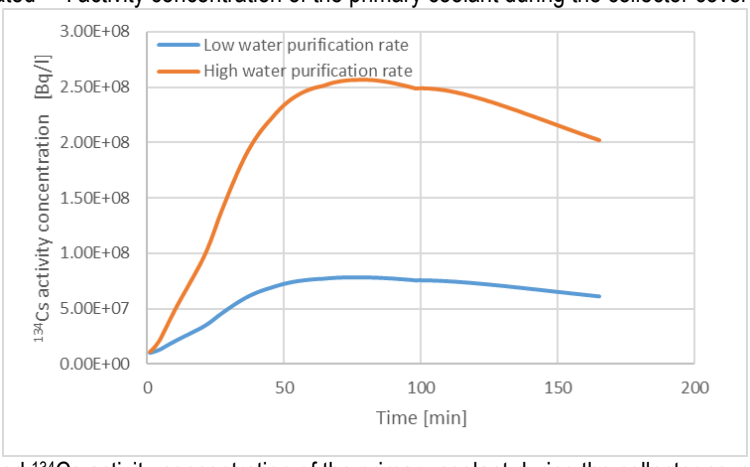

Fig. 43: Calculated ^{134}Cs activity concentration of the primary coolant during the collector cover opening event.

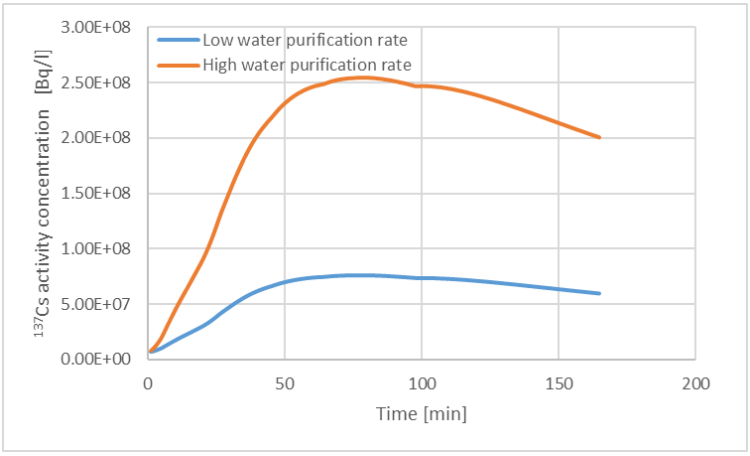

Fig. 44: Calculated ^{137}Cs activity concentration of the primary coolant during the collector cover opening event.

Similarly, to the 3-tube rupture scenario, in the further analyses only the data from high water purification rate cases were evaluated.
The maximum coolant activity concentrations were lower by about 30% in the broken circuit compared to the RING calculation. The stabilisation of the concentrations at 100 min time corresponds to the isolation of the affected steam generator, when the break flow stopped.

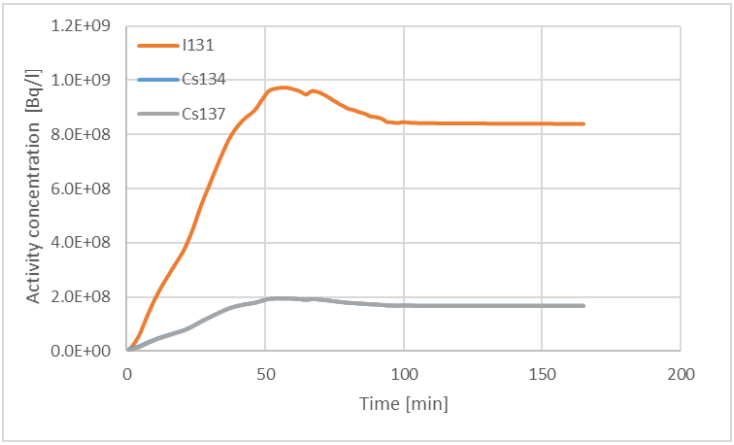

Fig. 45: ^{131}I, ^{134}Cs and ^{137}Cs corrected activity concentrations of the primary coolant during collector cover opening event (^{134}Cs and ^{137}Cs data are very close to each other and cannot be seen separately).

Integrated activity releases from the defective fuel rods

Parallel with the calculation of activity concentrations, the activity release from the leaking fuel rods are determined by the RING code. The calculated values for the three isotopes are summarized in Table 7.

Table 7: Integrated activity release from defective fuel rods during collector cover opening.

Isotope	Integrated release (Bq)
^{131}I	$2.78 \cdot 10^{14}$
^{134}Cs	$5.5 \cdot 10^{13}$
^{137}Cs	$5.51 \cdot 10^{13}$

Released activity to the steam generator

Taking into account the primary coolant activity and break flowrate, the release to the steam generator was calculated for the three isotopes.

The calculated results (Table 8) shows that roughly 40% of the activity released from the leaking fuel rods (Table 7) arrives to the secondary side of the steam generator.

This is the final result of the calculations. The activity release data to the steam generator can be used in further activity transport calculations to evaluate the doses in the rooms of the nuclear power plant and to simulate activity release to the environment.

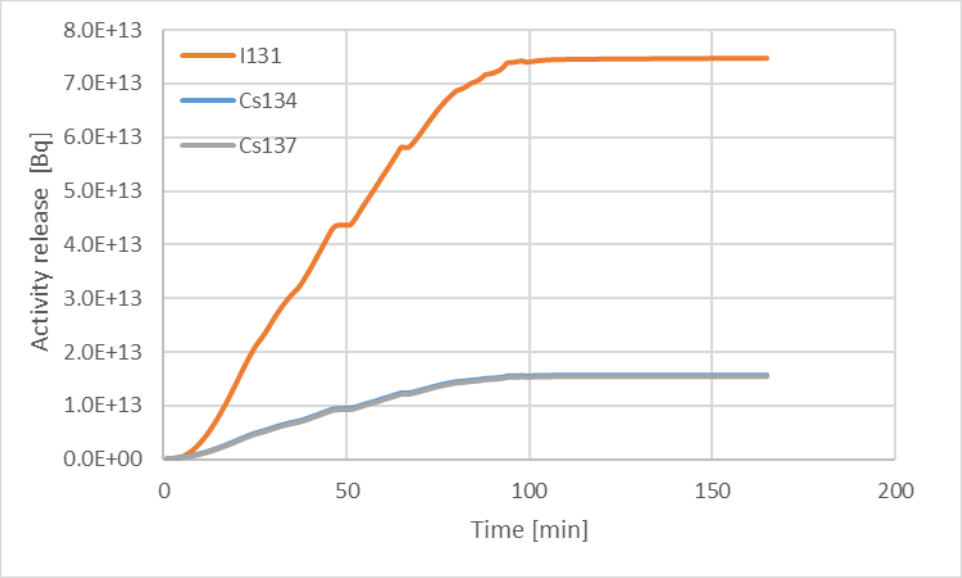

Fig. 46: ^{131}I, ^{134}Cs and ^{137}Cs activity release to the steam generator during the collector cover opening event (^{134}Cs and ^{137}Cs data are very close to each other and cannot be seen separately)

Table 8: Integrated activity release to steam generators during collector cover opening

Isotope	Integrated release (Bq)
^{131}I	$7.48 \cdot 10^{13}$
^{134}Cs	$1.57 \cdot 10^{13}$
^{137}Cs	$1.54 \cdot 10^{13}$

3.2.3 Summary

Activity release from defective fuel rods during SGTR accidents was calculated with the RING code. It was supposed that the transient activity release happened due to the change of reactor power, primary pressure and boric acid concentration. The corresponding input data and boundary conditions were collected from thermal hydraulic calculations for two scenarios:

- Break of 3 steam generator tubes and
- Opening of collector cover in the steam generator.

Low and high-water purification flowrates were used setting up initial activity concentrations for the calculated iodine and caesium isotopes. It was shown that in case of high purification rate higher activity release was obtained, since higher number of defective fuel rods corresponds to the activity concentration limit compared to low purification case. For this reason, only the high purification rate condition was used in the further analyses.

In the calculated scenarios 400 leaking fuel rods corresponded to the iodine activity concentration limits. According to the simulation of iodine spiking phenomena with the boundary conditions of the two scenarios 2.6% and 1.7% of fuel rod inventory was released to the primary coolant during the 3-tube break and collector cover opening transients, respectively. These values mean 0.023% and 0.014% of the core inventory of the ^{131}I, ^{134}Cs and ^{137}Cs isotopes (Fig. 47).

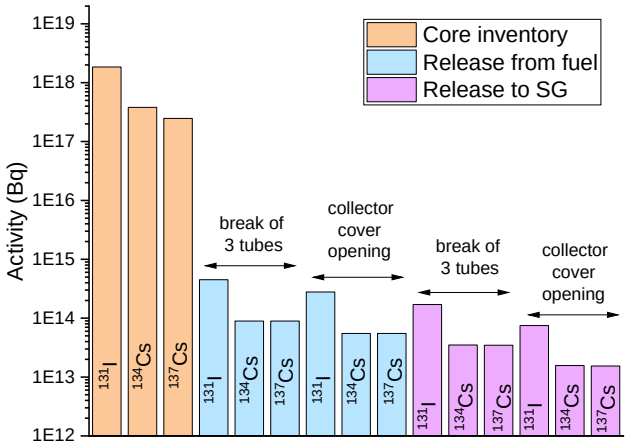

Fig. 47: Activity release and core inventory of ^{131}I, ^{134}Cs and ^{137}Cs isotopes during SGTR events.

The calculated results showed that the activity release from leaking fuel rods was higher in the case of 3 tube generator rupture compared to collector cover opening event (Fig. 48, Fig. 49 and Fig. 50).

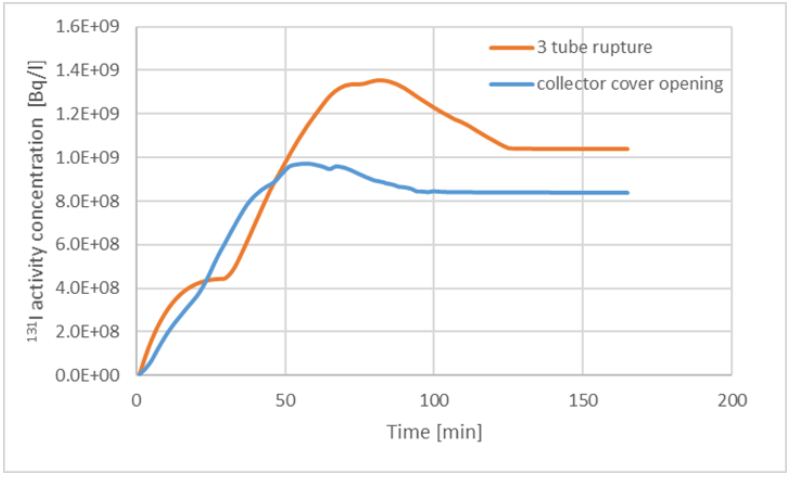

Fig. 48: ^{131}I activity concentration in the primary coolant during collector cover opening and 3 tube rupture events.

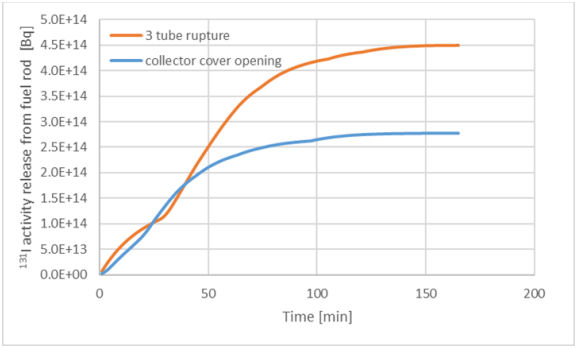

Fig. 49: The ^{131}I activity release from the defective fuel rod during the two scenarios.

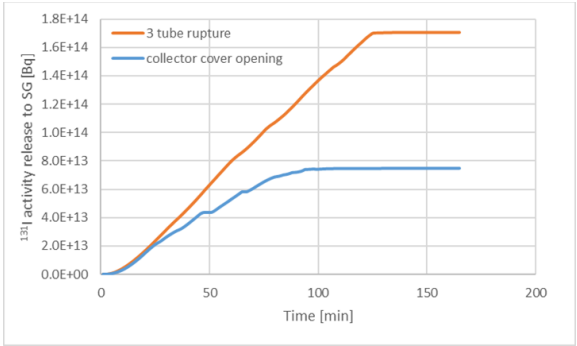

Fig. 50: The ^{131}I activity release to the steam generator during the two scenarios.

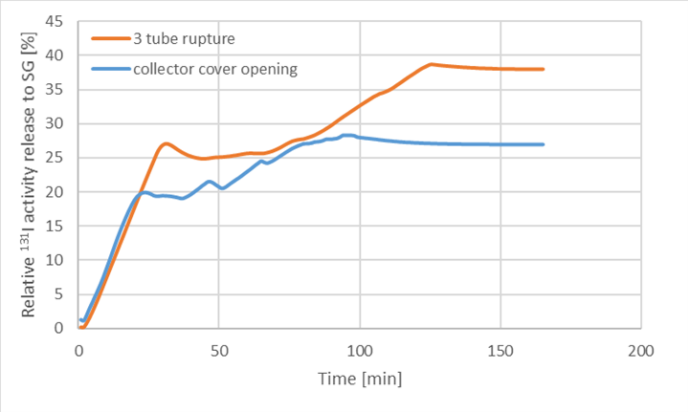

Fig. 51: The relative release to the SG was different in the two scenarios.

During the calculated period (roughly 3 hours) ≈ 30-40% of the activity released from the fuel rods into the primary coolant was transferred to the secondary side of steam generator (Table 9). The produced data can be used to evaluate the further consequences (environmental release, dose of NPP workers) of the simulated SGTR accidents.

Table 9: Integrated activity releases during SGTR events.

Isotope	Activity release from the defective fuel rod during 3 tube break	Activity release from the defective fuel rod during collector cover opening	Activity release to steam generator during 3 tube break	Activity release to steam generator during collector cover opening
^{131}I	$4.5 \cdot 10^{14}$	$2.78 \cdot 10^{14}$	$1.71 \cdot 10^{14}$	$7.48 \cdot 10^{13}$
^{134}Cs	$8.95 \cdot 10^{13}$	$5.5 \cdot 10^{13}$	$3.5 \cdot 10^{13}$	$1.57 \cdot 10^{13}$
^{137}Cs	$8.95 \cdot 10^{13}$	$5.51 \cdot 10^{13}$	$3.47 \cdot 10^{13}$	$1.54 \cdot 10^{13}$

3.3. Development of the RELAP5-3D code

BOKU analyzed the capability of RELAP5-3D to simulate iodine behavior during a SGTR scenario. It was concluded that the build - in model of the code is not sufficient to simulate the chemical transformation of FPs adequately.
Therefore, BOKU has developed an external function to improve the FP behaviour during the transient simulation. The function is completed and utilized in T2.5.

The following effects on iodine are included in the post processing function:

- Coolant purification system (VVER 1000 up to 30 kg/s).
- Pool scrubbing effect (based on Model of Pich and Schütz).
- Containment retention effect (VVER 1000 design leakage of 0.1%/day).

An extended description of the implementation can be found in the found in T4.1.

The plots below show the effect on the iodine concentration for one example scenario (VVER1000, SGTR, DEC-A). In this scenario no pathway for iodine to the containment was included.

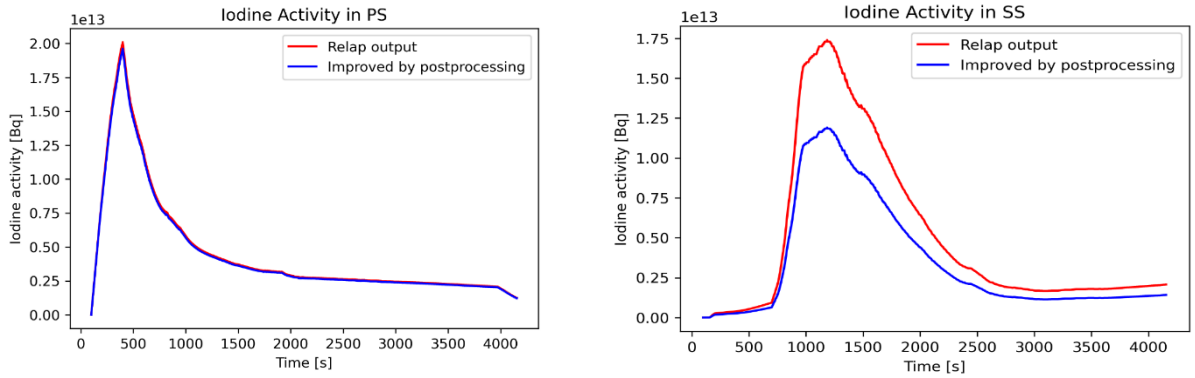

Fig. 52: On the left: iodine activity for one example scenario (VVER1000, SGTR, DEC-A) in primary side (PS). On the right: iodine activity for one example scenario (VVER1000, SGTR, DEC-A) in the secondary side (SS).

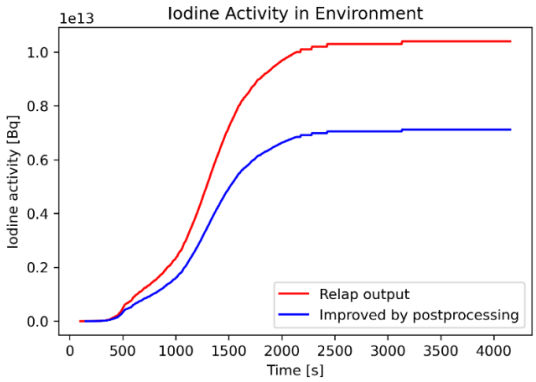

Fig. 53: iodine activity for one example scenario (VVER1000, SGTR, DEC-A) released to the environment.

The following conclusions can be made:

- The impact of the coolant purification system at the PS in the first hours of a transient scenario is only moderate.
- Pool Scrubbing at this scenario leads to a retention effect of about 30%.
- PS and SS retention effects reduce the iodine transported to the environment by about 30%.

3.4. Assessment of the FP/aerosol release in MELCOR code

3.4.1 Brief description of the code

MELCOR is a fully integrated, engineering-level computer code whose primary purpose is to model the progression of accidents in Light Water Reactor (LWR) NPPs [56]. A broad spectrum of severe accident phenomena is treated in MELCOR in a unified framework (latest versions are being extended to include phenomena for advanced reactor concepts, like sodium fast reactors, high temperature gas-cooled reactors and others [57]). These include thermal-hydraulic response in the reactor coolant system, reactor cavity, containment, and confinement buildings; core heat up, degradation, and relocation; core-concrete attack; hydrogen production, transport, and combustion; fission product release and transport behaviour. Current uses of MELCOR include estimation of severe accident source terms and their sensitivities and uncertainties in a variety of applications [56].

The MELCOR code consists of an executive driver and several major modules, or packages that together model the major systems of a reactor plant and their coupling. MELCOR modelling makes use of a "control volume" approach in describing the plant system. Reactor-specific geometry is imposed only in modelling the reactor core.

In MELCOR the RadioNuclide (RN) package models the behaviour of FP aerosols and vapours, from release from fuel and debris to their removal by engineered safety features, going through transport and deposition in the reactor cooling and containment systems. At present, just limited FP chemistry is considered in transport and deposition models (chemistry effects can be simulated in MELCOR just through the class reaction and class transfer models, which are controlled entirely by user-specified parameters). Rather than tracking all FP isotopes, the masses of all the isotopes of an element are modelled as a sum; that is, the total element mass, not its individual isotopes, is modelled. Furthermore, elements are combined into material classes, groups of elements with similar chemical behaviour. Fifteen material classes are typically used, thirteen containing FPs, plus water, and concrete oxides. Combination of classes to form new classes upon release, such as Cs + I to CsI, is permitted. The decay heat power per unit initial mass for each class is determined by the Decay Heat (DCH) package based on the class compositions (see **Table 10**) [56].

The aerosol dynamics models are based on MAEROS, a multisection, multicomponent aerosol dynamics code, whereas condensation and evaporation of radionuclide vapours on pool surfaces, heat structure surfaces and particle surfaces are evaluated by the rate equations from the TRAP-MELT2 code. Aerosols can deposit directly on surfaces such as heat structures and water pools or can agglomerate and eventually fall out once they exceed the largest size specified by the user for the aerosol size distribution. Some volatile FP species may revaporise from deposits if the necessary conditions prevail; resuspension can be also modelled, if activated.

Specific models are available for the removal of radionuclides by suppression pools and ponds, filter trapping, and spray scrubbing. The pool scrubbing model is based on the SPARC code.

Table 10: RN Class composition [58]

Class Name	Representative	Member Elements
1. Noble Gases	Xe	He, Ne, Ar, Kr, Xe, Rn, H, N
2. Alkali Metals	Cs	Li, Na, K, Rb, Cs, Fr, Cu
3. Alkaline Earths	Ba	Be, Mg, Ca, Sr, Ba, Ra, Es, Fm
4. Halogens	I	F, Cl, Br, I, At
5. Chalcogens	Te	O, S, Se, Te, Po
6. Platinoids	Ru	Ru, Rh, Pd, Re, Os, Ir, Pt, Au, Ni
7. Early Transition Elements	Mo	V, Cr, Fe, Co, Mn, Nb, Mo, Tc, Ta, W
8. Tetravalent	Ce	Ti, Zr, Hf, Ce, Th, Pa, Np, Pu, C
9. Trivalents	La	Al, Sc, Y, La, Ac, Pr, Nd, Pm, Sm, Eu, Gd, Tb, Dy, Ho, Er, Tm, Yb, Lu, Am, Cm, Bk, Cf
10. Uranium	U	U
11. More Volatile Main Group	Cd	Cd, Hg, Zn, As, Sb, Pb, Tl, Bi
12. Less Volatile Main Group	Ag	Ga, Ge, In, Sn, Ag
13. Boron	B	B, Si, P
14. Water	H_2O	H_2O
15. Concrete	- -	- -
16. Cesium Iodide	CsI	Classes 2 and 4
17. Cesium Molybdate	CsM	Classed 2 and 7

Release of radionuclides can occur from the fuel-cladding gap by exceeding a failure temperature criterion or losing intact geometry, from material in the core, and during core-concrete interactions in the reactor cavity using the VANESA release model. The radionuclides residing in the core fuel are assumed to be in elemental form but could combine with non-radioactive materials with which they might interact or even react with. An example is the interaction of Cs with steam to form CsOH, or even with structural, control rod materials or even concrete constituents (that might get also released as vapours and aerosols).
The release models apply to both geometry-like fuel conditions, refrozen fuel material and particulate debris. Before cladding failure, radionuclides released from fuel are transferred to the gap and are released to the surrounding atmosphere of control volume only upon cladding failure [56].

Four options are currently available for the release of radionuclides from the core components: the CORSOR, CORSOR-M, CORSOR-BOOTH, or modified ORNL-BOOTH model. The CORSOR-BOOTH model contains low and high burn-up options. In addition, the CORSOR and CORSOR-M release rates can be modified to be a function of the component surface-to-volume ratio as compared to a base value, derived from the experimental data on which CORSOR is based [58]. The CORSOR and CORSOR-Booth models are briefly summarized as follows.

CORSOR model

The CORSOR model is an empirical correlation of a variety of experimentally determined release fractions. Most of the data that are the basis for the CORSOR model come from the SASCHA tests at the Kernforschungszentrum in Karlsruhe. West Germany, and the hot cell tests (HI and HT Series) done at Oak Ridge National Laboratory. The SASCHA tests used simulated fuel doped with fission products to a level expected for fuel with a burnup of 44000 MWd/t. The samples were heated under a variety of atmospheres at pressures up to 2 bars. The Oak Ridge tests used irradiated fuel rods heated in atmospheres initially composed of steam and an inert carrier at a pressure of about 1 atm [59].

The original CORSOR model correlates the fractional release rate in exponential form,

$$f_i = A_i \exp\left(B_i T\right) \text{ for } T \geq T_i \tag{31}$$

where f_i is the release rate (fraction per minute), A_i and B_i are empirical coefficients based on experimental data, T is the core cell component temperature in Kelvin and the subscript i indicates the specific class.

Different values for A_i and B_i are defined for three separate temperature ranges [59]:
1. 900 – 1400 °C
2. 1400 – 2200 °C
3. > 2200 °C

If the cell temperature is below the lowest temperature range limit specified, no release is calculated [56].

CORSOR Booth model

The original CORSOR-Booth model considers mass transport limitations to radionuclide releases and uses the Booth model for diffusion with empirical diffusion coefficients for caesium releases. Release fractions for other classes are calculated relative to that for caesium. The classical or effective diffusion coefficient for caesium in the fuel matrix is given by:

$$D = D_0 \exp\left(-\frac{Q}{RT}\right) \tag{32}$$

where R is the universal gas constant (cal mol^{-1} K^{-1}), T (K) is the temperature, Q (cal mol^{-1}) is the activation energy, and the pre-exponential factor D_0 (m^2 s^{-1}) is a function of the fuel burn-up. For fuel with burn-up in excess of 30,000 MWD/MTU the model uses a value for D_0 five times larger than the value it uses for fuels with lower burn-up. The two default values for D_0, the transition burn-up value, and the activation energy Q, based on experimental data for the release of fission gases from fuel test samples, are all given in sensitivity coefficient array [60]. The caesium release fraction f at time t is calculated from an approximate solution of Fick's law for fuel grains of spherical geometry:

$$f = 6\sqrt{\frac{D't}{\pi}} - 3D't \text{ for } D't \leq \pi^{-2} \tag{33}$$

$$f = 1 - \frac{6}{\pi^2}\exp\left(-\pi^2 D' t\right) \text{ for } D' t \geq \pi^{-2} \tag{34}$$

where $D' = D/a^2$ and a is the radius of the equivalent spherical fuel grain.

The release rate (in mol/s) of Cs during a time interval t to $t + \Delta t$ from the fuel grain is calculated as:

$$\text{Release rate}_{\text{Cs}} = \frac{[(f\sum D'\Delta t)_{t+\Delta t} - (f\sum D'\Delta t)_t]V\rho}{(1-f)\Delta t} \tag{35}$$

where ρ (mol m^{-3}) is the molar density of UO_2 in the fuel, V (m^3) is the fuel volume and the summations are done over the time steps up to time $t + \Delta t$ and t, respectively.

The release rate formulation in the CORSOR-Booth model is also limited by mass transfer through the gas phase. The gas phase mass transport release rate from the fuel rod for species k, $\dot{m}_k$ (in mol/s), is calculated using an analogy from heat transfer as:

$$\frac{1}{\dot{m}_k} = \frac{d_{\text{fuel}} RT}{A_{\text{fuel}} Nu D_{\text{k,gas}} P_{\text{k,eq}}} \tag{36}$$

where:
d_{fuel} (m) is the diameter of the fuel pellet,
A_{fuel} (m^2) is the fuel rod flow contact area,
$D_{\text{k,gas}}$ (m^2/s) is the diffusivity of the class k in the gas mixture,
Nu is the Nusselt number,
R (J mol^{-1} K^{-1}) is the universal gas constant
$P_{\text{k,eq}}$(Pa) is the equilibrium vapour pressure of the class k at temperature T.

The effective release rate for Cs is a combination of the rates given by diffusion and by gas-phase mass transport. Therefore, the contribution from diffusion only is taken as:

$$\text{DIFF}_{\text{Cs}} = \left(\frac{1}{\text{Release rate}_{\text{cs}}} - \frac{1}{\dot{m}_{\text{Cs}}}\right)^{-1} \tag{37}$$

The diffusion release rate (in mol/s) for species other than Cs is given by multiplying the caesium release rate by an appropriate scaling factor S_k for each RN class k:

$$\text{DIFF}_k = \text{DIFF}_{\text{Cs}} S_k \tag{38}$$

Nominal values for S_k are given in sensitivity coefficient array. For certain conditions of cladding oxidation and temperature, the scaling factors must be modified for some classes.
The combined mass transport and diffusion release rate $\dot{m}_{tot,k}$ for class *k* is then:

$$\dot{m}_{tot,k} = \frac{1}{(\text{DIFF}_{\text{k}})^{-1} + (\dot{m}_k)^{-1}} \tag{39}$$

The fractional release rate for the inventory of class *k* is calculated as:

$$\dot{f}_k\left(\frac{\text{fraction}}{\text{s}}\right) = \frac{\dot{m}_{tot,k}}{\rho V}\left(F - \frac{P_{k,bulk}}{P_{k,eq}}\right) \quad (40)$$

Fuel - Cladding gap

Release of the radionuclides in the fuel-cladding gap (initial inventory plus masses from fuel release) occurs at the time of cladding failure. It is assumed that the gaps in each radial ring can communicate axially between core cells, so when the cladding temperature at any core cell reaches or exceeds the cladding failure temperature specified for that cell, or when the cladding intact geometry has been lost, the entire gap inventory in that ring is released. This cladding failure temperature (by default 1173 K) corresponds to an initial fracture of the fuel rod cladding [60], and is only used in the RN package for gap releases [56]. At the time this fuel rod failure criterion is met, no water is flowing through that core region and the fluid in contact with fuel is in gas phase (mostly steam and hydrogen).

3.4.2 Critical assessment of model applicability

According to what just said above, no FP release is estimated by MELCOR at temperatures lower than 900ºC. During SGTR sequences in DBA and DEC-A conditions calculated in R2CA/WP2.3, clad temperature never comes even close to that threshold. In addition, the CORSOR model has an empirical nature and extrapolation of the exponential law in the previous section would not make any sense. In other words, below 900ºC no FP is released. Thus, the application for MELCOR FP release model should be ruled out under the conditions of interest here investigated.

In the case of the CORSOR Booth mode, the code calculates the release from the core to the fuel gap, but the condition of fuel cladding failure temperature limits its application for the modelling of the iodine spiking.

3.4.3 Potential enhancements

Based on the assessment of the applicability of the code release models is not planned any enhancements. In order to model FP behaviour during SGTR sequences in DBA and DEC-A conditions an external function will be built to model iodine spiking phenomenon. Based on [57], the enhanced-diffusional release during reactor shutdown and any forced-convective release driven by temperature and pressure changes, are considered to estimate the iodine (I^{131}) release rate.

Diffusion and first-order model

During reactor shutdown, the coolant which has entered the rod remains in the liquid phase and dissolves the iodine that is deposited on the internal rod surfaces. In the absence of any temperature or pressure fluctuations, this iodine leaching process can be described by either a diffusion or first-order kinetic process. In both representations, the release rate, $R_{diff}(t)$ (atom/s) from the defective rod into the RCS is given by the time-dependent relation [57]:

$$R_{diff}(t) = kN_{g0}e^{(-(\lambda+k)t} \quad (41)$$

where:

N_{g0} is the initial iodine inventory in the gap (atom),
k is the escape rate constant of the inventory in the gap (s^{-1}).
λ is the radioactive decay constant (s^{-1}).

It is assumed that the iodine release into the gap stops at shutdown and that the iodine inventory can only be depleted from that moment on [57].

Forced-convection model

Iodine spiking is enhanced under coolant depressurization and temperature transients. When the RCS pressure is reduced or the RCS temperature is increased, non-condensable gases that are trapped in the plenum at the top of the rod can expand, forcing iodine-rich water out of the rod and into the coolant. If a defect is located at the top of the rod, the gases can escape from the plenum and the rod can then entirely fill with water as the steam condenses on shutdown. The change of the fluid density in the gap due a temperature or pressure change in the RCS, can produce the possible expulsion of iodine-rich water.

As a consequence of gas expansion in the plenum, or water expansion in the rod, a forced-convective release will result until a pressure or temperature equalization is achieved. The release rate expression for this transport process is given by [57]:

$$R_{conv}(t) = k_0 N_{g0} e^{(-(\lambda + f^{-1} k_0)t} \tag{42}$$

where:

$$k_0 = \frac{\Delta P(0) h^2}{12 \mu l^2} \tag{43}$$

h = fuel to clad gap thickness (m).
l = fuel stack length (m).
μ = fluid viscosity in the fuel to clad gap (kg/m.s).
$\Delta P(0)$ = pressure differential between the coolant and internal rod atmosphere at the beginning of the time step (Pa).

The parameter f depends on the axial location of the defect [47]. If the plenum is gas-filled (bottom-end defect):

$$f = \frac{\Delta P(0) \xi V_p}{P_c V_{gap}} \tag{44}$$

while if the rod is entirely filled with water (top-end defect):

$$f = \frac{\Delta P(0)}{\beta} \tag{45}$$

where:

$V_g = \xi V_p$ is the volume of gas in plenum, (m^3),
V_{gap} - is the fuel-to-clad gap volume (m^3),
V_p - is the plenum volume (m^3),
ξ - is the volumetric fraction of gas in the plenum,
P_c – is the coolant pressure (Pa),
β – is the fluid expansion coefficient (Pa).

According to the model [57] the release rate considering the processes of diffusion, $R_{diff}(t)$ and convection $R_{conv}(t)$ might be written as:

$$R_c(t) = R_{diff}(t) + R_{conv}(t) \tag{46}$$

Estimated released activity to the RCS

To get the release rate to be applicable in the best estimation calculations (DEC-A scenario), a defect at the bottom end of the rod was considered. The above model parameters were fitted to data collected from fifteen NPPs. Their values, gathered in Table 2 of [57], are:

- Average measured steady-state coolant activity = 179 µCi/kg.
- Steady-state escape rate constant, ν = 9.1.10^{-7} s^{-1}.
- Transient escape rate constant, κ = 3.6.10^{-5} s^{-1}.
- Volumetric fraction of gas in plenum ξ = 0.18.

Fig. 54 shows the estimated released activity of ^{131}I to the RCS. The value of RCS pressure and temperature correspond to modeled DEC-A scenario (isolable main steam line break (MSLB) with the double ended rupture of three steam generator tubes at the cold leg side tube sheet).

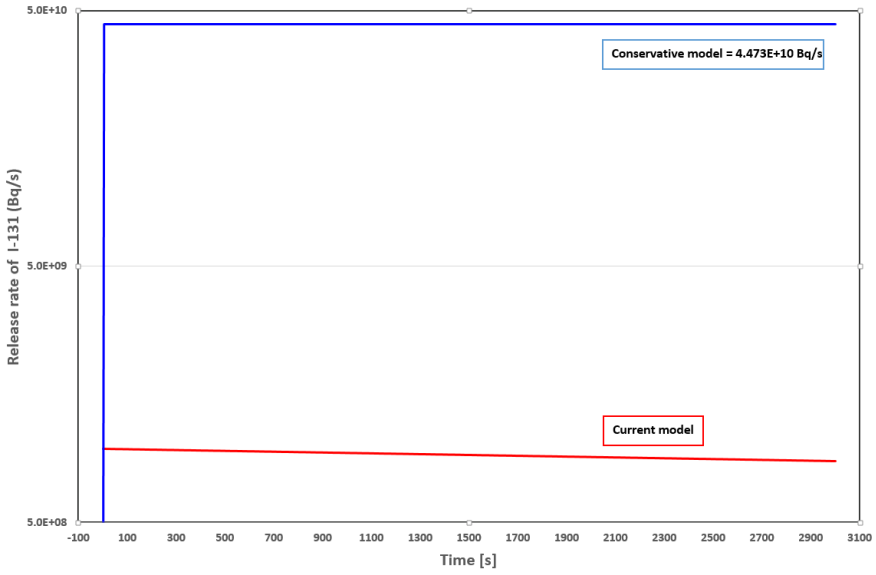

Fig. 54: Release activity of the 131I into the RCS (scenario MSLB + 3 SGTR).

3.5. Calculation methods for iodine spiking in SGTR

The initial analysis of SGTR with iodine spike is based on the coolant activity data provided by the Kurchatov's Institute in the report [61]. The report contains results of calculations of the radioactive content in the fuel and the fuel gap for 3 and 4-year fuel cycles of VVER-1000 (V-320) reactor with TVSA fuel, as well as the results of calculation of coolant activity with and without the iodine spike based on the limiting values for the fuel cladding defects of gas leakage and direct fuel contact type which are prescribed by the regulatory requirements. The report does not describe the methodology applied for calculating the activity of the primary circuit coolant in the case of the iodine spike though it refers to the methodology which is not publicly available. Earlier version of the methodology [62] is accessible, however applicability of this methodology and of various coefficients used therein to the modern fuel types and their operation cycles is not known.

Contrary, the method described in NUREG-0800 [63] provides engineering approach that is not excessively complicated to require developing a dedicated computational code on the one hand and on the other hand is acceptable to U.S.NRC for justifying the reactor design and operation safety. With respect to considering the iodine spike in SGTR analyses the approach requires to evaluate two separate cases (see, for example,

paragraph 15.6.3 III.6 of NUREG-0800 [63]): case A with the spike that has occurred before the initiating event (pre-accident iodine spike) and case B with the spike occurring due to primary circuit depressurization caused by the initiating event. For case A it is assumed that iodine concentration in the primary circuit coolant increases up to the maximal value specified in the plant technical specification. For case B the iodine release rate from the leaked fuel rods to the primary coolant (expressed in activity units per unit time) increases to a value 500 times greater than the release rate corresponding to the iodine concentration at the equilibrium value stated in the technical specification. According to [64], the equilibrium iodine concentration is identical for technical specifications of all PWRs of different vendors and corresponds to 1 μCi/g. The same value is specified as a normal operation limit for VVER-1000 nuclear power plants (see, for example, table 6.2.2-1 of the technical specification of Zaporizhzhia NPP Unit 6 [65]).

Paragraph 2.2 of Appendix F of the U.S.NRC regulatory guide RG 1.183 [66]allows to use lower multiplier of 335 for case B in SGTR accident analysis.

In [64] the following formula is specified for estimating the transient iodine release rate from plant spike events data:

$$R = \frac{L_\tau (A - A_0 e^{-L_\tau \tau})}{1 - e^{-L_\tau \tau}} \quad (47)$$

where R – transient iodine release rate (Ci/h).
Lτ – total iodine removal rate (1/h).
A – maximum transient RCS iodine activity (Ci).
A0 – steady-state RCS iodine activity (Ci).
τ – time from iodine spike initiating event to maximum iodine concentration (h).

From this formula the equilibrium iodine release rate can be calculated as R0 = Lτ ×A0.

The total iodine removal rate is estimated using formula (2) of [64]:

$$L_\tau = L_d + L_p; \quad L_p = \frac{F(1 - 1/DF)}{M} \quad (48)$$

Where:

Ld = 0.0035996 1/h – decay constant of 131I.
F: purification system flow rate (kg/h).
M: RCS mass inventory (kg).
DF: purification system decontamination factor.

The assumed iodine spike duration to be applied in SGTR analysis should be 8 hours according to paragraph 2.2 of appendix F of RG 1.183 [66]. Shorter spike durations may be considered if it can be shown that the activity released by the 8-hour spike exceeds that available for release from the fuel gap of all fuel rods.
To compare the actual VVER-1000 spike events versus the approach specified in NUREG-0800 [63] and regulatory guide RG 1.183 [66], information on the spike events at NPPs with VVER-1000 reactor operating in Ukraine for last 10 years were collected and analyzed (this information could be submitted by Ukrainian Utility NNEG Energoatom only with request). It was found that the scope of data available is insufficient considering that reported data:

- Provides the peak values for the iodine activity only with no information on activity change with time.
- Do not include information on actual purification system performance during the spike event, which is needed to estimate the total iodine removal rate using formula (2) of [64], given above.

Considering the above, the evaluation of the applicability of NUREG-0800 and RG 1.183 approach for estimating the iodine spike for VVER-1000 nuclear fuel could not be performed based on the currently available data.

[6] https://www-nds.iaea.org/relnsd/vcharthtml/VChartHTML.html

4. Summary and conclusions

Achievements on modelling FP release from defective rods during a SGTR transient and iodine spiking have been obtained and presented in this deliverable.
JRC has reprogrammed in modern Fortran the implementation of the semi-empirical model ANS 5.4-2010 by V. Peri in the TRANSURANUS code to predict the release-to-birth-ratio of some short-lived gaseous and volatile FPs.
NINE developed an upgraded model for radioactive FP release from defective fuel rods, currently being tested in TRANSURANUS. This model is structured in two successive steps: (1) FP release from the fuel to the fuel-cladding gap and (2) FP release from the fuel-cladding gap to the coolant. The first intra-granular step considers the formation of both unstable FPs and stable isotopes of FGs within the fuel grains, and their diffusion towards the grain boundaries. The grains are assumed homogeneous and spherical. Furthermore, a new diffusion model that takes into account the possibility to have fuel oxidation has been modelled. Such model considers a correction factor on the high temperature component of the single atom diffusion coefficient by Turnbull, that is successively used in the extended mechanistic model by Speight, in which the intra-granular diffusivity is given by two contributions: a term accounting for the fraction of in-solution intra-granular gas atoms, available for single atoms diffusion and a term accounting for the mobility of intra-granular bubbles, formed by the trapping of FGs, through an effective diffusion mechanism. The results of fission gas release model has been compared with experimental data for CONTACT 1 experiment of the IFPE database, considering different diffusion models and diffusion equation solvers. Moreover, the isotopes production has been verified by means of the comparison with the Monte Carlo transport code Serpent. The intra-granular diffusion process is the source for the concentration of FPs and FGs in the fuel-cladding gap. From there, the release from the defective cladding is modelled with a phenomenological first-order rate theory model. The model has been used to estimate escape rate constants under equilibrium conditions during the simulated CRUSIFON1bis experiments,
Complementary with this modelling activity, POLIMI developed a methodology to bound a priori the numerical error on the prediction of radioactive FP/gas release [6]. The methodology is tailored to state-of-the-art SDAs and aims to determine the number of time-steps of modes used in the computation of the numerical solution. A suitable upper bound of the numerical error is defined and studied to produce a set of reference tables collecting fitting factors for the error bounds. The procedure to bound the error is: (1) fix the demanded error upper bound, (2) estimate the non-dimensional characteristics of the constant irradiation history (or the average characteristics for transient irradiation history) and choose the number of time-steps and the number of modes for which the fit function provides a value below the demanded upper bound. The methodology is applicable both in constant and transient conditions, it is suitable for implementation in simulation codes of interest for the current task and to reproduce reactor conditions pivotal for the project.
POLIMI also developed a physics-based model to describe the intra-/inter granular behaviour of radioactive FG/FP in the fuel, to reproduce the dynamics of the radioactive release and its evolution during irradiation. This development constitutes a milestone in the modelling of radioactive gas without calibration of specific parameters, as in the ANS 5.4-2010 methodology, under both constant and transient conditions. The model has been implemented in SCIANTIX and tested (as a standalone code) against the CONTACT1 irradiation experiment, from the IFPE database. Results include the comparison of the release-to-birth ratio of several short-lived isotopes of xenon and krypton with both the experimental measurements and the predictions given by the semi-empirical ANS 5.4-2010 methodology [7].
In order to assess the aforementioned model from an integral point of view, the coupling interface between the integral fuel performance code TRANSURANUS and SCIANTIX has been upgraded, to account for the TRANSURANUS restart option. Then, the coupled code TRANSURANUS//SCIANTIX has been used to reproduce the CONTACT1 and the HATAC C2 irradiation experiment. The analysis of the simulations of the two complementary experimental cases reveals the potential of the coupled version of TRANSURANUS with SCIANTIX [8].

Concerning the modelling of iodine spiking, EK further developed the RING code against new 18 nuclear power plants data (during power transients, reactor shutdown and start-up). The targeted developments have been oriented to overcome limitations in previous version of the code, and the introduction of new caesium spiking

models (^{134}Cs and ^{137}Cs). The upgraded RING code is applied to the simulation of iodine and caesium spiking effect in SGTR, and collector cover opening conditions. In addition, it allows to precise the activity release according to the specific power and pressure histories of the two events. In the updated transient model of the RING code, the release accelerates as a function of the variation in core power, primary pressure, and boric acid concentration.

BOKU analyzed the capability of RELAP5-3D to simulate iodine behavior during a SGTR scenario. It was concluded that the build - in model of the code is not sufficient to simulate the chemical transformation of FPs adequately. Therefore, BOKU is developing an external function to improve the FP behaviour during the transient simulation.

SSTC NRS reviewed the open literature about the investigation of fission product release from fuel rods under primary to secondary leaks. Main attention was paid on investigation approaches for iodine spike-effect modelling. In particular, to compare the actual VVER-1000 spike events versus the approach specified in NUREG-0800 [63] and regulatory guide RG 1.183 [66], information on the spike events at NPPs with VVER-1000 reactor operating in Ukraine for last 10 years were collected and analyzed (this information could be submitted by Ukrainian Utility NNEG Energoatom only with request). It was concluded that the scope of data available is insufficient considering that reported data provides the peak values for the iodine activity only with no information on activity change with time, and do not include information on actual purification system performance during the spike event, which is needed to estimate the total iodine removal rate. Therefore, the applicability of NUREG-0800 and RG 1.183 approach for estimating the iodine spike for VVER-1000 nuclear fuel could not be performed based on the currently available data.

CIEMAT reviewed the experimental database and available open technical documentation on fission product release during SGTR DBA sequences and iodine spiking models. As a result an external user function with a more accurate description of iodine spiking than the one used for WP2.3 calculations (based on very conservative assumptions) has been built considering a model of the release rate of iodine that considers the enhanced-diffusional release during reactor shutdown and includes any forced-convective release that may occur because of the temperature and pressure changes during the shutdown event.

IRSN proposed a new methodology for evaluating the release of radioactive isotopes from the fuel, called the decoupling approach. By treating separately the release problem of (stable) elements, and the decay/release problem of radioactive isotopes, this approach allows to perform accurate assessment of the element release, and to reuse this assessment for the calculation of radioactive isotope release. The decoupling approach uses two separate tools: the coupling of TRANSURANUS and MFPR-F codes, developed in collaboration with JRC, and a simple calculation tool for the formation, decay, and transmutation of radioactive isotopes. This approach has been applied as an illustration to an irradiation case taken from the Halden database (Ifa-650.10).

At UJV, TRANSURANUS code calculations were used to refine the conservative assumptions regarding the number of the failed rod in the core at the initiation of the SGTR. The gap inventory of ^{135}Xe, ^{133}Xe, ^{131}I and ^{137}Cs were assessed by TRANSURANUS model for both an intact fuel rod and a fuel rod with an assumed prior cladding breach. The calculated gap inventories were compared to the coolant activities measured in a VVER-1000 plant. Several cycles with varying number of leaking fuel rods were analyzed. No clear conclusion could be made for the release rates during the normal operation, including small activity spikes following power changes. On the other hand, the shutdown spike activity of ^{137}Cs always corresponds well to the gap inventory of the leaking rods assuming no enhanced diffusion from the fuel as a result of the cladding failure. This conclusion helps to justify the application of the TRANSURANUS code for the gap inventory analysis.

References

[1] K. Lassmann, "TRANSURANUS: a fuel rod analysis code ready for use," *Nuclear Materials for Fission Reactors*, pp. 295–302, 1992, doi: 10.1016/b978-0-444-89571-4.50046-3.

[2] D. Pizzocri, T. Barani, and L. Luzzi, "SCIANTIX: A new open-source multi-scale code for fission gas behaviour modelling designed for nuclear fuel performance codes," *Journal of Nuclear Materials*, vol. 532, p. 152042, 2020, doi: 10.1016/j.jnucmat.2020.152042.

[3] M. Charles, J. J. Abassin, D. Baron, M. Bruet, and P. Melin, "Utilization of Contact Experiments To Improve the Fission Gas Release Knowledge in Pwr Fuel Rods.," in *IAEA Specialists Meetiing on Fuel Element Performance Computer Modelling, Preston*, 1983, pp. 1–18.

[4] M. Bruet, J. Dodelier, P. Melin, and M.-L. Pointund, "CONTACT 1 and 2 experiments: Behaviour of PWR fuel rod up to 15000 MWd/tU," in *IAEA Specialists' Meetting on Water Reactor Fuel Element Perfomance Computer Modelling*, 1980, pp. 235–244.

[5] J. A. Turnbull and C. E. Beyer, "Background and Derivation of ANS-5.4 Standard Fission Product Release Model," 2010, doi: 10.2172/1033086.

[6] G. Zullo, D. Pizzocri, and L. Luzzi, "On the use of spectral algorithms for the prediction of short-lived volatile fission product release: Methodology for bounding numerical error," *Nuclear Engineering and Technology*, vol. 54, no. 4, pp. 1195–1205, 2022, doi: 10.1016/J.NET.2021.10.028.

[7] G. Zullo, D. Pizzocri, A. Magni, P. Van Uffelen, A. Schubert, and L. Luzzi, "Towards grain-scale modelling of the release of radioactive fission gas from oxide fuel. Part I: SCIANTIX," *Nuclear Engineering and Technology*, 2022, doi: 10.1016/J.NET.2022.02.011.

[8] G. Zullo, D. Pizzocri, A. Magni, P. van Uffelen, A. Schubert, and L. Luzzi, "Towards grain-scale modelling of the release of radioactive fission gas from oxide fuel. Part II: Coupling SCIANTIX with TRANSURANUS," *Nuclear Engineering and Technology*, Aug. 2022, doi: 10.1016/J.NET.2022.07.018.

[9] H. Faure-Geors, D. Baron, and C. Struzik, "HATAC experiments (1965-1990) Fission Gas Release at High Burn-up, Effect of a Power Cycling," 1990.

[10] V. Peri, "Fuel performance modelling in the Loviisa nuclear power plant with TRANSURANUS," *School of Science, Aalto University, 2014*, Aug. 2014, Accessed: Oct. 18, 2022. [Online]. Available: https://aaltodoc.aalto.fi:443/handle/123456789/13880

[11] G. Zullo, D. Pizzocri, A. Magni, P. Van Uffelen, A. Schubert, and L. Luzzi, "Towards grain-scale modelling of the release of radioactive fission gas from oxide fuel. Part II: Coupling SCIANTIX with TRANSURANUS," *Nuclear Engineering and Technology*, vol. 54, no. 12, pp. 4460–4473, Dec. 2022, doi: 10.1016/J.NET.2022.07.018.

[12] J. A. Turnbull, R. J. White, and C. Wise, "The diffusion coefficient for fission gas atoms in uranium dioxide," in *Water reactor fuel element computer modelling in steady state, transient and accident conditions*, 1988, pp. 174–181.

[13] D. Pizzocri, C. Rabiti, L. Luzzi, T. Barani, P. van Uffelen, and G. Pastore, "PolyPole-1: An accurate numerical algorithm for intra-granular fission gas release," *Journal of Nuclear Materials*, vol. 478, pp. 333–342, 2016, doi: 10.1016/j.jnucmat.2016.06.028.

[14] G. Pastore, D. Pizzocri, C. Rabiti, T. Barani, P. van Uffelen, and L. Luzzi, "An effective numerical algorithm for intra-granular fission gas release during non-equilibrium trapping and resolution," *Journal of Nuclear Materials*, vol. 509, pp. 687–699, 2018, doi: 10.1016/j.jnucmat.2018.07.030.

[15] R. S. Barnes, "A theory of swelling and gas release for reactor materials," *Journal of Nuclear Materials*, vol. 2, pp. 135–148, 1964.

[16] A. D. Whapham, "Electron microscope observation of the fission-gas bubble distribution in UO\textsubscript{2}," *Nuclear applications*, pp. 123–130, 1966, doi: 10.13182/NT66-A27492.

[17] R. J. White and M. O. Tucker, "A new fission-gas release model," *Journal of Nuclear Materials*, vol. 118, no. 1, pp. 1–38, 1983, doi: 10.1016/0022-3115(83)90176-9.

[18] G. Pastore, L. Luzzi, V. di Marcello, and P. van Uffelen, "Physics-based modelling of fission gas swelling and release in UO2 applied to integral fuel rod analysis," *Nuclear Engineering and Design*, vol. 256, pp. 75–86, 2013, doi: 10.1016/j.nucengdes.2012.12.002.

[19] C. A. Friskney and M. v. Speight, “A calculation on the in-pile diffusional release of fission products forming a general decay chain,” *Journal of Nuclear Materials*, vol. 62, pp. 89–94, 1976.
[20] R. J. White, “The development of grain-face porosity in irradiated oxide fuel,” *Journal of Nuclear Materials*, vol. 325, no. 1, pp. 61–77, 2004, doi: 10.1016/j.jnucmat.2003.10.008.
[21] J. A. Turnbull, C. A. Friskney, J. R. Findlay, F. A. Johnson, and A. J. Walter, “The diffusion coefficients of gaseous and volatile species during the irradiation of uranium dioxide,” *Journal of Nuclear Materials*, vol. 107, no. 2–3, pp. 168–184, 1982, doi: 10.1016/0022-3115(82)90419-6.
[22] M. S. Veshchunov, “Modelling of grain face bubbles coalescence in irradiated UO\textsubscript{2} fuel,” *Journal of Nuclear Materials*, vol. 374, no. 1–2, pp. 44–53, 2008, doi: 10.1016/j.jnucmat.2007.06.021.
[23] L. C. Bernard, J. L. Jacoud, and P. Vesco, “An efficient model for the analysis of fission gas release,” *Journal of Nuclear Materials*, vol. 302, no. 2–3, pp. 125–134, 2002, doi: 10.1016/S0022-3115(02)00793-6.
[24] R. J. J. White, R. C. C. Corcoran, R. S. Barnes, and P. J. Barnes, “A Summary of Swelling Data Obtained from the AGR/Halden Ramp Test Programme,” *R&T/NG/EXT/REP/0206/02*, no. 5, pp. 1–192, 2006.
[25] A. H. Booth, “A method of calculating fission gas diffusion from UO\textsubscript{2} fuel and its application to the X-2-f loop test,” *Atomic Energy of Canada Limited*, 1957.
[26] F. S. Ham, “Theory of diffusion-limited precipitation,” *Journal of Physics and Chemistry of Solids*, vol. 6, no. 4, pp. 335–351, 1958, doi: 10.1016/0022-3697(58)90053-2.
[27] M. v. Speight, “A Calculation on the Migration of Fission Gas in Material Exhibiting Precipitation and Re-solution of Gas Atoms Under Irradiation,” *Nuclear Science and Engineering*, vol. 37, no. 2, pp. 180–185, 1969, doi: 10.13182/nse69-a20676.
[28] C. Vitanza, E. Kolstad, and U. Graziani, “Fission gas release from UO2 pellet fuel at high burn-up,” *OECD HALDEN REACTOR PROJECT*, pp. 361–366, 1979.
[29] G. Zullo, D. Pizzocri, A. Magni, P. van Uffelen, A. Schubert, and L. Luzzi, “Towards grain-scale modelling of the release of radioactive fission gas from oxide fuel. Part II: Coupling SCIANTIX with TRANSURANUS,” *Nuclear Engineering and Technology*.
[30] M. O. Tucker and J. A. Turnbull, “The morphology of interlinked porosity in nuclear fuels,” *Proceedings of the Royal Society of London. A. Mathematical and Physical Sciences*, vol. 343, no. 1634, pp. 299–314, 1975, doi: 10.1098/rspa.1975.0067.
[31] M. O. Tucker, “The spacing of intergranular fission gas bubbles in irradiated UO\textsubscript{2},” *Journal of Nuclear Materials*, vol. 74, pp. 34–40, 1978.
[32] M. O. Tucker, “A simple description of interconnected grain edge porosity,” *Journal of Nuclear Materials*, vol. 79, no. 1, pp. 199–205, 1979, doi: 10.1016/0022-3115(79)90447-1.
[33] J. Leppänen, M. Pusa, T. Viitanen, V. Valtavirta, and T. Kaltiaisenaho, “The Serpent Monte Carlo code: Status, development and applications in 2013,” *Ann Nucl Energy*, vol. 82, pp. 142–150, Aug. 2015, doi: 10.1016/J.ANUCENE.2014.08.024.
[34] D. R. Olander, “Mechanistic interpretations of UO2 oxidation,” *Journal of Nuclear Materials*, vol. 252, no. 1–2, pp. 121–130, Jan. 1998, doi: 10.1016/S0022-3115(97)00291-2.
[35] B. v. Dobrov, V. v. Likhanskii, V. D. Ozrin, A. A. Solodov, M. P. Kissane, and H. Manenc, “Kinetics of UO2 oxidation in steam atmosphere,” *Journal of Nuclear Materials*, vol. 255, no. 1, pp. 59–66, May 1998, doi: 10.1016/S0022-3115(97)00364-4.
[36] A. R. Massih, “UO2 fuel oxidation and fission gas release,” 2018.
[37] D. R. Olander, “Oxidation of UO2 by High-Pressure Steam,” *http://dx.doi.org/10.13182/NT86-A33806*, vol. 74, no. 2, pp. 215–217, 2017, doi: 10.13182/NT86-A33806.
[38] J. D. Higgs, B. J. Lewis, W. T. Thompson, and Z. He, “A conceptual model for the fuel oxidation of defective fuel,” *Journal of Nuclear Materials*, vol. 366, no. 1–2, pp. 99–128, 2007, doi: 10.1016/j.jnucmat.2006.12.050.
[39] Y. S. Kim, “Fission Gas Release from UO$_{2+x} in Defective Fuel Rods,” in *International Topical Meeting on LWR Fuel Performance, Park City, Utah, April 10-13 2000, American Nuclear Society, cf. Nucl. Tech*, 2000, vol. 130, no. 1, pp. 9–17. doi: 10.13182/NT00-A3073.

[40] J. C. Killeen and J. A. Turnbull, “An experimental and theoretical treatment of the release of 85Kr from hyperstoichiometric uranium dioxide,” *Proc. Workshop Chemical Reactivity of Oxide Fuel and Fission Product Release, Gloucestershire, England, K.A. Simpson and P. Wood, eds., Central Electricity Generating Board*, pp. 387–404, Apr. 1987.

[41] P. Van Uffelen, G. Pastore, V. Di Marcello, and L. Luzzi, “Multiscale modelling for the fission gas behaviour in the TRANSURANUS Code,” *Nuclear Engineering and Technology*, vol. 43, no. 6, pp. 477–488, 2011, doi: 10.5516/NET.2011.43.6.477.

[42] K. Lassmann and H. Benk, “Numerical algorithms for intragranular fission gas release,” *Journal of Nuclear Materials*, vol. 280, no. 2, pp. 127–135, 2000, doi: 10.1016/S0022-3115(00)00044-1.

[43] K. Forsberg and A. R. Massih, “Diffusion theory of fission gas migration in irradiated nuclear fuel UO2,” *Journal of Nuclear Materials*, vol. 135, no. 2–3, 1985, doi: 10.1016/0022-3115(85)90071-6.

[44] K. Forsberg and A. R. Massih, “Fission gas release under time-varying conditions,” *Journal of Nuclear Materials*, vol. 127, no. 2–3, 1985, doi: 10.1016/0022-3115(85)90348-4.

[45] J. A. Turnbull, “The treatment of radioactive fission gas release measurements and provision of data for development and validation of the ANS-5.4 model,” *OECD HALDEN REACTOR PROJECT*, 2001.

[46] P. T. Elton and K. Lassmann, “Calculational methods for diffusional gas release,” *Nuclear Engineering and Design*, vol. 101, no. 3, pp. 259–265, 1987, doi: 10.1016/0029-5493(87)90054-9.

[47] von S. R. de Groot and P. Mazur, *Non-Equilibrium Thermodynamics*. 1963. Accessed: Nov. 02, 2022. [Online]. Available: https://www.abebooks.de/Non-Equilibrium-Thermodynamics-Groot-Mazur-North-Holland-Publishing/30763855635/bd

[48] C. Sari and G. Schumacher, “Oxygen redistribution in fast reactor oxide fuel,” *Journal of Nuclear Materials*, vol. 61, no. 2, pp. 192–202, Aug. 1976, doi: 10.1016/0022-3115(76)90083-0.

[49] B. J. Lewis, “A generalized model for fission-product transport in the fuel-to-sheath gap of defective fuel elements,” *Journal of Nuclear Materials*, vol. 175, no. 3, pp. 218–226, Dec. 1990, doi: 10.1016/0022-3115(90)90210-E.

[50] M. S. Veshchunov, “Mechanisms of fission gas release from defective fuel rods to water coolant during steady-state operation of nuclear power reactors,” *Nuclear Engineering and Design*, vol. 343, pp. 57–62, 2019, doi: 10.1016/J.NUCENGDES.2018.12.021.

[51] A. Harrer, G. Kurka, R. Warlop, G. Lasne, and M. Viver, “Resultats de l’Experience CRUSIFON 2 Compte-Rendu DMG No.61/80 (Action 4172-60),” 1980.

[52] A. Harrer, G. Kurka, R. Warlop, G. Lasne, and M. Viver, “Resultats de l’Experience CRUSIFON 1 bis (dossier No.4) Compte-Rendu DMG No. 40/81 (Action 4172-60),” 1981.

[53] Berta Bürger and Zoltán Hózer, “Improvement of the iodine and caesium spiking models in the RING code, EK-2021-437-1-4-M0, T4.2. Fission product release from defective fuel rod during SGTR transient,” 2021.

[54] Z. Hózer and N. Vajdda, “Simulation of leaking fuel rods,” in *ENS TopFuel, May*, 2001, pp. 27–30.

[55] Z. Hózer, “Simulation of leaking fuel rods in a VVER reactor,” *Ann Nucl Energy*, vol. 70, pp. 122–129, 2014, doi: 10.1016/J.ANUCENE.2014.03.002.

[56] “MELCOR Computer Code Manuals Vol. 2: Reference Manual Version 2.2.14959, SAND2019-12537 O,” 2019.

[57] B. J. Lewis, F. C. Iglesias, A. K. Postma, and D. A. Steininger, “Iodine spiking model for pressurized water reactors,” *Journal of Nuclear Materials*, vol. 244, no. 2, pp. 153–167, Apr. 1997, doi: 10.1016/S0022-3115(96)00723-4.

[58] “MELCOR Computer Code Manuals Vol. 1: Primer and Users’ Guide Version 2.2.14959, SAND2019-12536 O,” 2019. https://www.nrc.gov/reading-rm/doc-collections/nuregs/contract/cr6119/v1/index.html (accessed Aug. 10, 2022).

[59] D. A. Powers, J. L. Sprung, and C. D. Leigh, “Scan of an Unpublished Report: ‘Fission Product Behavior During Severe LWR Accidents: Recommendations for the MELCOR Code System,’” Jan. 2020, doi: 10.2172/1599281.

[60] “MELCOR Best Practices As Applied In The State-of-the-Art Reactor Consequence Analyses (SOARCA) Project (NUREG/CR-7008) | NRC.gov.” https://www.nrc.gov/reading-rm/doc-collections/nuregs/contract/cr7008/index.html (accessed Aug. 10, 2022).

[61] "Calculations of the fission products inventory under the cladding of hermetic and unhermetic fuel elements of VVER-1000 fuel assemblies (TVSA, TVS-2) with deep fuel burnup (60 MWd/kgU for the fuel element) and the activity of the primary coolant. Report of the RRC 'Kurchatov Institute'.," 2004.
[62] L. L. M. and P. B. G., "Method for calculating the nuclide activity of the primary circuit coolant of water-water energy reactor. IAE-1968, Kurchatov's Institute.," 1970.
[63] "NUREG-0800. Standard Review Plan (https://www.nrc.gov/reading-rm/doc-collections/nuregs/staff/sr0800/index.html)."
[64] A. J. P., "Iodine Spiking Data from Commercial PWR Operations. EGG-NERD-8395. Idaho National Engineering Laboratory.," 1989.
[65] "Technical specification of the safe operation of Unit 6 of Zaporizhzhia NPP. 06.GT.00.RG.01-19, 2019.".
[66] "[10] Regulatory Guide 1.183: Alternative Radiological Source Term for Evaluating Design Basis Accidents at Nuclear Power Reactors. U.S.NRC," 2000.
[67] J. H. Evans, "Bubble diffusion to grain boundaries in UO2 and metals during annealing: a new approach," *Journal of Nuclear Materials*, vol. 210, no. 1–2, pp. 21–29, 1994, doi: 10.1016/0022-3115(94)90218-6.
[68] L. Verma, L. Noirot, and P. Maugis, "Modelling intra-granular bubble movement and fission gas release during post-irradiation annealing of UO2 using a meso-scale and spatialized approach," *Journal of Nuclear Materials*, vol. 528, p. 151874, 2020, doi: 10.1016/j.jnucmat.2019.151874.
[69] L. Verma, L. Noirot, and P. Maugis, "A new spatially resolved model for defects and fission gas bubbles interaction at the mesoscale," *Nucl Instrum Methods Phys Res B*, vol. 458, no. October 2018, pp. 151–158, 2019, doi: 10.1016/j.nimb.2018.10.028.
[70] A. Moal, V. Georgenthum, and O. Marchand, "SCANAIR: A transient fuel performance code: Part One: General modelling description," *Nuclear Engineering and Design*, vol. 280, pp. 150–171, Dec. 2014, doi: 10.1016/J.NUCENGDES.2014.03.055.
[71] M. S. Veshchunov and V. I. Tarasov, "Modelling of irradiated UO2 fuel behaviour under transient conditions," *Journal of Nuclear Materials*, vol. 437, no. 1–3, pp. 250–260, Jun. 2013, doi: 10.1016/j.jnucmat.2013.02.011.